UNIVERSITY OF CALIFORNIA
Los Angeles

Post-Inflationary Higgs Relaxation and the Origin of Matter

A dissertation submitted in partial satisfaction
of the requirements for the degree
Doctor of Philosophy in Physics

by

Louis Yang

2017

ABSTRACT OF THE DISSERTATION

Post-Inflationary Higgs Relaxation and the Origin of Matter

by

Louis Yang
Doctor of Philosophy in Physics
University of California, Los Angeles, 2017
Professor Alexander Kusenko, Chair

The recent measurement of the Higgs boson mass implies a relatively slow rise of the Standard Model Higgs potential at large scales, and a possible second minimum at even larger scales. Consequently, the Higgs field may develop a large vacuum expectation value during inflation. The relaxation of the Higgs field from its large postinflationary value to the minimum of the effective potential represents an important stage in the evolution of the Universe. During this epoch, the time-dependent Higgs condensate can create an effective chemical potential for the lepton number, leading to a generation of the lepton asymmetry in the presence of some large right-handed Majorana neutrino masses. The electroweak sphalerons redistribute this asymmetry between leptons and baryons. This Higgs relaxation leptogenesis can explain the observed matter-antimatter asymmetry of the Universe even if the Standard Model is valid up to the scale of inflation, and any new physics is suppressed by that high scale. The baryonic isocurvature perturbations generated by the relaxation leptogenesis can also explain the excess found in the cosmic infrared background (CIB) anisotropy.

We begin this dissertation by reviewing the development of the large vacuum expectation value (VEV) of the Higgs and other scalar fields during inflation. We then discuss the postinflationary relaxation of the Higgs field in full detail, and present the relaxation leptogenesis framework using the Standard Model Higgs field as an example.

Next, we extend the relaxation leptogenesis to the elementary Goldstone Higgs (EGH) framework and the pseudoscalar scenario. In the EGH paradigm, the electroweak (EW) scale is not fundamental but radiatively generated. This allows one to disentangle the EW scale from the vacuum expectation of the elementary Higgs field, and construct a very flat scalar potential directions along which the relaxation leptogenesis mechanism can be implemented with larger parameter space.

In December 2015, the ATLAS and CMS Collaborations have reported evidence of a diphoton excess which may be interpreted as a pseudoscalar boson S with a mass around 750 GeV. To explain the diphoton excess, such a boson is coupled to the Standard Model gauge fields via $SF\tilde{F}$ operators, which provide the chemical potential to the lepton asymmetry. Although the diphoton excess turns out to be a statistical fluctuation in 2016, a similar pseudoscalar with greater mass remains a viable model for relaxation leptogenesis mechanism.

Finally, we discuss the imprint of relaxation leptogenesis on the CIB anisotropy. Observations of CIB exhibit significant fluctuations on small angular scales, whose origin remains a question. We consider the possibility that small-scale fluctuations in matter-antimatter asymmetry could lead to variations in star formation rates which are responsible for the CIB fluctuations. We show that the Higgs relaxation leptogenesis mechanism can produce such small-scale baryonic isocurvature perturbations which can explain the observed excess in the CIB fluctuations.

The dissertation of Louis Yang is approved.

Roberto Peccei

Terence Chi-Shen Tao

Alexander Kusenko, Committee Chair

University of California, Los Angeles

2017

To my family and friends

Table of Contents

List of Figures

Acknowledgments

First, I would like to thank my advisor Alexander Kusenko, who constantly introduces me to the various exciting topics in particle physics and cosmology, and provides helpful guidance through out my Ph.D. research. I would also like to thank Doctor Lauren Pearce, who discuss and collaborate productively with me on most of my research projects. In addition, I want to thanks Professor Marco Peloso, Professor Francesco Sannino, Helene Gertov, and Professor Masahiro Kawasaki for the creative collaborations. This thesis contains parts that are adapted from five publications including substantial text overlap.

Sections 1.2, 1.3, and Chapter 2 are based on A. Kusenko, L. Pearce, and L. Yang, "Postinflationary Higgs Relaxation and the Origin of Matter-Antimatter Asymmetry," Phys. Rev. Lett. **114**, 061302 (2014), arXiv:1410.0722 [hep-ph]; and L. Yang, L. Pearce, and A. Kusenko, "Leptogenesis via Higgs Condensate Relaxation," Phys. Rev. D **92**, 043506 (2015), arXiv:1505. 07912 [hep-ph].

Chapter 3 is a version of H. Gertov, L. Pearce, F. Sannino, and L. Yang, "Baryogenesis via Elementary Goldstone Higgs Relaxation," Phys. Rev. D **93**, 115042 (2016), arXiv:1601.07753 [hep-ph].

Chapter 4 is a version of A. Kusenko, L. Pearce, and L. Yang, "Leptogenesis via the 750 GeV Pseudoscalar," Phys. Rev. D **93**, 115005 (2016), arXiv:1604.02382 [hep-ph].

Chapter 5 is a version of M. Kawasaki, A. Kusenko, L. Pearce, and L. Yang, "Relaxation leptogenesis, isocurvature perturbations, and the cosmic infrared background," Phys. Rev. D **95**, 103006 (2017), arXiv:1701.02175 [hep-ph].

Vita

2006 – 2010	B.S. in Physics, National Tsing Hua University (NTHU), Hsinchu, Taiwan.
2011 – Present	Ph.D. Candidate in Physics, University of California, Los Angeles (UCLA).
2016	Dissertation Year Fellowship, Graduate Division, UCLA.

Publications

[1] Masahiro Kawasaki, Alexander Kusenko, Lauren Pearce, and Louis Yang, "Relaxation leptogenesis, isocurvature perturbations, and the cosmic infrared background," Phys. Rev. D **95**, 103006 (2017), arXiv:1701.02175 [hep-ph].

[2] Alexander Kusenko, Lauren Pearce, and Louis Yang, "Leptogenesis via the 750 GeV pseudoscalar," Phys. Rev. D **93**, 115005 (2016), arXiv:1604.02382 [hep-ph].

[3] Helene Gertov, Lauren Pearce, Francesco Sannino, and Louis Yang, "Baryogenesis via Elementary Goldstone Higgs Relaxation," Phys. Rev. D **93**, 115042 (2016), arXiv:1601.07753 [hep-ph].

[4] Louis Yang, Lauren Pearce, and Alexander Kusenko, "Leptogenesis via Higgs Condensate Relaxation," Phys. Rev. D **92**, 043506 (2015), arXiv:1505.07912 [hep-ph].

[5] Lauren Pearce, Louis Yang, Alexander Kusenko, and Marco Peloso, "Leptogenesis via neutrino production during Higgs condensate relaxation," Phys. Rev. D **92**, 023509 (2015), arXiv:1505.02461 [hep-ph].

[6] Alexander Kusenko, Lauren Pearce, and Louis Yang, "Postinflationary Higgs relaxation and the origin of matter-antimatter asymmetry," Phys. Rev. Lett. **114**, 061302 (2015), arXiv:1410.0722 [hep-ph].

[7] Chung-Chi Lee, Chao-Qiang Geng, and Louis Yang, "Singularity phenomena in viable f(R) gravity," Prog. Theor. Phys. **128**, 415–427 (2012), arXiv:1201.4546 [astro-ph.CO].

[8] Louis Yang, Chung-Chi Lee, and Chao-Qiang Geng, "Gravitational Waves in Viable f(R) Models," JCAP **1108**, 029 (2011), arXiv:1106.5582 [astro-ph.CO].

[9] Louis Yang, Chung-Chi Lee, Ling-Wei Luo, and Chao-Qiang Geng, "Observational Constraints on Exponential Gravity," Phys. Rev. D **82**, 103515 (2010), arXiv:1010.2058 [astro-ph.CO].

CHAPTER 1

Post-Inflationary Higgs Relaxation

The recent discovery of a Higgs boson with mass 125 GeV [7, 8] implies that the Higgs potential is very shallow and may even develop a second minimum, assuming that the standard model is valid at high energy scales [9]. During cosmological inflation, the Higgs field may be trapped in a quasistable second minimum or, alternatively, may develop a stochastic distribution of vacuum expectation values due to the flatness of the potential [10–12]. In both scenarios, the Higgs field relaxes to its vacuum state after inflation via a coherent motion. In this chapter, we explore this epoch of Higgs relaxation.

In Sec. 1.1, we review how a scalar field such as the Higgs field can obtain a large vacuum expectation value during inflation through quantum fluctuation. (See also [13] for a complete review.) Next, in Sec. 1.2, we briefly review the cosmology of the reheating stage of the universe including the evolution of the scale factor and the temperature. Finally, in Sec. 1.3, we discuss the detail evolution of the Higgs field after the inflation including the perturbative and non-perturbative decays of the Higgs field.

1.1 Quantum Fluctuation in the Inflationary Universe

We begin with describing the universe by the isotropic Friedmann–Lemaitre–Robertson–Walker (FLRW) metric

$$ds^2 = dt^2 - a^2(t)\, d\vec{x}^2, \tag{1.1}$$

where t is the cosmic time and $a(t)$ is the scale factor. During inflation, the universe can be well approximated as a de Sitter spacetime, where the scale factor increases exponentially in

time $a(t) = a_0 e^{Ht}$, and the Hubble parameter

$$H^2 = \frac{\dot{a}}{a} = \frac{\rho}{3M_{pl}^2} \tag{1.2}$$

is almost a constant. ($M_{pl} \equiv 1/\sqrt{8\pi G} = 2.435 \times 10^{18}$ GeV is the reduced Planck mass.) One usually quantifies the length of inflation by the number of e-folds, which is given by $N = Ht$. The constant expansion rate of the spacetime provides an event horizon located at the distance $r = H^{-1}$.

We are interested in the behavior of scalar fields during inflation. The equation of motion of a scalar field ϕ in a FLRW metric is given by

$$\ddot{\phi} + 3H\dot{\phi} - \frac{1}{a^2}\nabla^2\phi + \frac{dV(\phi)}{d\phi} = 0, \tag{1.3}$$

where an overhead dot represents the derivative with respect to the cosmic time t, and $\nabla = (\partial_1, \partial_2, \partial_3)$ is the usual spatial gradient. Notice that the expansion of the background spacetime generates an additional $3H\dot{\phi}$ term in Eq. (1.3), which provides a Hubble friction to the motion of ϕ. If one approximates the potential of ϕ as a harmonic oscillator, $V(\phi) \simeq \frac{1}{2}m_{\text{eff}}^2\phi^2$, with the effective mass $m_{\text{eff}}^2 = V''(\phi)$, the classical relaxation time (oscillation period) of ϕ in the absence of the Hubble friction term is

$$\tau \sim m_{\text{eff}}^{-1} \sim \sqrt{V''(\phi)}^{-1}. \tag{1.4}$$

During inflation, the relevant time scale is the Hubble time scale H^{-1}. Thus, if a scalar field ϕ has a mass $m_{\text{eff}}^2 \ll H^2$, there is insufficient time for the scalar field to oscillate or change. Any non-zero field values of ϕ remains "frozen" until the end of inflation period. More precisely, for $m_{\text{eff}}^2 \ll H^2$, the oscillator is in the overdamped regime, and the Hubble friction term dominates over the first term of Eq. (1.3)

$$\ddot{\phi} \ll 3H\dot{\phi}. \tag{1.5}$$

In this case, the terminal speed of ϕ is given by the slow-roll approximation as

$$\dot{\phi} \simeq \frac{-1}{3H}\frac{dV}{d\phi} \tag{1.6}$$

so ϕ can only change slowly via classical motion. However, scalar fields can still obtain non-zero field from quantum effect. In the following sections, we will explain how scalar fields in the slow-roll regime ($m^2 \ll H^2$) can develop large field values from quantum fluctuation during inflation. But before we start the analysis, let us note that if the scalar field is very massive, $m^2 \gg H^2$, non-zero field value of ϕ can always relax via classical motion within a few Hubble time H^{-1} so quantum fluctuations are suppressed for very massive scalar fields.

1.1.1 Quantization of Scalar Fields in de Sitter Space

To understand the growth of the vacuum expectation of a scalar field ϕ in a changing spacetime, we first consider the case where the scalar field ϕ is massless and non-interacting, namely $V'(\phi) = 0$. We expand $\phi(\vec{x}, t)$ in the momentum Fourier modes[1] as

$$\phi(\vec{x}, t) = \int \frac{d^3k}{(2\pi)^{3/2}} \left[a_k^\dagger \psi_k(t) e^{i\vec{k}\cdot\vec{x}} + a_k \psi_k^*(t) e^{-i\vec{k}\cdot\vec{x}} \right], \tag{1.7}$$

where $a_k^\pm$ are the creation and annihilation operators after quantization [10, 11, 14, 15]. The time dependence of the k mode, $\psi_k(t)$, satisfies the equation of motion

$$\ddot{\psi}_k(t) + 3H\dot{\psi}_k(t) + \vec{k}^2 e^{-2Ht} \psi_k(t) = 0, \tag{1.8}$$

which has a solution

$$\psi_k(t) = \frac{iH}{k\sqrt{2k}} \left(1 + \frac{k}{iH} e^{-Ht}\right) \exp\left(\frac{ik}{H} e^{-Ht}\right). \tag{1.9}$$

We can see that the solution (1.9) is the physical one because (1) in the limit that $k \gg H$ while $kt \sim$ const., the short-wavelength solution

$$\psi_k \to \frac{i}{\sqrt{2k}} e^{-ikt} e^{ik/H} \tag{1.10}$$

recovers the plane wave solution in Minkowski space; (2) for long-wavelength mode satisfying $ke^{-Ht} < H$, the solution

$$\psi_k \to \frac{iH}{k\sqrt{2k}} \tag{1.11}$$

[1] In our notation, $k = \left|\vec{k}\right|$ is the comoving momentum or comoving wave number, which is time independent. The physical momentum or wave number is $p = k/a(t)$, which decreases as the space expands.

ceases to oscillate corresponding to mode that is outside the event horizon.

The quantum fluctuation of ϕ can be characterized by the variance of the field, $\langle\phi^2\rangle$. The solution of ϕ in the de Sitter space yields an vacuum expectation value

$$\left\langle 0\left|\phi^2\left(t\right)\right|0\right\rangle = \int \frac{d^3k}{\left(2\pi\right)^3}\left|\psi_k\left(t\right)\right|^2 = \int \frac{d^3k}{\left(2\pi\right)^3}\left(\frac{e^{-2Ht}}{k}+\frac{H^2}{2k^3}\right). \tag{1.12}$$

Note this is expressed in terms of the comoving momentum k but not the physical momentum ($p = k/a = ke^{-Ht}$). If we rewrite this in terms of the physical momentum p, we find

$$\left\langle\phi^2\right\rangle = \int \frac{d^3p}{\left(2\pi\right)^3 p}\left(\frac{1}{2}+\frac{H^2}{2p^2}\right). \tag{1.13}$$

The first term in the parentheses describes the usual contribution from the vacuum fluctuation in Minkowski space. This term has UV divergence but it can be fixed by the usual renormalization procedure. The second term in the parentheses is due to the expansion of space and it appears only when the Hubble parameter H is large and nonzero. This term is especially interesting because it implies that particles can be created from the vacuum of an expanding universe. By comparing it with the usual $\langle\phi^2\rangle$ in Minkoswki space, we find Eq. (1.13) represents a state with nonzero occupation number

$$n_p = \frac{H^2}{2p^2}. \tag{1.14}$$

Note that the contribution to $\langle\phi^2\rangle$ from low p diverges in Eq. (1.13). This happens only in the pure de Sitter universes where the inflation stage exists forever. In a realistic inflationary universe, the exponential expansion phase only lasts for a finite period of time t. If the inflationary period starts at $t = 0$, the longest quantum fluctuation, which exists the horizon at $t = 0$, only has a physical momentum $p \simeq He^{-Ht}$ at time t. On the other hand, fluctuations with wavelengths much shorter than the size of horizon H^{-1} do no feel the expansion of the space, and their spectra are indistinguishable from that in Minkowski space. (This is illustrated in Fig. 1.1) Therefore, in a realistic inflation theory, the quantum fluctuation for a massless scalar field is finite and is given by

$$\left\langle\phi^2\right\rangle \approx \frac{H^2}{2\left(2\pi\right)^3}\int_{He^{-Ht}}^{H}\frac{d^3p}{p^3} = \frac{H^3}{4\pi^2}t. \tag{1.15}$$

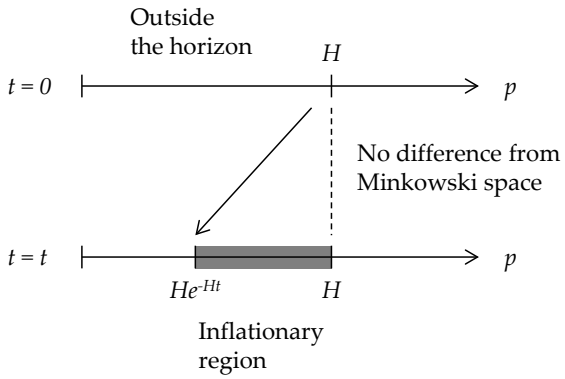

Figure 1.1: The spectrum of the quantum fluctuation generated in a realistic inflation theory. For mode $p \gg H$, the spectrum is the same as that in Minkowski space. For mode $p = H$ leaving the horizon at $t = 0$, it grows to $p = He^{-Ht}$ at $t = t$. Inflation which lasts for a finite time t generates the quantum fluctuation in $He^{-Ht} \lesssim p \lesssim H$.

Similarly, one can show for scalar fields with nonzero mass m and $m < H$, the quantum fluctuation is

$$\left\langle \phi^2 \right\rangle = \frac{3H^4}{8\pi^2 m^2} \left[1 - \exp\left(\frac{-2m^2}{H} t \right) \right]. \tag{1.16}$$

Note for $m^2 t < H$, the massive result (1.16) reduces to the massless one (1.15), which is a very useful approximation when a scalar field only experiences a short period of inflation.

To better understand the physical interpretation of these results, we observe that the $\langle \phi^2 \rangle$ we computed are dominated by the large occupation number n_p from the exponentially long wavelength mode ($p \sim He^{-Ht}$). Those fluctuations are also characterized by long correlation length. A calculation in de Sitter space on the correlation functions of scalar fields shows [16]

$$\left\langle \phi\left(\vec{x}, t\right) \phi\left(\vec{y}, t\right) \right\rangle \approx \left\langle \phi^2\left(\vec{x}, t\right) \right\rangle \left(1 - \frac{1}{Ht} \ln Hl \right). \tag{1.17}$$

For large separations $H^{-1} \lesssim l \lesssim H^{-1} e^{Ht}$, the magnitudes of the scalar fields are highly correlated. Thus, we can treat the long-wavelength quantum fluctuations of a scalar field created during inflation as a weakly inhomogeneous (semi)classical field. In order to simplify the analysis of the postinflationary evolution of the quantum field, we identify the classical

field value by the vacuum expectation value (VEV) of ϕ as

$$\phi_0 \equiv \sqrt{\langle \phi^2 \rangle}. \tag{1.18}$$

1.1.2 Stochastic Approach

Another approach to analyze the quantum fluctuation during inflation is to consider the diffusion process [17, 18]. One can interpret the generation of the nonzero vacuum expectation value of scalar fields as the scalar field ϕ going through several quantum jumps or quantum tunnelings away from its equilibrium minimum in the potential $V(\phi)$. The entire process is similar to a particle undergoing Brownian motion, and can be described by the diffusion equation [19]

$$\frac{\partial P(\phi, t)}{\partial t} = D \frac{\partial^2 P(\phi, t)}{\partial \phi^2}. \tag{1.19}$$

Here D is the diffusion coefficient to be determined. $P(\phi, t)$ is the probability distribution to find the field value ϕ in a patch of the space at time t. To determine the diffusion coefficient D, we can consider the case of a massless scalar field (1.15), where expectation value of ϕ^2 is given by

$$\left\langle \phi^2(t) \right\rangle \equiv \int_{-\infty}^{\infty} \phi^2 P(\phi, t)\, d\phi = \frac{H^3}{4\pi^2} t. \tag{1.20}$$

Taking the time derivative, the diffusion coefficient can be found by

$$\frac{H^3}{4\pi^2} = \int \phi^2 \frac{\partial P}{\partial t} d\phi = D \int \phi^2 \frac{\partial^2 P}{\partial \phi^2} d\phi = 2D, \tag{1.21}$$

where in the last equality we assume that $P(\phi, t)$ is normalized as $\int_{-\infty}^{\infty} P(\phi, t)\, d\phi = 1$. We can also compute the probability distribution by solving Eq. (1.19). With the initial condition $P(\phi, 0) = \delta(\phi)$, we find

$$P(\phi, t) = \sqrt{\frac{2\pi}{H^3 t}} \exp\left(\frac{-2\pi^2 \phi^2}{H^3 t} \right), \tag{1.22}$$

which can consistently reproduces the massless result of (1.15).

For massive or interacting scalar fields [$V'(\phi) \neq 0$], the generated ϕ field can move toward its minimum in the potential following its equation of motion. Thus, for $V'(\phi) \neq 0$, we need

to add an additional drift term $-\frac{\partial}{\partial\phi}\left[P\mu\left(\phi,t\right)\right]$ to the diffusion equation, whereμ is the drift coefficient. The slow-roll condition (1.6) of scalar fields during inflation provides the drift coefficient being

$$\mu=\frac{\partial\phi}{\partial t}=\frac{-1}{3H}\frac{dV}{d\phi}, \tag{1.23}$$

so the diffusion equation for the massive or interacting case $\left[V'\left(\phi\right)\neq 0\right]$ is [20]

$$\frac{\partial P\left(\phi,t\right)}{\partial t}=\frac{H^3}{8\pi^2}\frac{\partial^2 P\left(\phi,t\right)}{\partial\phi^2}+\frac{1}{3H}\frac{\partial}{\partial\phi}\left[P\left(\phi,t\right)\frac{dV}{d\phi}\right]. \tag{1.24}$$

This diffusion equation is also known as the **Fokker-Planck equation**. Again, we can reproduce the result we obtained from the quantization approach (1.16) for the massive scalar with a potential $V\left(\phi\right)=\frac{1}{2}m^2\phi^2$. Considering the case where the distribution of ϕ is in equilibrium $\frac{\partial P}{\partial t}=0$, the Fokker-Planck equation (1.24) can reduce to

$$\frac{\partial P\left(\phi\right)}{\partial\phi}=-\frac{8\pi^2}{3H^4}m^2\phi P\left(\phi\right), \tag{1.25}$$

which has a solution

$$P\left(\phi\right)=N\exp\left(\frac{-4\pi^2m^2}{3H^4}\phi^2\right), \tag{1.26}$$

with some normalization factor N. Integrading this distribution with ϕ^2, we obtain the vacuum expectation value of ϕ^2 as

$$\left\langle\phi^2\right\rangle=\frac{3H^4}{8\pi^2m^2}, \tag{1.27}$$

which agrees with the result of Eq. (1.16) when $t\to\infty$.

For a scalar field ϕ with a general form of the potential $V\left(\phi\right)$, we have the equilibrium Fokker-Planck equation ($\frac{\partial P}{\partial t}=0$) as

$$\frac{\partial P\left(\phi\right)}{\partial\phi}=-\frac{8\pi^2}{3H^4}P\left(\phi\right)\frac{dV\left(\phi\right)}{d\phi}. \tag{1.28}$$

The general solution to the equilibrium Fokker-Planck equation can be easily obtained as

$$P\left(\phi\right)=N\exp\left[-\frac{8\pi^2}{3H^4}V\left(\phi\right)\right]. \tag{1.29}$$

From this probability distribution (1.29), we see the scalar field ϕ can have non-vanishing transition probability for $V(\phi) \lesssim H^4$. For the potential of the form $V(\phi) = \beta_n \phi^{2n}$, $n \in \mathbb{N}$, the expectation value is

$$\left\langle \phi^2 \right\rangle = \left(\frac{3H^4}{8\pi^2 \beta_n} \right)^{1/n} \frac{\Gamma\left(\frac{3}{2n}\right)}{\Gamma\left(\frac{1}{2n}\right)}, \tag{1.30}$$

which can also be estimated by

$$V\left(\sqrt{\left\langle \phi^2 \right\rangle}\right) \sim \beta_n \left(H^{4/n} / \beta_n^{1/n} \right)^n \sim H^4. \tag{1.31}$$

(See Appendix A for the derivation.) The physical interpretation of Eq. (1.31) is that the expanding background in the de Sitter space provides quantum fluctuations with energy density in the order of H^4. Therefore, any scalar fields with $m^2 \ll H^2$ during inflation can receive a VEV ϕ such that $V(\phi) \sim H^4$. Note that if the scalar field is very massive $m^2 \gg H^2$, the quantum fluctuation is suppressed via the classical relaxation.

1.1.3 Quantum Fluctuation of the Inflaton

In the above analysis, we have assumed the Hubble parameter H is independent from the VEV of the scalar field ϕ. In general, the VEV of ϕ can affect the expansion rate of the universe via its energy density so more generally one should write the diffusion equation (1.24) as

$$\frac{\partial P(\phi, t)}{\partial t} = -\frac{\partial j(\phi, t)}{\partial \phi}, \tag{1.32}$$

where $j(\phi, t)$ is the probability current in (ϕ, t)-space given by

$$-j(\phi, t) = \frac{\partial}{\partial \phi} \left[\frac{H^3 P(\phi, t)}{8\pi^2} \right] + \frac{P(\phi, t)}{3H} \frac{dV}{d\phi}. \tag{1.33}$$

If a scalar field ϕ, like the inflaton I, dominates the energy density ρ of the universe via its potential energy $V(\phi)$, the Hubble parameter is determined by the VEV of ϕ via

$$H^2(\phi) = \frac{\rho}{3M_{pl}^2} \simeq \frac{1}{3M_{pl}^2} V(\phi), \tag{1.34}$$

which gives the probability current

$$-j(\phi, t) = \frac{H^3}{8\pi^2} \frac{\partial P}{\partial \phi} + \frac{P}{8\pi^2} \frac{\partial H^3}{\partial \phi} + \frac{P}{3H} \frac{dV}{d\phi}. \tag{1.35}$$

Using the relation that

$$\frac{\partial H^3}{\partial \phi} = \frac{3}{2} H^3 \frac{1}{V} \frac{dV}{d\phi}, \tag{1.36}$$

we find the probability current $j(\phi, t)$ for the universe with the potential energy of ϕ dominates the energy density is

$$-j(\phi, t) = \frac{1}{3H} \left[\frac{3H^4}{8\pi^2} \frac{\partial P}{\partial \phi} + \left(\frac{9H^4}{16\pi^2} \frac{1}{V} + 1 \right) P \frac{dV}{d\phi} \right] \tag{1.37}$$

$$= \frac{1}{3H} \left[\frac{8V^2}{3m_{pl}^4} \frac{\partial P}{\partial \phi} + \left(1 + \frac{4V}{m_{pl}^4} \right) P \frac{dV}{d\phi} \right], \tag{1.38}$$

where $m_{pl} = \sqrt{8\pi} M_{pl} = 1.22 \times 10^{19}\,\text{GeV}$ is the Planck mass. Next, we want to find the equilibrium distribution, $\partial P/\partial t = 0$, in this case. The solution to Eq. (1.32) with $j(\phi, t) \neq 0$ corresponds to a constant probability current flowing from $\phi = -\infty$ to $\phi = \infty$, which is not accessible by any physical initial condition [18]. Thus, we should restrict to the cases where $j(\phi, t) = 0$. Furthermore, the stochastic approach is valid only when the potential energy of ϕ is less than the Planck scale [$V(\phi) \ll m_{pl}^4$] so we approximate Eq. (1.38) as

$$\frac{\partial \ln P(\phi)}{\partial \phi} = -\frac{3m_{pl}^4}{8V^2} \frac{dV}{d\phi} = \frac{3m_{pl}^4}{8} \frac{d}{d\phi} \left[V^{-1}(\phi) \right]. \tag{1.39}$$

The solution to Eq. (1.39) is

$$P(\phi) = N \exp \left[\frac{3m_{pl}^4}{8V(\phi)} \right], \tag{1.40}$$

where the normalization N is determined by $\int P(\phi)\, d\phi = 1$. Since this distribution $P(\phi)$ has a clear-cut maximum at $\phi = 0$ [assuming $\phi = 0$ is the minimum of $V(\phi)$], one find the equilibrium probability distribution in this case is

$$P(\phi) = \exp \left[-\frac{3m_{pl}^4}{8} \left(\frac{1}{V(0)} - \frac{1}{V(\phi)} \right) \right] \tag{1.41}$$

upto an unimportant sub-exponential factor. Note that one can also obtain the result (1.41) via the instanton approach as first done by Hawking and Moss [21, 22]. Tunneling problem in quantum field theory is described by the instanton solution connecting the two states. In a de Sitter space, the transition rate per unit volume of both the field ϕ and the background

metric $g_{\mu\nu}$ experience quantum tunneling from the minimum $\phi = 0$ to $\phi = \phi_1$ is proportional to

$$\frac{\Gamma}{V} \propto \exp\left[S_E\left(0\right) - S_E\left(\phi_1\right)\right], \tag{1.42}$$

where the Euclidean action S_E in de Sitter space is given by

$$S_E\left(\phi\right) = -\frac{3m_{pl}^4}{8V\left(\phi\right)}. \tag{1.43}$$

Since in equilibrium, the probability of the field being at a value ϕ is proportional to the transition rate Γ of the field to that value ϕ, Eq. (1.42) recovers the result of stochastic approach (1.41).

1.1.4 Quantum Fluctuation of the Higgs Field

The extension of these results to multiple scalar fields is straightforward. In the case of the standard model Higgs, the system has both the inflaton I and the Higgs field Φ in the early universe. While the energy density of the universe is primarily controlled by the inflaton potential $V\left(I\right)$, the Higgs field as a spectator field still experience the exponential expansion of the space and can develop a large vacuum expectation value by the end of inflation. In this case, the quantum fluctuation of the Higgs field can be well described by the analysis in Sec. 1.1.2.

The standard model Higgs field has a tree-level potential

$$V(\Phi) = m^2\Phi^\dagger\Phi + \lambda\left(\Phi^\dagger\Phi\right)^2, \tag{1.44}$$

where Φ is an SU(2) doublet. Using a gauge transformation, one can write the classical field as $\Phi = \left\{0, e^{i\theta}\phi\right\}/\sqrt{2}$, where $\phi(x)$ is real. For energy scale above the electroweak scale ($\mu \gg v_{EW}$), this potential can be fairly approximated by the quartic potential

$$V\left(\phi\right) = \frac{1}{4}\lambda\phi^4, \tag{1.45}$$

with a running quartic coupling $\lambda\left(\phi\right) \lesssim 0.1$ for $\phi \gg v_{EW}$ whose evolution can be obtained by solving the RGEs. From Eq. (1.29), we see the equilibrium distribution for a potential

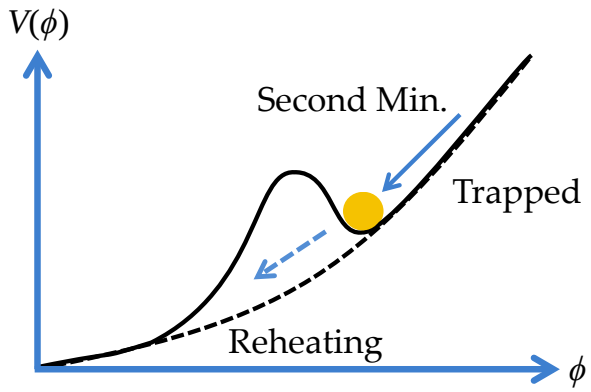

Figure 1.2: Illustration for the initial condition 1 (IC-1)—A metastable vacuum at large VEV which is later destabilized during reheating.

with $n = 4$ is given by

$$P(\phi) = N \exp\left(-\frac{2\pi^2 \lambda \phi^4}{3H^4}\right). \tag{1.46}$$

which gives the equilibrium Higgs VEV as [23] (see also Appendix A)

$$\phi_I = \sqrt{\langle \phi^2 \rangle} = \sqrt{\frac{\Gamma(3/4)}{\Gamma(1/4)}} \left(\frac{3}{2\pi^2 \lambda}\right)^{1/4} H \cong 0.36 \frac{H}{\lambda^{1/4}}. \tag{1.47}$$

During inflation, the Hubble parameter can be as large as $H \sim 10^{12}$ GeV [24, 25], which gives a Higgs VEV in the order of $\phi_I \sim 10^{12}$ GeV as well. With this large VEV, the Higgs field is sensitive to higher scale physics. One can consider two possible modifications to the standard model Higgs potential at high energy scales: (1) the Higgs potential might have a metastable vacuum at the large VEV due to higher-dimensional operators; (2) there could also be interaction between the Higgs field and the inflaton.

1.1.4.1 Initial Condition 1 (IC-1): Metastable Vacuum at Large VEVs

The Higgs quartic coupling λ, although constant at tree-level, are modified by both loop and finite temperature corrections. Due to the contribution from the top quark Yukawa coupling, λ turns negative at the scale around $\phi \sim 10^{12}$ GeV, which generates a second minimum at Planckian scale. The result is that the electroweak vacuum at $\phi = v_{EW} = 246.22$ GeV is

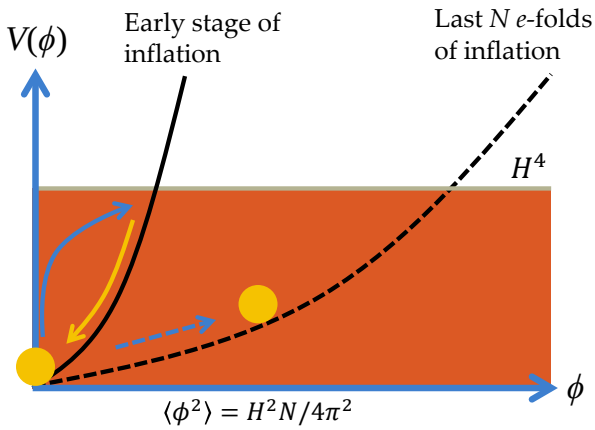

Figure 1.3: Illustration for the initial condition 2 (IC-2)—Delayed quantum fluctuation of the Higgs field due to the Higgs-inflaton couplings.

only metastable at zero temperature [9].

At the large VEVs, the Higgs potential may be sensitive to the effects of higher-dimensional operators

$$\mathcal{O}_{\phi,n} = \frac{\phi^n}{\Lambda_{\phi,n}^{n-4}} \qquad n \geq 6, \tag{1.48}$$

which can raise the second minimum and consequently stabilize the electroweak vacuum. If such operators lift the second minimum but don't eliminate it, one can have a metastable vacuum at large Higgs VEVs. The Higgs VEV may take an initial large value during inflation, similar to the initial VEV of the inflaton field itself in chaotic inflation models (see Fig. 1.2 for the illustration). During inflation, such a VEV evolves towards the false vacuum from above, and then remains trapped in this false vacuum until destabilized by thermal corrections in reheating. Subsequently, the field rolls to the global minimum at $\phi = 0$, until electroweak symmetry is broken at a significantly later time.

1.1.4.2 Initial Condition 2 (IC-2): Delayed Quantum Fluctuation due to the Higgs-Inflaton Couplings

At large VEV, the Higgs field can also be sensitive to the Higgs-inflaton coupling of the form

$$\mathcal{L}_{\phi \mathrm{I}} = -c \frac{(\Phi^\dagger \Phi)^{m/2} I^n}{M_{pl}^{m+n-4}}, \tag{1.49}$$

where I is the inflaton field and Φ is the Higgs field. Such couplings can contribute significantly to the effective mass of the Higgs field as

$$\Delta m_{\mathrm{eff},\phi}^2 (\phi, I) = \frac{\partial^2 V(\phi, I)}{\partial \phi^2} = cm(m-1) \frac{\phi^{m-2} I^n}{M_{pl}^{m+n-4}}. \tag{1.50}$$

During the early stages of the inflation, the inflaton VEV $\langle I \rangle$ is large (superplanckian) and provides a large effective mass to the Higgs field. As explained in Sec. 1.1, when $m_{\mathrm{eff},\phi} \gtrsim H$ the expansion of the universe is not sufficiently rapid to maintain the field at large VEVs, hence, suppressing the quantum fluctuation of the Higgs. At the later time of inflation, $\langle I \rangle$ decreases; consequently this term becomes negligible and the Higgs VEV starts to develop (see Fig. 1.3). The evolution of the distribution of the Higgs field is then determined by the Fokker-Planck equation (1.33). If the Higgs VEV grows during the last N_{last} e-folds of inflation, one can approximate the resulting average VEV as

$$\phi_0 \simeq \min \left(\sqrt{N_{\mathrm{last}}} \frac{H}{2\pi}, \ \phi_I \right). \tag{1.51}$$

In both cases, the spectra of the Higgs field fluctuation are modified, which we will discuss in detail in Chapters 2 and 5. In the following sections, we will study the relaxation of the Higgs VEV in these possible scenarios during reheating.

1.2 Reheating

Now that we have established that the Higgs field can develop a large VEV during inflation, we are interested in its subsequent evolution to its equilibrium value. Relaxation begins when the Hubble parameter is comparable to the effective mass of the Higgs field, $H(I) \approx$

$m_{\text{eff}}(\phi)$, which is within the reheating epoch. Therefore, this relaxation is sensitive to finite temperature effects due to the plasma, and so we now proceed to discuss reheating.

In this dissertation, we consider the case that the energy density is never dominated by the Higgs field so the expansion history of the universe is unaffected by the present of Higgs VEV. Inflaton oscillations dominate until the transition to the radiation dominated era, which occurs when the inflaton decay width is comparable to the Hubble parameter, $\Gamma_I \sim H_{RH}$, which typically occurs after the Higgs field has lost a significant portion of its energy. Consequently, the reheat temperature $T_{RH} \sim \sqrt{\Gamma_I M_{pl}}$, is generally only weakly constrained [26].

For simplicity, we assume coherent oscillations begin instantly at the end of the inflationary epoch, and as a simple model, we assume that the inflaton decays entirely to radiation at a constant rate,

$$\dot{\rho}_r + 4H(t)\rho_r = \Gamma_I \rho_I, \tag{1.52}$$

where

$$\rho_I = \frac{\Lambda_I^4}{a(t)^3} e^{-\Gamma_I t} \tag{1.53}$$

is the energy density of the inflaton field and Λ_I is the energy scale of inflation. The evolution of the Hubble parameter is given by

$$H(t) \equiv \frac{\dot{a}}{a} = \frac{1}{M_{pl}} \sqrt{\frac{\rho_r + \rho_I}{3}}. \tag{1.54}$$

This is a complete system of equations for $a(t)$, $\rho_r(t)$ that may be solved independently of the evolution of the Higgs condensate. Note in this simplified inflation model, Λ_I and Γ_I completely determine the expansion history of the universe after inflation. Throughout this and next chapters, we take $t = 0$ to be the beginning of the coherent oscillation of the inflaton field; during the coherent oscillation epoch, the universe evolves as if it were matter dominated, until the radiation from reheating dominates at $t_{RH} \equiv 1/\Gamma_I$.

Before the reheating is complete ($0 < t < t_{RH}$), one can approximate the scale factor as $a = (1 + t/t')^{2/3}$, and the inflaton energy as

$$\rho_I = \frac{4M_{pl}^2}{3(t+t')^2} = \frac{\Lambda_I^4}{a(t)^3}, \tag{1.55}$$

where

$$t' \equiv \sqrt{\frac{4}{3}} \frac{M_{pl}}{\Lambda_I^2} \tag{1.56}$$

is a characteristic time scale for the relaxation of inflaton. By solving the system of equations (1.52), (1.53), and (1.54) with these approximations, one can find the evolution of the radiation density

$$\rho_r(t) = \frac{2}{5}\sqrt{3} M_{pl} \Gamma_I \Lambda_I^2 a^{-3/2} \left(1 - a^{-5/2}\right) \tag{1.57}$$

$$= \frac{4}{5} M_{pl}^2 \Gamma_I \frac{1}{t + t'} \left[1 - \left(\frac{t'}{t + t'}\right)^{5/3}\right]. \tag{1.58}$$

For $0 < t < t'$, the radiation energy increases linearly as $\rho_r \approx \Gamma_I \Lambda_I^4 t$ while the decay of inflaton energy is negligible $\rho_I \approx \Lambda_I^4$. For $t' < t < t_{RH}$, the energy densities of both radiation and inflaton decrease:

$$\rho_r \approx \frac{4}{5} M_{pl}^2 \frac{\Gamma_I}{t} = \frac{2}{5}\sqrt{3} m_{pl} \Gamma_I \Lambda_I^2 a^{-3/2}, \tag{1.59}$$

$$\rho_I \approx \frac{4}{3} M_{pl}^2 \frac{1}{t^2}. \tag{1.60}$$

The radiation energy density reaches maximum

$$\rho_{r,\,\max} = \left(\frac{3}{8}\right)^{8/5} \sqrt{\frac{4}{3}} M_{pl} \Gamma_I \Lambda_I^2 \cong 0.24\, M_{pl} \Gamma_I \Lambda_I^2 \tag{1.61}$$

at $t_{\max} = \left[(8/3)^{3/5} - 1\right] t' \cong 0.80\, t'$.

During reheating, the effective temperature of the plasma is defined using the radiation density as

$$\rho_r = \frac{g_* \pi^2}{30} T^4, \tag{1.62}$$

where the effectively massless degrees of freedom for $T \gtrsim 300$ GeV is $g_* = 106.75$ in the standard model. The maximum temperature of the plasma during reheating is

$$T_{\max} = \left[\frac{30}{\pi^2 g_*} \left(\frac{3}{8}\right)^{8/5} \sqrt{\frac{4}{3}} M_{pl} \Gamma_I \Lambda_I^2\right]^{1/4} \cong 0.92\, g_*^{-1/4} \left(M_{pl} \Gamma_I \Lambda_I^2\right)^{1/4}. \tag{1.63}$$

For $t \gg t'$, the temperature evolves as

$$T = T_{RH} \left(\frac{t_{RH}}{t}\right)^{1/4} = T_{RH} \left(\frac{a}{a_{RH}}\right)^{3/8}, \tag{1.64}$$

until it reaches the reheat temperature

$$T_{RH} = \left(\frac{24}{\pi^2 g_*}\right)^{1/4} \sqrt{M_{pl}\Gamma_I} \cong 1.25\, g_*^{-1/4} \sqrt{M_{pl}\Gamma_I} \tag{1.65}$$

at t_{RH}. Subsequently, radiation dominates the energy density and the temperature evolves as

$$T = \left(\frac{45}{2\pi^2 g_*}\right)^{1/4} \sqrt{\frac{M_{pl}}{t}}. \tag{1.66}$$

1.3 Evolution of the Higgs VEV

We now turn our attention to the relaxation of the Higgs VEV, which evolves as [27]

$$\ddot{\phi} + 3H\,(t)\,\dot{\phi} + \frac{\partial V_\phi\,[\phi, T(t)]}{\partial \phi} + \Gamma_H \dot{\phi} = 0, \tag{1.67}$$

where $V_\phi(\phi, T)$ is the Higgs effective potential, including modifications from the decays of the condensate [23]. Γ_H describes the effect of the perturbative decay of the condensate. In the first subsection below, we discuss the one-loop corrected potential, including two-loop corrections to the renormalization group equations (RGE). Subsequently, we consider the non-perturbative decay of the Higgs condensate, followed by perturbative decay. Finally, we present a numerical analysis of the evolution of the Higgs condensate.

1.3.1 Effective Potential

The Standard Model Higgs potential computed to a fixed order in perturbation theory is generally gauge-dependent, although the value of the potential at the extrema are not (see, for example, [28, 29]). One can ensure gauge-invariant results by removing the gauge-dependence of the potential using Nielsen identities [30–32]. Here we use the Landau gauge, which has good numerical agreement with the corrected potential [28, 33]. In our analysis, we have used the one-loop corrected potential [34], with running couplings [including two-loop corrections to the renormalization group (RG) equations[2], as given in [9]]. The one-loop

[2]Note the L-loop effective potential improved by $(L+1)$-loop RGE resums all Lth-to-leading logarithm contributions [34–36].

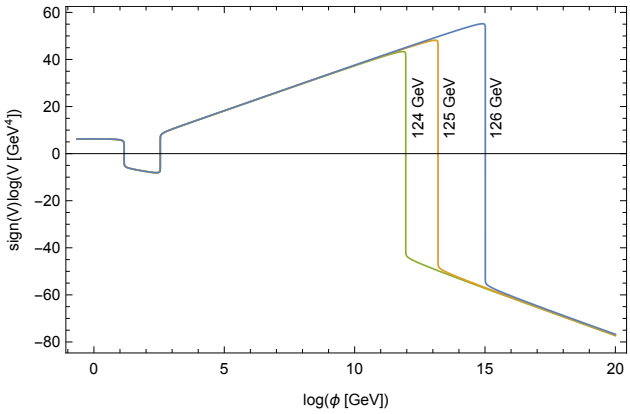

Figure 1.4: The Higgs effective potential at zero temperature including 1-loop contribution and 2-loop corrections to the RGEs. The blue, yellow, and green lines indicate the potential with the Higgs mass $M_h = 126$, 125, and 124 GeV, respectively. The top quark pole mass is taken to be $M_t = 173.07$ GeV.

zero-temperature effective potential is

$$\begin{aligned} V_\phi^{1-\text{loop}} = \frac{1}{2}m_\phi^2\phi^2 + \frac{\lambda}{4}\phi^4 + \frac{1}{(4\pi)^2}\left\{\frac{m_H(\phi)^4}{4}\left[\ln\left(\frac{m_H(\phi)^2}{\mu^2}\right) - \frac{3}{2}\right]\right. \\ + \frac{3m_G(\phi)^4}{4}\left[\ln\left(\frac{m_G(\phi)^2}{\mu^2}\right) - \frac{3}{2}\right] + \frac{3m_W(\phi)^4}{2}\left[\ln\left(\frac{m_W(\phi)^2}{\mu^2}\right) - \frac{5}{6}\right] \\ \left. + \frac{3m_Z(\phi)^4}{4}\left[\ln\left(\frac{m_Z(\phi)^2}{\mu^2}\right) - \frac{5}{6}\right] - 3m_t(\phi)^4\left[\ln\left(\frac{m_t(\phi)^2}{\mu^2}\right) - \frac{3}{2}\right]\right\}, \end{aligned} \tag{1.68}$$

where μ is the renormalization scale and the tree-level masses for the W bosons, Z boson, top quark, Higgs boson, and Goldstone mode are

$$\begin{aligned} m_W^2 = \frac{g^2\phi^2}{4}, \qquad m_Z^2 = \frac{(g^2+g'^2)\phi^2}{4}, \quad m_t = \frac{y_t\phi}{\sqrt{2}}, \\ m_H^2 = m_\phi^2 + 3\lambda\phi^2, \quad m_G^2 = m_\phi^2 + \lambda. \end{aligned} \tag{1.69}$$

Figure 1.4 illustrates this Higgs effective potential at various Higgs mass M_h. Depending on the precise value of M_h, the Planckian vacuum appears at around $\phi \gtrsim 10^{12}$ GeV. Quantum fluctuation during inflation can bring the Higgs field into this Planckian vacuum and end the universe by a big crunch. To preserve the history of our universe, one can introduce higher dimensional operator to completely stabilize the electroweak vacuum as discussed

in Sec. 1.1.4.1 as IC-1. One can also consider the Higgs-inflaton couplings which limit the growth of the Higgs VEV to below this instability scale (IC-2 in Sec. 1.1.4.2). Finally, one can also constrain the inflation scale Λ_I to reduce the resulting quantum fluctuation of the Higgs VEV without any modification to the standard model Higgs potential.

To consider the relaxation of the Higgs field during reheating, one needs to include the thermal corrections to the potential. The one-loop finite temperature contribution to the Higgs potential is [37, 38],

$$\Delta V_T(\phi, T) = -\frac{T^2}{2\pi^2}\left[6m_W^2 J_B\left(\frac{m_W}{T}\right) + 3m_Z^2 J_B\left(\frac{m_Z}{T}\right) + 12m_t^2 J_F\left(\frac{m_t}{T}\right)\right], \tag{1.70}$$

where

$$J_B(y) = \sum_{n=1}^{\infty} \frac{1}{n^2} K_2(ny), \tag{1.71}$$

$$J_F(y) = \sum_{n=1}^{\infty} \frac{(-1)^{n+1}}{n^2} K_2(ny), \tag{1.72}$$

$K_\alpha(x)$ is the modified Bessel function of the second kind, and we have ignored the contributions from Higgs bosons and Goldstone mode, which only dominate when $\phi \lesssim v_{EW}$. We emphasize that we do not use the high temperature expansion, as during reheating the condition $T(t) \gg \phi(t)$ is not satisfied at all times. The renormalization scale μ is taken to be $\sqrt{\phi^2 + T^2}$.

We note that two-loop corrections to the effective potential may be significant at the boundary of the metastability region [9]; however, a self-consistent analysis at two-loop order would include finite temperature effects in the RG equations, which is beyond the scope of this dissertation.

After the Higgs VEV passes through zero, it generally oscillates around its minimum at $\phi = 0$, which remains a minimum for $T \gg v_{EW}$. The amplitude of the oscillation decreases due to Hubble friction term. During this oscillation, the Higgs condensate can then decay perturbatively and non-perturbatively into Standard Model particles. The non-perturbative decay happens much faster than the perturbative decay and is the dominant channel, as pointed out by [23].

1.3.2 Non-Perturbative Decay

The non-perturbative decay of the Higgs field is due to the backreaction of the produced particles. The oscillation of the Higgs field provides a time-dependent mass term for all the coupled particles, which can cause resonant production of the particles. The produced particles then induce an effective mass term to the Higgs condensate as a backreaction; this attenuates the oscillation of the Higgs field until the resonant production is off [23, 39].

The non-perturbative decay channel of Higgs is dominated by $h \to WW, ZZ$. The Lagrangian containing the Standard Model weak gauge fields and the Higgs sector is

$$\mathcal{L} = \frac{1}{2} g^{\mu\nu} \partial_\mu \phi \partial_\nu \phi - V_\phi(\phi, T) + g^{\mu\nu} \left[\frac{1}{4} g^2 W_\mu^+ W_\nu^- + \frac{1}{8} \left(g^2 + g'^2 \right) Z_\mu Z_\nu \right] \phi^2 + \mathcal{L}_{A,\,\mathrm{kin}}, \quad (1.73)$$

where the kinetic terms of the gauge fields can be expanded as

$$\begin{aligned} \mathcal{L}_{A,\,\mathrm{kin}} = & -\frac{1}{2} \left(\nabla_\mu W_\nu^+ - \nabla_\nu W_\mu^+ \right) \left(\nabla^\mu W^{\nu-} - \nabla^\nu W^{\nu-} \right) \\ & - \frac{1}{4} \left(\nabla_\mu Z_\nu - \nabla_\nu Z_\mu \right)^2 + O(g)(\text{non-Abelian terms}). \end{aligned} \quad (1.74)$$

Since the non-Abelian contributions are small at the beginning of the resonant production of W and Z bosons, we ignore those terms [23, 39]. We also work specifically in flat FLRW spacetime, $g_{\mu\nu} = a^2(\tau)\,\eta_{\mu\nu}$, with conformal time $\tau = \int a^{-1} dt$. The resonant production of the weak gauge fields, $A_\mu = W_\mu^\pm$ or Z_μ, in momentum space is then described by

$$A_0\left(\vec{k}, \tau\right) = \frac{-ikA_L'\left(\vec{k}, \tau\right)}{k^2 + a^2 m_A^2(\phi)}, \quad (1.75)$$

$$A_{T,i}'' + \omega_k^2(\phi)\, A_{T,i} = 0, \quad (1.76)$$

and

$$A_L'' + \omega_k^2(\phi)\, A_L + \frac{2k^2}{\omega_k^2(\phi)} \partial_\tau \ln(a m_A)\, A_L' = 0, \quad (1.77)$$

where $\omega_k = \sqrt{k^2 + a^2 m_A^2(\phi)}$ and prime denotes differentiation with respect to conformal time $d\tau$. $\vec{A}_T\left(\vec{k}, t\right)$ and $A_L\left(\vec{k}, t\right)$ are the transverse and longitudinal components of the spatial component $\vec{A}\left(\vec{k}, t\right)$, respectively. The mass term $m_A^2(\phi)$ is given in Eq. (1.69) and

can include the thermal correction by replacing $\phi^2 \to \phi^2 + C_A T^2$ where we use $C_W = 2/3$, and $C_Z < 1$ is determined by diagonalizing the mass matrix [40]. Due to extra friction term in Eq. (1.77) for the longitudinal component A_L, we expect the resonance production of this mode to be suppressed. A_0, which depends only on A_L through Eq. (1.75), should also be suppressed [39]. Hence, we focus on the transverse mode A_T only.

Resonant production of particles can be understood as the amplification of vacuum fluctuations. The number of particles in each mode produced from the vacuum is

$$n_k = \frac{1}{2\omega_k}\left[\left|A'_\mu(\vec{k},\tau)\right|^2 + \omega_k^2\left|A_\mu(\vec{k},\tau)\right|^2\right] - \frac{1}{2}. \tag{1.78}$$

The initial conditions are taken to be the WKB approximation of the vacuum solution,

$$A_T(k,0) = \frac{1}{\sqrt{2\omega_k}}; \quad A'_T(k,0) = -i\sqrt{\frac{\omega_k}{2}}, \tag{1.79}$$

which satisfy $n_k(0) = 0$ and the Wronskian condition $AA'^* - A^*A' = i$.

Fig. 1.5 shows the amplification of the W field, which increases each time the Higgs VEV passes through zero. The number density n_k is shown in Fig. 1.6. It has a sequence of flat steps, which are separated by peaks. Those peaks occur when $\phi = 0$; due to the rapidly changing mass, the number of particles is not well defined at these points. Particle number is well defined only when ϕ reaches a local maxima or minima. We approximate the particle number of A_μ quanta within each oscillation of ϕ by its value when $\dot{\phi} = 0$, which is supported by the flatness of the steps in Fig. 1.6. The resonant production begins once the Higgs VEV starts to oscillate at $\tau \sim 800/\phi_0$. The decrease of n_k at $\tau \sim 2500/\phi_0$ indicates the system has a stochastic resonance, which is a distinctive feature of parametric resonance in an expanding universe [41]. The resonant production then ceases at $\tau \sim 3300/\phi_0$ because the amplitude of ϕ has decreased to the order of T.

If we approximate the oscillation of the Higgs VEV by $\phi(\tau) = \phi_m \cos(\omega_\phi \tau)$, we can write Eq. (1.76) as a Mathieu equation of the form

$$\frac{d^2 A_T}{dz^2} + \left(m^2 + b^2\cos^2 z\right) A_T = 0 \tag{1.80}$$

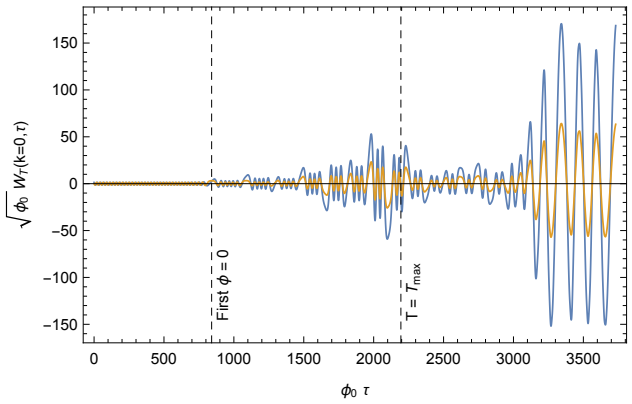

Figure 1.5: Real and imaginary parts (blue and yellow lines) of $W_T(\tau)$ for $k = 0$ for IC-1, with the parameters $\Lambda_I = 10^{15}$ GeV, $\Gamma_I = 10^9$ GeV, $\phi_0 = 10^{15}$ GeV. The Higgs mass is set at $M_h = 126$ GeV, and the top quark mass is $M_t = 173.07$ GeV. The metastable vacuum is produced by the higher dimensional operator $\mathcal{O}_{\phi,10}$ with $\Lambda_{\phi,10} = 6.52 \times 10^{15}$ GeV. The vertical lines designate the first time the Higgs VEV crosses zero, and the time of maximum reheating, from left to right.

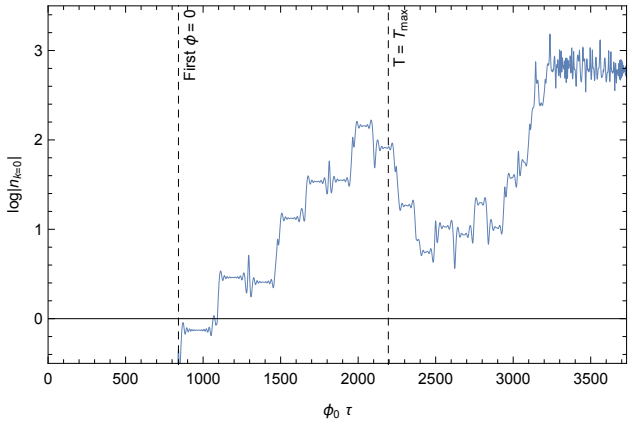

Figure 1.6: $\log[n_k(\tau)]$ for $k = 0$, with the same parameters as Fig. 1.5. Note $n_k(\tau)$ stops increasing at $\tau \sim 3300/\phi_0$ because the amplitude of ϕ has decreased to the order of T. The effective mass of W was then dominated by T instead of ϕ.

where $z = \omega_\phi \tau$, $m^2 \approx \left[k^2 + a^2 m_A^2 \left(\phi = 0, T\right)\right] / \omega_\phi^2$ and $b^2 \approx a^2 m_A^2 \left(\phi_m, T = 0\right) / \omega_\phi^2$. The Mathieu equation has an instability only when $b \gtrsim m^2$. Thus, resonant production is suppressed for

$$k > k_{\rm max} \approx \sqrt{a \omega_\phi m_A \left(\phi_m, 0\right) - a^2 m_A^2 \left(0, T\right)}. \tag{1.81}$$

The produced W and Z fields induce an effective mass for the Higgs field as a backreaction,

$$m_{\phi,W}^2 = -\frac{1}{2} g^2 \left\langle W_\mu^+ W^{\mu -} \right\rangle \tag{1.82}$$

$$m_{\phi,Z}^2 = -\frac{1}{4} \left(g^2 + g'^2\right) \left\langle Z_\mu Z^\mu \right\rangle \tag{1.83}$$

where the expectation value of $A = W$, Z can be approximated as [23, 41]

$$g^{\mu\nu} \left\langle A_\mu A_\nu \right\rangle \cong \frac{-2}{a^2} \left\langle A_T^2 \right\rangle \approx \frac{-1}{\pi^2 a^2} \int_0^\infty \frac{k^2 dk}{\omega_k} n_k. \tag{1.84}$$

In general, the integral in Eq. (1.84) will need to be regularized. However, in our case there is no significant contribution from n_k values with $k \gtrsim k_{\rm max}$, and so the integral is finite. The upper limit can be approximated by $k_{\rm max}$. One can then include the non-perturbative decay of the Higgs by adding the induced mass terms Eqs. (1.82) and (1.83) into the Higgs potential in Eq. (1.67).

Fig. 1.7 shows an example of the Higgs evolution with the non-perturbative decay for the IC-1 scenario (see Sec. 1.1.4.1). The increasing effective masses from W and Z affect the oscillation of Higgs when $m_{\phi,A}^2 \gtrsim T$; these decrease the amplitude of the Higgs oscillation. When the Higgs VEV decreases to $\phi \lesssim T$, the resonant production of W and Z end, because the non-perturbative decay channel is blocked by the large W and Z thermal masses. In this case, one has only to consider perturbative decay channels, discussed in Sec. 1.3.3.

Note the generated W and Z bosons can decay perturbatively into fermions. This decay could in principle obstruct the resonant production of W and Z in the usual Standard Model case [42, 43]. However, in the parameter space that we are interested in, the average decay times of W and Z bosons $\left\langle \Gamma_{W,Z} \right\rangle^{-1}$ are longer than the semiperiod of the Higgs oscillation. Thus, we have ignored the decay of W and Z in our analysis.

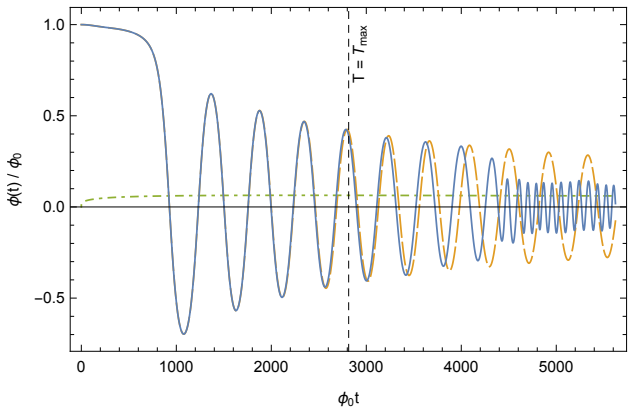

Figure 1.7: Non-perturbative decay of the Higgs condensate for IC-1, with the same parameters as Fig. 1.5. The blue solid (yellow dashed) line corresponds to evolution of the Higgs VEV with (without) non-perturbative decay. The green dash-dotted line corresponds to the temperature of the plasma. The vertical dashed line indicates the time of maximum reheating.

The analysis in this section can be further improved by using a lattice gauge theory [43, 44]. However, as Fig. 1.7 demonstrates, the non-perturbative decay of the Higgs condensate is relevant only after several oscillations, whereas in our later analysis, we will be primarily interested in the cosmological consequence of the first few oscillation of the Higgs VEV.

1.3.3 Perturbative Decay—Thermalization

The perturbative decay of the Higgs condensate is described by the friction term $\Gamma_H \dot{\phi}$ in the equation of motion (1.67). The decay width can be computed through the imaginary part of the self-energy operator

$$\Gamma_H = \frac{\mathrm{Im}\Pi}{m_{\rm eff}}, \tag{1.85}$$

where $m_{\rm eff} = \mathrm{Re}\sqrt{\partial^2 V_\phi(\phi, T)/\partial\phi^2}$ is the effective mass of the Higgs boson. In a finite-temperature thermal background, Γ_H corresponds to the thermalization rate of the Higgs condensate.

Here we consider the fermionic decay channels, motivated by the large top Yukawa coupling. (The dominant bosonic channels, WW and ZZ, are included in the non-perturbative

calculation, which dominates their perturbative contribution.) In the thermal bath of fermions, there are additional excitations which are the removals of antiparticles from the Fermi sea (holes). The dispersion relations for particles and holes are [40, 45, 46]

$$\hat{\omega}_p - \hat{k} - \frac{g_T^2}{\hat{k}} - \frac{g_T^2}{2\hat{k}}\left(1 - \frac{\hat{\omega}_p}{\hat{k}}\right)\ln\left|\frac{\hat{\omega}_p + \hat{k}}{\hat{\omega}_p - \hat{k}}\right| = 0, \tag{1.86}$$

$$\hat{\omega}_h + \hat{k} + \frac{g_T^2}{\hat{k}} - \frac{g_T^2}{2\hat{k}}\left(1 + \frac{\hat{\omega}_h}{\hat{k}}\right)\ln\left|\frac{\hat{\omega}_h + \hat{k}}{\hat{\omega}_h - \hat{k}}\right| = 0, \tag{1.87}$$

where $\hat{\omega}(k) = \omega/T$, $\hat{k} = k/T$, and the subscripts p and h refer to particles and holes respectively. Eq. (1.87) can also be expressed as

$$\hat{\omega}_h = \hat{k}\coth\left(\frac{\hat{k}^2}{g_T^2} + \frac{\hat{k}}{\hat{\omega}_h + \hat{k}}\right), \tag{1.88}$$

which is a convenient form for numerical purposes. We will specify the necessary coefficient g_T below. In these equations, we have made the approximation that the left- and right-handed fermions have the same thermal mass $m(T) = g_T T$; generically, this is not true because they are in different representations of the Standard Model gauge group. However, this difference, which is much smaller than the difference between the particle and hole contributions, is negligible [40].

The dominant fermionic contribution to the thermalization of the Higgs condensate is from the top quark, due to the large top-Higgs Yukawa coupling. The thermal mass of the left-handed top quark is [40]

$$g_{T,t} = \sqrt{\frac{1}{6}g_s^2 + \frac{3M_W^2 + \frac{1}{9}(M_Z^2 - M_W^2) + M_t^2 + M_b^2}{8v_{EW}^2}}, \tag{1.89}$$

where M_i are the physical masses at $T = 0$, and the strong coupling $g_s \cong 1.220$.

The presence of particles and holes in the fermionic plasma provides two thermalization processes for the Higgs condensate. A Higgs boson can decay into a pair of particles or a pair of holes respectively if

$$m_{\text{eff}} = 2\omega_i(k_i); \quad i = p, h \tag{1.90}$$

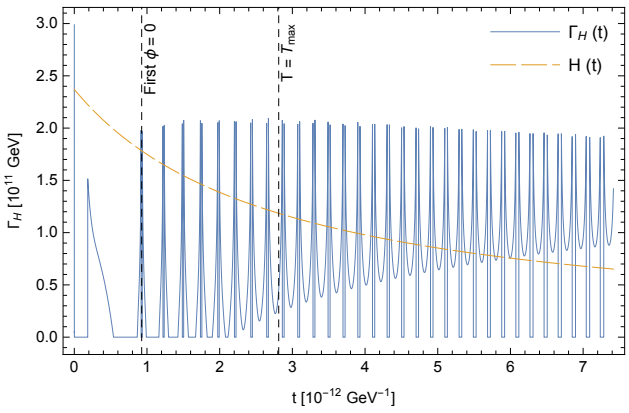

Figure 1.8: Higgs thermalization rate (Γ_H) through the top quark compared with the Hubble parameter for IC-1, with the same parameters as Fig. 1.5. The vertical dashed lines designate the first time the Higgs VEV crosses zero, and the time of maximum reheating, from left to right.

is satisfied. The contribution of each process to the decay width is

$$\frac{\mathrm{Im}\Pi_{\mathrm{dec}}}{T^2} = \frac{y_t^2}{4\pi g_T^4} \sum_{i=p,h} \hat{k}_i^2 \left(\hat{\omega}_i^2 - \hat{k}_i^2\right)^2 (1 - 2n_i)\,, \tag{1.91}$$

where y_t is the top Yukawa coupling, and

$$n_{h,p} = \frac{1}{\exp\left(\hat{\omega}_{h,p}\right) + 1} \tag{1.92}$$

are the fermion distribution functions. Although this decay channel is blocked when $m_\phi < 2\min\left[\omega_h\left(k\right)\right]$, a Higgs boson can also be absorbed by a hole to produce a particle. The contribution of this absorption channel to the width is

$$\frac{\mathrm{Im}\Pi_{\mathrm{abs}}}{T^2} = \frac{y_t^2}{2\pi g_T^4} \sum_i \hat{k}_i^2 \left(\hat{\omega}_p^2 - \hat{k}_i^2\right) \left(\hat{\omega}_h^2 - \hat{k}_i^2\right) (n_h - n_p) \tag{1.93}$$

where the index i sums over the solutions of

$$m_{\mathrm{eff}} + \omega_h\left(k_i\right) = \omega_p\left(k_i\right). \tag{1.94}$$

The total thermalization rate is then the sum of two channels $\mathrm{Im}\Pi = \mathrm{Im}\Pi_{\mathrm{abs}} + \mathrm{Im}\Pi_{\mathrm{dec}}$.

For IC-1, Fig. 1.8 shows the thermalization rate of the Higgs condensate through the top quark compared with the Hubble parameter. We see the thermalization rate is comparable

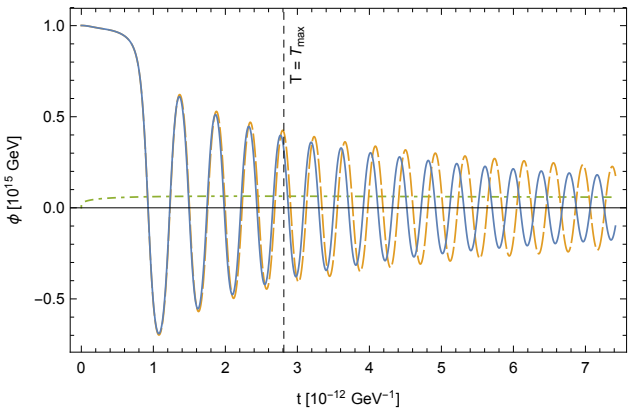

Figure 1.9: Perturvative decay of the Higgs condensate for IC-1 through top quark, with the same parameters as Fig. 1.5. The blue solid (yellow dashed) line corresponds to evolution of the Higgs VEV with (without) the thermalization. The green dash-dotted line corresponds to the temperature of the plasma. The vertical dashed line indicates the time of maximum reheating.

to the Hubble parameter only after the maximum reheating has been reached. Therefore, the evolution of the Higgs VEV is affected only at the later time of reheating as shown in Fig. 1.9.

We have repeated the above analysis with the bottom quark in place of the top quark and verified numerically that its contribution is negligible; we also note that plasma effects can delay thermalization [47]. We also remark that particularly for IC-2, the thermalization rate is frequently much smaller than the Hubble parameter.

1.3.4 Numerical Results

Figures 1.10 and 1.11 illustrate the typical evolution of the Higgs VEV (and temperature) as functions of time for IC-1 and IC-2, respectively. For IC-1, we have used the operator

$$\mathcal{O}_{\phi,10} = \frac{\phi^{10}}{\Lambda_{\phi,10}^{6}} \tag{1.95}$$

with $\Lambda_{\phi,10} = 6.52 \times 10^{15}$ GeV to lift the second minimum generating a metastable vacuum at $\phi = 10^{15}$ GeV (as discussed in Sec. 1.1.4.1). The inflationary parameters are chosen to be

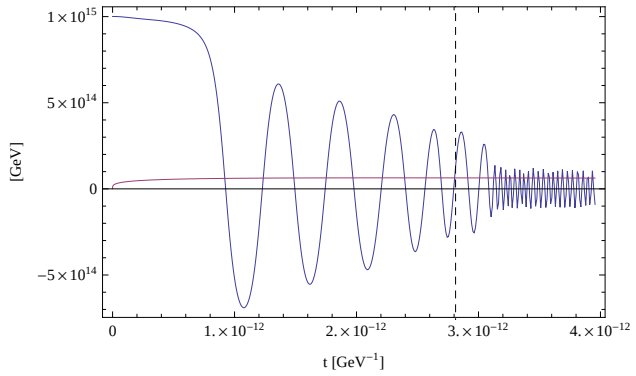

Figure 1.10: The evolution of the Higgs VEV for IC-1 (blue line) and temperature (purple line) as a function of time, with the parameters $\Lambda_I = 10^{15}$ GeV and $\Gamma_I = 10^9$ GeV. This plot includes both the effect of non-perturbative decay and thermalization. The vertical line designate the time of maximum reheating.

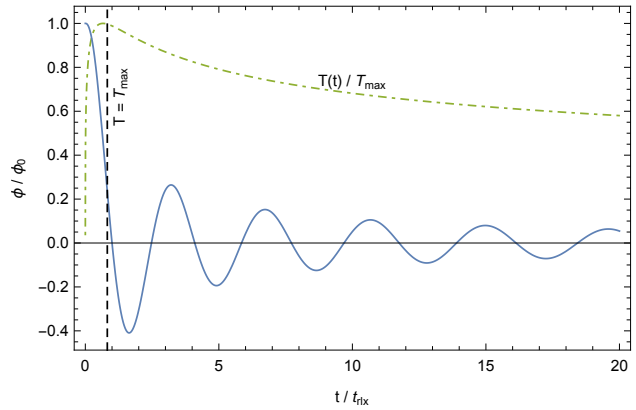

Figure 1.11: The evolution of the Higgs VEV for IC-2 (blue solid line) and temperature (green dash-dotted line) as a function of time, with the parameters $\Lambda_I = 10^{16}$ GeV, $\Gamma_I = 10^9$ GeV, and $N_{\rm last} = 48$. The resulting initial Higgs VEV is $\phi_0 = 2.6 \times 10^{13}$ GeV, and the first time Higgs VEV crosses zero is at $t_{\rm rlx} = 3.4 \times 10^{-14}$ GeV^{-1}. The maximum reheat temperature is $T_{\rm max} = 2 \times 10^{14}$ Gev. This plot includes both the effect of non-perturbative decay and thermalization, although the effect of condensate decay is not appreciable in this case.

$\Lambda_I = 10^{15}$ GeV and $\Gamma_I = 10^9$ GeV in this IC-1 plot. For IC-2, the relevant parameters are $\Lambda_I = 10^{16}$ GeV and $\Gamma_I = 10^9$ GeV, and we have assumed $N_{\text{last}} = 48$ to determine ϕ_0, which does not probe the Planckian vacuum. For both plots, we use 126 GeV and 173.07 GeV for the masses of the Higgs boson and top quark, respectively.

In IC-1 scenario, the initial VEV $\phi_0 = 10^{15}$ GeV is determined by the metastable vacuum generated by the operator (1.95). In IC-2 scenario, though the Higgs VEV is constrained to grow only in the last N_{last} e-folds of inflation, it may still reach a large value if H_I is large; for these inflationary parameters, $H_I = 2.4 \times 10^{13}$ GeV. The initial velocities of the Higgs VEV are set to zero in our analysis.

In scenario IC-1, the Higgs VEV remains approximately constant at short times, until reheating is sufficient to destabilize the second minimum, whereas in IC-2 the field relaxes as soon as the Hubble parameter becomes sufficiently small. Subsequent oscillations have a larger amplitude in the IC-1 scenario; this is due to the difference in Λ_I values, which result in less Hubble friction, and that the additional term (1.95) contributes to the velocity of the VEV.

A notable feature in Fig. 1.10 is that shortly after maximum reheating, the Higgs condensate begins to oscillate more rapidly. This is due to the non-perturbative decay of the Higgs condensate, as illustrated in Fig. 1.7 above. (In the IC-2 scenario, such features are not relevant due to the rapid decay of the amplitude of oscillation.)

We see that both the thermal decay of the condensate and the non-perturbative decay of the condensate have little effect on first approach of the VEV to zero. In the next section, we will introduce a leptogenesis model which generates lepton asymmetry using the relaxation of the Higgs VEV. In this scenario, the lepton asymmetry is produced primarily during the first swing, and therefore, these decay processes have little effect on the total asymmetry generated.

CHAPTER 2

Leptogenesis via the Higgs Condensate Relaxation

As we discussed in the previous chapter, during the inflationary era, the Higgs field may develop a stochastic distribution of vacuum expectation values (VEVs) due to the flatness of its potential [10–12, 14, 15, 21, 23, 48], or it may be trapped in a quasi-stable minimum. In both cases, the Higgs field relaxes to its vacuum state via a coherent motion, during which time the Sakharov conditions [49], necessary for baryogenesis, are satisfied by the time-dependent Higgs condensate and the lepton-number-violating Majorana masses in the neutrino sector. At large VEVs, the Higgs field may be sensitive to physics beyond the Standard Model, which can generate an effective chemical potential which increases the energy of leptons in comparison to antileptons. Through the scattering of neutrinos and Higgs bosons in the plasma produced by the decays of the inflaton, the system can produce a net lepton asymmetry during reheating. The electroweak sphalerons then redistribute this into baryons asymmetry matching the cosmological observations.

In this chapter, we will discuss this Higgs relaxation leptogenesis model in detail. The structure of this chapter is as follows. In the next section, we reexamine the two mechanisms by which the Higgs field can acquire a large vacuum expectation value during inflation. Next, we introduce a higher-dimensional operator, involving only Standard Model fields, which represents new physics at some high energy scale. In Sec. 2.2, we demonstrate that, while the Higgs VEV is in motion, this operator induces an effective chemical potential which distinguishes leptons from antileptons. We derive the resulting Boltzmann equation for lepton number in Sec. 2.4. In Sec. 2.5, we derive the analytical estimation for the resulting asymmetry. Then, we present a numerical analysis covering a variety of initial conditions and scales for new physics, and we identify the allowed parameter space for a successful

leptogenesis.

2.1 Initial Conditions for the Higgs VEV

We begin by motivating our project with the observation that the Higgs field can acquire a large vacuum expectation value (VEV) for a variety of reasons during inflation; therefore, an epoch of post-inflationary Higgs relaxation is a general feature of many cosmological scenarios. In this work we are interested in generating an excess of leptons over antileptons during this epoch.

When we generate the lepton asymmetry during this epoch of Higgs relaxation, we will find that the resulting asymmetry depends on the initial value of the VEV, denoted $\sqrt{\langle\phi^2\rangle} = \phi_0$. During inflation, quantum fluctuations of the Higgs field were ongoing, and therefore different patches of the Universe had slightly different VEVs at the end of inflation. Regions that begin with slightly different ϕ_0 values consequently develop different baryon asymmetries. This produces unacceptably large baryonic isocurvature perturbations [50–54], which are constrained by CMB observations [24]. Therefore, in order to suppress isocurvature perturbations in the late universe, it is necessary to have a small variation in these values.

In this section, we examine the conditions for suppressing the variation between different spacetime regions in the two initial conditions we introduced in Sec. 1.1.4: by trapping the Higgs field in a false vacuum (IC-1), and through quantum fluctuations (IC-2), which are suppressed by a Higgs-inflaton coupling until the later stage of inflation.

The Standard Model Higgs boson has a tree-level potential

$$V(\Phi) = m^2\Phi^\dagger\Phi + \lambda(\Phi^\dagger\Phi)^2, \tag{2.1}$$

where Φ is an SU(2) doublet. The classical field may be written as

$$\Phi = \frac{1}{\sqrt{2}}\begin{pmatrix} 0 \\ e^{i\theta}\phi \end{pmatrix}, \tag{2.2}$$

where $\phi(x)$ is a real scalar field. The parameters m and λ, although constant at tree-level, are modified by both loop and finite temperature corrections as discussed in Sec. 1.3. For the experimentally preferred top quark mass and Higgs boson mass, loop corrections result in a negative running coupling λ at sufficiently large VEVs, with the result that the $\phi = v_{EW} = 246.22$ GeV minimum is metastable at zero temperature [9]. We note, however, that a stable vacuum is possible within current experimental uncertainties [9].

The running of the quartic coupling produces a shallow potential, which has the consequence that that a large VEV develops during inflation due to quantum fluctuations, at least in the regime in which the Standard Model vacuum is stable [23]. We consider this sort of scenario in subsection IC-2 below. Alternatively, the metastability of the electroweak vacuum is frequently possible within the inflationary paradigm [55–57], and the Higgs potential may be sensitive to higher-dimensional operators which lift the second minimum. We consider this scenario in the subsequent subsection.

2.1.1 IC-1: Metastable Vacuum at Large VEVs

As we mentioned in Sec. 1.1.4.1, at the large VEVs, the Higgs potential may be sensitive to the effects of higher-dimensional operators, which can lift the second minimum and consequently stabilize the electroweak vacuum. The Higgs VEV may take an initial large value during inflation, similar to the initial VEV of the inflaton field itself in chaotic inflation models. During inflation, such a VEV evolves towards the false vacuum from above, and then remains trapped in this false vacuum until destabilized by thermal corrections in reheating. Subsequently, the field rolls to the global minimum at $\phi = 0$, until electroweak symmetry is broken at a significantly later time.

In order to lift the second minimum, we consider terms of the form

$$\mathcal{L}_{\text{lift}} = -\frac{\phi^{10}}{\Lambda_{\text{lift}}^{6}}. \tag{2.3}$$

This non-renormalizable operator may be viewed as an effective operator arising from integrating out heavy states in loops.

During inflation, thermal corrections in the supercooled universe are insufficient to destabilize the metastable vacuum. We also ensure that the quantum fluctuations (discussed in detail in the next subsection) do not destabilize the vacuum by requiring that the potential barrier height $\Delta V \gg H_I^4$, where H_I is the Hubble parameter near the end of inflation. In order to suppress the above-mentioned isocurvature perturbations, we will ensure that fluctuations about the false minimum are able to relax back to the minimum, for which it is sufficient to ensure $m_{\text{eff}} \sim \sqrt{d^2V/d\phi^2} > H_I$ in the region probed by quantum fluctuations.

As a specific example, we consider the Higgs potential with one loop corrections [9] with the experimentally preferred values $M_h = 126$ GeV and $M_t = 173.07$ GeV. Taking $\Lambda_{\text{lift}} = 6.52 \times 10^{15}$ GeV gives a metastable minimum near $\phi = 10^{15}$ GeV, with a potential barrier height of $\Delta V \approx 10^{53}$ GeV^4. We will consider $H_I \sim 10^{11}$ GeV; in addition to being insufficient to probe the region beyond the barrier, this is less than the effective mass $m_{\text{eff}} \sim 10^{13}$ GeV in the region probed by quantum fluctuations. Provided that the maximum reheat temperature is greater than $\sim 5 \times 10^{13}$ GeV, thermal corrections during reheating are sufficient to destabilize this vacuum.

2.1.2 IC-2: Quantum Fluctuations

The running coupling constant λ results in a shallow potential, and during inflation, scalar fields with slowly rising potentials generically develop large VEVs. Qualitatively, the scalar field in a de Sitter space can develop a large VEV via quantum effects, such as Hawking-Moss instantons [10, 21] or stochastic growth [11, 14, 15] as we discussed in Chapter 1. The field then relaxes to its equilibrium value via a classical motion, which requires a time

$$\tau_\phi \sim m_{\text{eff}}^{-1} \sim \left(\sqrt{d^2V/d\phi^2}\right)^{-1}. \tag{2.4}$$

If the universe expands sufficiently quickly during inflation, then relaxation is too slow and quantum jumps occur frequently enough to maintain a large VEV. Specifically, large VEVs occur if the Hubble parameter $H_I = \sqrt{8\pi/3}\Lambda_I^2/M_{pl} \gg \tau_\phi^{-1}$. For field values ϕ that satisfy this relation, Hubble friction is sufficient to prevent the system from relaxing to its

equilibrium value $\phi = 0$. Averaged over superhorizon scales, the mean Higgs VEV is such that $V(\phi_I) \sim H_I^4$ [10, 21, 23], provided that this VEV does not probe the second vacuum in the case that the electroweak vacuum is quasistable.

Although the average vacuum expectation value is ϕ_I, there is variation between the VEVs of different horizon-sized patches. Consequently, different patches of the observable universe began with different ϕ_0 values, and as discussed above, this generically results in unacceptably large isocurvature perturbations. However, also as mentioned, the Higgs potential is sensitive to the effects of higher-dimensional operators at large VEVs; here we use such operators to limit the growth of the Higgs VEV to the last several e-folds of inflation. This has the result that the isocurvature perturbations are limited to smaller angular resolution scales than have been experimentally probed. Specifically, in Sec. 1.1.4.2, we introduce one or more couplings between the Higgs and inflaton field of the form

$$\mathcal{L}_{\phi \mathrm{I}} = -c \frac{(\Phi^\dagger \Phi)^{m/2} I^n}{M_{pl}^{m+n-4}}, \tag{2.5}$$

which increases the effective mass of the Higgs field during the early stages of inflation, when $\langle I \rangle$ is large (superplanckian, in the case of chaotic inflation). As explained above, when $\tau_\phi^{-1} \sim m_{\mathrm{eff}}(\phi_I) \sim H_I$ the expansion of the universe is not sufficiently rapid to trap the field at large VEVs. At the end of slow-roll inflation, $\langle I \rangle$ decreases; consequently this term becomes negligible and the Higgs acquires a large vacuum expectation value.

If the Higgs VEV grows during the last N_{last} e-folds of inflation, it reaches the average value

$$\phi_0 = \min\left(\phi_I, \sqrt{N_{\mathrm{last}}} H_I / 2\pi\right). \tag{2.6}$$

Provided $N_{\mathrm{last}} \lesssim 48$, the baryonic isocurvature perturbations develop only on the smallest angular scales which are not yet constrained. (We will examine this condition in detail in Chapter 5.)

We emphasize that operators of the form (2.5) may be viewed as effective operators arising from integrating out heavy states in loops. We note that the change in $\langle I \rangle$ during the slow-roll phase of inflation is model-dependent, and consequently the allowed range of

parameters c, m, and n differs from model to model. This range may be quite narrow, and so this scenario may require some fine-tuning.

As a concrete example, we consider only the term,

$$V_{\rm mix} = \frac{1}{2}\frac{I^{2n}}{M^{2n-2}}\phi^2, \tag{2.7}$$

which induces an effective mass $m_{\rm eff}(\langle I\rangle) = \langle I\rangle^n / M^{n-1}$ for the Higgs field. We define I_1 as the VEV of the inflaton field value at the end of slow roll inflation, and I_2 as the VEV of the inflaton field 48 e-folds before the end of slow roll inflation. To ensure that the Higgs VEV grows only during the last $N_{\rm last}$ e-folds, we must choose parameters such that $m_{\rm eff}(I_2) \approx H_I$. We illustrate this approach with quartic inflation (although this is disfavored observationally; see Ref. [24]). With the inflaton potential $V_I = \lambda_I I^4$, slow roll inflation ends when the inflaton as a vacuum expectation value of $I_1 = m_{pl}/\sqrt{2\pi}$. The number of e-folds during the time in which the inflaton evolves from $\langle I\rangle$ to I_1 is

$$N\left(\langle I\rangle \to I_1\right) = \pi\left(\frac{\langle I\rangle}{m_{pl}}\right)^2 - \frac{1}{2}, \tag{2.8}$$

which gives

$$I_2 = \sqrt{\frac{N_{\rm last} + \frac{1}{2}}{\pi}}\, m_{pl}. \tag{2.9}$$

(Although this field value is superplanckian, this is a feature of quartic inflation which does not necessarily apply to other inflationary models.) The Hubble parameter at this field value is given by

$$H_I^2\left(I_2\right) = \frac{8\pi}{3m_{pl}^2}\lambda_I I_2^4 = \frac{8\pi}{3}\left(\frac{N_{\rm last}+\frac{1}{2}}{\pi}\right)^2 \lambda_I m_{pl}^2. \tag{2.10}$$

The quartic coupling λ_I must be $\lesssim 10^{-13}$ in order to avoid large CMB temperature anisotropies, which gives $M \sim 10^6 m_{pl}$ for $n = 2$ and $M \sim 100\, m_{pl}$ for $n = 4$. In this way, a coupling between the Higgs field and the inflaton field can prevent the Higgs VEV from growing until the last several e-folds of inflation, suppressing the scale of isocurvature perturbations. As this example illustrates, the constraints on the Higgs-inflaton coupling depends on the shape of the inflaton potential. Although we have demonstrated an explicit calculation using a quartic inflationary potential, a similar calculation can be done with other potentials.

Our analysis of the final asymmetry will depend only on the VEV of the Higgs field at the end of inflation, which as noted above is $\phi_0 = \min\left(\phi_I, \sqrt{N_{\rm last}} H_I/2\pi\right)$ provided that the parameters in whatever inflationary model is used are chosen such that the Higgs VEV does not begin to grow until the last $N_{\rm last}$ e-folds of inflation. Therefore, we do not specify a specific inflationary model in our analysis, and we take the inflationary scale Λ_n and the inflaton decay rate Γ_I to be free parameters.

2.2 Effective Chemical Potential

In Sec. 1.1.4, we observed that the Higgs potential may be sensitive to the effects of higher dimensional operators, which are normally suppressed by powers of a high scale. In Sec. 2.1, we have seen how such operators can be used to make a quasistable minimum in the Higgs potential or to suppress the growth of the Higgs VEV until the end stages of inflation. Now, we consider an operator, involving only Standard Model fields, which generates an effective external chemical potential for leptons (and also baryons). This operator is

$$\mathcal{O}_6 = -\frac{1}{\Lambda_n^2}\phi^2 \partial_\mu j^\mu_{B+L}, \tag{2.11}$$

where j^μ_{B+L} is the fermion current of all fermions which carry $\mathrm{SU}(2)_\mathrm{L} \times \mathrm{U}(1)_\mathrm{Y}$ charge. We observe that the zeroth component of (2.11) is the $B + L$ charge density.

We now consider how an operator of this form can be generated. Within the Standard Model itself, one can use quark loops and the CP-violating phase of the CKM matrix [58, 59] to generate an effective operator of the form

$$\mathcal{O}_6 = -\frac{1}{\Lambda_n^2}\phi^2 \left(g^2 W\tilde{W} - g'^2 A\tilde{A}\right), \tag{2.12}$$

where W and A are the $\mathrm{SU}(2)_\mathrm{L}$ and $\mathrm{U}(1)_\mathrm{Y}$ gauge fields respectively. This term is small due to the small Yukawa couplings and small CP-violating phase.

However, a term of the same form can be generated by replacing some or all of the quarks with heavier fermions, which may have larger Yukawa couplings and/or CP-violating phases. The scale in the denominator may be T, due to thermal loops, or the mass scale of

these fermions, M_n [58–61]. In the latter case, it is important that the fermions not acquire masses through the Higgs mechanism; otherwise, the Higgs VEV dependence in this term cancels out. Such fermions may acquire soft masses similarly to higgsinos and gauginos in supersymmetric models.

This operator could be generated in a UV-complete model. As a concrete example, we mention the fully renormalizable Lagrangian

$$\begin{aligned}\mathcal{L}_{hd} = & g\bar{\psi}_{1i}\gamma^\mu\psi_{1i}W_\mu + g'\bar{\psi}_{1i}\gamma^\mu\psi_{1i}A_\mu + y_i e^{i\delta_i}\phi\bar{\psi}_{1i}\psi_2 \\ & + M_{ij}\bar{\psi}_{1i}\psi_{1j} + m\bar{\psi}_2\psi_2 + h.c.,\end{aligned} \tag{2.13}$$

where ψ_{1i} are a set of SU(2) doublets, while ψ_2 is a singlet under both SU(2) and U(1). Despite the explicit mass terms, this Lagrangian is invariant under SU(2) rotations provided that both right and left components of the ψ_{1i} doublets couple vectorially to gauge bosons. The phases of the ψ_{1i} doublets may be fixed by eliminating the phases in the mass matrix. Provided that $i \geq 3$, there are more phases δ_i than can be eliminated by rotating the Higgs field ϕ and the singlet ψ_2. Fermionic loops such as those in [58, 59], which involve sums of the Yukawa couplings $y_i e^{i\delta_i}$ due to insertions of the Higgs VEV $\langle\phi\rangle$ generate an effective operator of the form (2.12). In this case, the scale in the $\mathcal{O}_6$ operator is $\Lambda_n \sim M \sim m$.

Once an effective operator of the form (2.12) is generated, it may be transformed into (2.11) through the electroweak anomaly equation [62]. However, this is only justified if the electroweak sphalerons are in thermal equilibrium [63, 64]. Otherwise, the operator (2.12) involves the Chern-Simons number density, which is not changed by Higgs relaxation unless the phase of the Higgs VEV evolves. At least for slowly evolving Higgs VEVs, the sphaleron transition rate per unit volume at finite temperature is

$$\Gamma_{\rm sp} = k\alpha_W^5 T^4 \exp(-v/2T), \tag{2.14}$$

where the exponential factor accounts for the suppression due to being in the broken phase. As both the Higgs VEV and the temperature are quickly evolving in the scenario considered here, it may be difficult to arrange for the electroweak sphalerons to be in thermal equilibrium. However, additional gauge groups which couple to fermions can contribute to the

anomaly and generate the requisite term, as discussed in Appendix A in [3]. For our purposes, we simply consider a scenario with operator (2.11) without specifying the mechanism by which it is generated.

Returning to equation (2.11), we observe that integrating by parts and dropping an unimportant boundary term gives

$$\mathcal{O}_6 = -\partial_\mu \left(\frac{\phi^2}{\Lambda_n^2} \right) j^\mu_{B+L}. \tag{2.15}$$

In the case where $\Lambda_n = M_n$ a constant [for example, the mass scale of a fermionic loop, as outlined around Eq. (2.13)], this becomes

$$\mathcal{O}_{6,M_n} = -\frac{1}{M_n^2} (\partial_\mu \phi^2) j^\mu_{B+L}. \tag{2.16}$$

If thermal loops generate this term instead, then this becomes

$$\mathcal{O}_{6,T} = -\partial_\mu \left(\frac{\phi^2}{T^2} \right) j^\mu_{B+L} \approx -\frac{1}{T^2} (\partial_\mu \phi^2) j^\mu_{B+L}, \tag{2.17}$$

provided that the temperature is slowly varying on the time scales of the Higgs oscillation. In the IC-1 scenario specifically, the Higgs VEV remains trapped until there is sufficient reheating, which generally ensures that the temperature will be slowly varying during the evolution of the Higgs condensate. Since the Higgs VEV varies only in time, these equations become

$$\mathcal{O}_{6,\Lambda_n} = -\frac{1}{\Lambda_n^2} (\partial_0 \phi^2) j^0_{B+L}. \tag{2.18}$$

For each fermionic species, its contribution to this term can be combined with its kinetic energy term, $\bar{\psi}(i\partial\!\!\!/)\psi$, which is equivalent to the replacement

$$i\partial_0 \to i\partial_0 - (\partial_0 \phi^2)/\Lambda_n^2. \tag{2.19}$$

This effective raises the energy of antiparticles, $E \to E + (\partial_0 \phi^2)/\Lambda_n^2$, while lowering it for particles, $E \to E - (\partial_0 \phi^2)/\Lambda_n^2$. This can be interpreted as an external chemical potential; further remarks along these lines are discussed in Appendix B.1. In the presence of a lepton-number-violating interaction, the system will relax to its equilibrium state, in which the

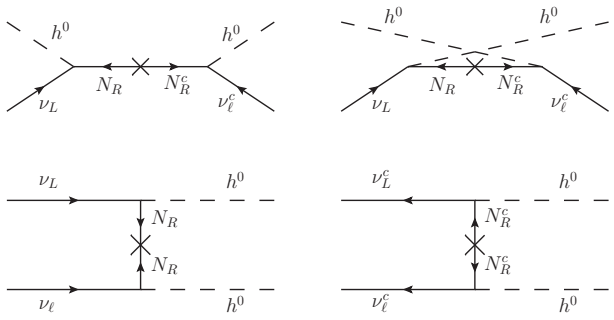

Figure 2.1: Some diagrams that contribute to lepton number violation via exchange of a heavy Majorana neutrino.

number of particles exceeds the number of antiparticles. For future reference, we define the effective external chemical potential,

$$E_0 = \frac{\partial_0 \phi^2}{\Lambda_n^2}. \tag{2.20}$$

As an effective chemical potential, this operator spontaneously breaks not only CP, but in fact, CPT [65]. This operator has been used previously in spontaneous baryogenesis models utilizing gauge [44, 62, 66–68] or gravitational [69] interactions.

2.3 Lepton Number Violating Processes

The universe can relax to its equilibrium state with nonzero lepton and baryon number only if there exists some lepton-number or baryon-number violating process. In order to induce such processes, we consider a minimal extension of the Standard Model with the usual seesaw mass matrix in the neutrino sector [70–73]. In theories with a nonzero Majorana mass, the effective lepton number L is the sum of the lepton numbers of the charged leptons and the helicities of the light neutrinos. This is conserved in the limits $M_R \to \infty$ and $M_R \to 0$, but it is not conserved for a finite M_R. Insertions of the Majorana mass induce lepton-number-violating processes such as those shown in Fig. 2.1.

We further require that the Majorana mass M_R be significantly greater than both the maximum reheat temperature and the initial mass of the Higgs bosons within the condensate

$[m_{\text{eff}}(\phi_0)]$, which suppresses the production of right-handed neutrinos both from thermal production and the decay of the Higgs condensate. Consequently, the contribution from the typical leptogenesis scenario [74] is strongly suppressed.

The lepton-number-violating diagrams shown in Fig. 2.1 necessarily involve the exchange of the heavy right-handed neutrino in order to violate lepton number, and therefore are comparatively suppressed, leading to a naturally small value for the asymmetry.

In order to calculate the thermally averaged cross section $\langle \sigma v \rangle$ for these processes in the early universe, we need to know the number densities of neutrinos and Higgs bosons. These can be produced directly through the decay of the inflaton, or in the thermal plasma through weak interactions, involving weak bosons with masses $m_W \propto \phi(t)$. Generically these weak interactions may be in or out of equilibrium the plasma created by inflaton decay; however, when $\phi(t) \sim 0$, these interactions will be in equilibrium and equilibrate the distributions of charged and neutral leptons. To be concrete, we will use a thermal number density of each of these species. The calculation of the cross section and reaction rate are given in Appendix B.2.

We note that y^2/M_R is set by the mass scale of the left-handed neutrinos, such that

$$\frac{y^2 v_{EW}^2}{2M_R} \approx 0.1 \text{ eV}. \tag{2.21}$$

The cross section found in Appendix B.2 is to a good approximation a function of y^2/M_R only. There is a resonance in the s-channel contribution to the cross section; however, we found numerically that this resonance does not change the result appreciably. This is not unexpected as the energy scale, which is set by the temperature, remains below the right-handed Majorana mass scale at all times.

As we will discuss below, sphaleron processes later convert this lepton charge asymmetry into a baryon asymmetry, as in the typical leptogenesis scenario [74].

2.4 Boltzmann Transport Equation

The reactions discussed in Sec. 2.3 are generally not sufficient to establish equilibrium, due to the suppression from the large Majorana mass. (Recall that we have assumed $\phi_0 \ll M_R$ and $T_{\max} \ll M_R$ in order to suppress the typical leptogenesis mechanism.) The relaxation of the system towards equilibrium can be described by a system of Boltzmann equations, based on detailed balance. The rate of change in the neutrino number density is [75]

$$\begin{aligned}\dot{n}_{\nu_L} + 3Hn_{\nu_L} = -\sum_{\ell=e,\mu,\tau}\Bigg[&\frac{n_{\nu_L}n_{h^0}}{n^{eq}_{\nu_L}n^{eq}_{h^0}}\gamma^{eq}(\nu_L h^0 \to \bar{\nu}_\ell h^0) - \frac{n_{\bar{\nu}_\ell}n_{h^0}}{n^{eq}_{\bar{\nu}_\ell}n^{eq}_{h^0}}\gamma^{eq}(\bar{\nu}_\ell h^0 \to \nu_L h^0)\\ &+ \frac{n_{\nu_L}n_{\nu_\ell}}{n^{eq}_{\nu_L}n^{eq}_{\nu_\ell}}\gamma^{eq}(\nu_L\nu_\ell \to h^0h^0) - \frac{n^2_{h^0}}{n^{eq\,2}_{h^0}}\gamma^{eq}(h^0h^0 \to \nu_L\nu_\ell)\\ &+\frac{n_{\nu_L}n_{\bar{\nu}_\ell}}{n^{eq}_{\nu_L}n^{eq}_{\bar{\nu}_\ell}}\gamma^{eq}(\nu_L\bar{\nu}_\ell \to h^0h^0) - \frac{n^2_{h^0}}{n^{eq\,2}_{h^0}}\gamma^{eq}(h^0h^0 \to \nu_L\bar{\nu}_\ell)\Bigg],\end{aligned} \tag{2.22}$$

where $\gamma^{eq}(A \to B)$ is the equilibrium spacetime rate for the process $A \to B$. We will assume that interactions are sufficiently fast that the Higgs bosons have their equilibrium density, and in equilibrium, the rate for the process $A \to B$ is equal to the rate of $B \to A$. Therefore this simplifies to

$$\begin{aligned}\dot{n}_{\nu_L} + 3Hn_{\nu_L} = -\sum_{\ell=e,\mu,\tau}\Bigg[&\left(\frac{n_{\nu_L}}{n^{eq}_{\nu_L}} - \frac{n_{\bar{\nu}_\ell}}{n^{eq}_{\bar{\nu}_\ell}}\right)\gamma^{eq}(\nu_L h^0 \leftrightarrow \bar{\nu}_\ell h^0) + \left(\frac{n_{\nu_L}n_{\nu_\ell}}{n^{eq}_{\nu_L}n^{eq}_{\nu_\ell}} - 1\right)\gamma^{eq}(\nu_L\nu_\ell \leftrightarrow h^0h^0)\\ &+\left(\frac{n_{\nu_L}n_{\bar{\nu}_\ell}}{n^{eq}_{\nu_L}n^{eq}_{\bar{\nu}_\ell}} - 1\right)\gamma^{eq}(h^0h^0 \leftrightarrow \nu_L\bar{\nu}_\ell)\Bigg],\end{aligned} \tag{2.23}$$

while for antineutrinos we find the similar equation

$$\begin{aligned}\dot{n}_{\bar{\nu}_L} + 3Hn_{\bar{\nu}_L} = -\sum_{\ell=e,\mu,\tau}\Bigg[&\left(\frac{n_{\bar{\nu}_L}}{n^{eq}_{\bar{\nu}_L}} - \frac{n_{\nu_\ell}}{n^{eq}_{\nu_\ell}}\right)\gamma^{eq}(\bar{\nu}_L h^0 \leftrightarrow \nu_\ell h^0) + \left(\frac{n_{\bar{\nu}_L}n_{\bar{\nu}_\ell}}{n^{eq}_{\bar{\nu}_L}n^{eq}_{\bar{\nu}_\ell}} - 1\right)\gamma^{eq}(\bar{\nu}_L\bar{\nu}_\ell \leftrightarrow h^0h^0)\\ &+\left(\frac{n_{\bar{\nu}_L}n_{\nu_\ell}}{n^{eq}_{\bar{\nu}_L}n^{eq}_{\nu_\ell}} - 1\right)\gamma^{eq}(h^0h^0 \leftrightarrow \bar{\nu}_L\nu_\ell)\Bigg].\end{aligned} \tag{2.24}$$

Since we are interested in the order of magnitude of the final asymmetry, we simplify to the case in which there is only a single neutrino species. Subtracting Eq. (2.23) from Eq. (2.24)

gives a Boltzmann-type equation for the difference $n_L = n_{\nu_L} - n_{\bar{\nu}_L}$,

$$\dot{n}_L + 3Hn_L = -2\left(\frac{n_{\nu_L}}{n_{\nu_L}^{eq}} - \frac{n_{\bar{\nu}_L}}{n_{\bar{\nu}_L}^{eq}}\right)\gamma^{eq}(\nu_L h^0 \leftrightarrow \bar{\nu}_L h^0) - \left(\frac{n_{\nu_L}^2}{n_{\nu_L}^{eq\,2}} - 1\right)\gamma^{eq}(\nu_L\nu_L \leftrightarrow h^0 h^0) + \left(\frac{n_{\bar{\nu}_L}^2}{n_{\bar{\nu}_L}^{eq\,2}} - 1\right)\gamma^{eq}(\bar{\nu}_L\bar{\nu}_L \leftrightarrow h^0 h^0). \tag{2.25}$$

The rates $\gamma^{eq}(A \leftrightarrow B)$ refer to the process $A \leftrightarrow B$ in equilibrium, but in the presence of the $\mathcal{O}_6$ operator, which alters the energy of particles and antiparticles. Consequently, these reaction rates are not generally equal to the rates one would find in the absence of the $\mathcal{O}_6$ operator; however, the difference appears at a higher order in E_0/T [63] and so we will neglect it. This has the consequence that the rates for $h^0h^0 \leftrightarrow \nu_L\nu_L$ and $h^0h^0 \leftrightarrow \bar{\nu}_L\bar{\nu}_L$ are equal. We will use the subscript 0 to denote reaction rates calculated without the $\mathcal{O}_6$ operator.

We next substitute $n_{\nu_L}^{eq} = e^{E_0/T} n_0^{eq}$ and $n_{\bar{\nu}_L}^{eq} = e^{-E_0/T} n_0^{eq}$, where $n_0^{eq} = T^3/\pi^2$ is the equilibrium number of left-handed neutrinos (or antineutrinos), when $E_0 = 0$. Expanding the resulting equation to lowest order in E_0/T gives

$$\dot{n}_L + 3Hn_L \approx -\frac{2}{n_0^{eq}}\left(n_L - \frac{E_0}{T}n_L^{\rm tot}\right)\gamma_0^{eq}(\bar{\nu}_L h^0 \leftrightarrow \nu_L h^0) - \frac{1}{n_0^{eq\,2}}\left(n_L^{\rm tot} n_L - \frac{E_0}{T}n_L^{\rm tot\,2}\right)\gamma_0^{eq}(\nu_L\nu_L \leftrightarrow h^0 h^0), \tag{2.26}$$

where we have introduced the notation $n_L^{\rm tot} = n_{\nu_L} + n_{\bar{\nu}_L}$, and we have dropped terms quadratic in the asymmetry (e.g., n_L^2). Approximating $n_L^{\rm tot} \approx 2n_0^{eq}$, the equation becomes

$$\dot{n}_L + 3Hn_L \approx -\frac{2}{n_0^{eq}}\left(n_L - \frac{2E_0}{T}n_0^{eq}\right)\left[\gamma_0^{eq}(\bar{\nu}_L h^0 \leftrightarrow \nu_L h^0) + \gamma_0^{eq}(\nu_L\nu_L \leftrightarrow h^0 h^0)\right], \tag{2.27}$$

$$= -\frac{2}{\pi^2}T^3\left\langle\sigma v\,(T)\right\rangle_0\left(n_L - \frac{2}{\pi^2}T^2 E_0\right), \tag{2.28}$$

where $\langle\sigma v\,(T)\rangle_0$ is the net thermally averaged cross section and its relation to reaction rates are calculated in Appendix B.2. From this equation, we observe that the equilibrium asymmetry is

$$n_{L,eq} = \frac{2E_0}{T}n_0^{eq} = \frac{2}{\pi^2}T^2\frac{\partial_0\phi^2}{\Lambda_n^2}. \tag{2.29}$$

However, the relevant reactions are generally not fast enough to equilibrate to this value before the Higgs VEV approaches zero at $t_{\rm rlx}$. In this work, we solve the differential equation

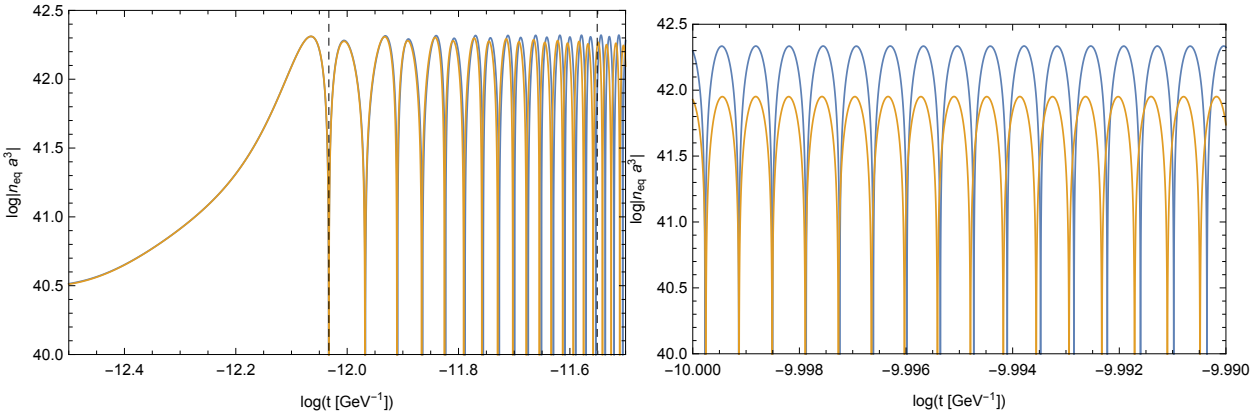

Figure 2.2: The comoving density of equilibrium lepton asymmetry $N_{L,eq} = n_{L,eq}a^3$ for IC-1, with the parameters $\Lambda_I = 10^{15}$ GeV and $\Gamma_I = 10^9$ GeV. Yellow (Blue) line corresponds to the result with (without) the thermalization through the top quark. The left diagram corresponds to times before maximum reheating, whereas the right diagram corresponds to times after maximum reheating.

(2.28) numerically to obtain the final lepton asymmetry. An analytical approximation to the late-time lepton asymmetry will be discussed in the next section.

During subsequent oscillations of the Higgs VEV, the chemical potential changes sign. However, due to the large suppression in the cross section, significant washout can be avoided if the Higgs oscillation amplitude decreases rapidly. This is in contrast to Ref. [67], in which washout was avoided by using coherent oscillations of the inflaton field to modify the sphaleron transition rate.

We note that this is modified by the decay of the Higgs condensate; however, as discussed above, the Higgs condensate does not typically thermalize until after reheating. Fig. 2.2 demonstrates the effect of thermalization on the equilibrium density. However, since the lepton asymmetry will be generated primarily during the first oscillation of the Higgs VEV, the effect of the thermalization of the Higgs condensate is negligible.

2.5 Resulting Asymmetry

In this section, we consider the lepton asymmetry produced by these Higgs-neutrino interactions during the relaxation of the Higgs VEV, as outlined above. We first derive the analytic approximation for the late-time lepton asymmetry, which agrees with the numerical result within one order of magnitude. Next, we analyze the time-evolution of the lepton asymmetry numerically. We present four characteristic examples, covering both IC-1 and IC-2, along with the scale of the $\mathcal{O}_6$ operator Λ_n set to the temperature T (motivated by thermal loops) and a constant M_n (motivated by loops of heavy fermions). In all scenarios, we use the Boltzmann equation (2.28), with the cross sections calculated in Appendix B.2, and the calculation of the Higgs condensate equation of motion presented in Sec. 1.3. We show the time-evolution of the lepton asymmetry in all four scenarios; subsequently, we present an analysis of the parameter space in which a sufficiently large late-time lepton asymmetry can be generated.

2.5.1 Analytical Approximation for the Late-Time Lepton Asymmetry

The Boltzmann equation (2.28) can be analyzed in two regimes: during the relaxation of the Higgs field ($E_0 \neq 0$) and during the subsequent cooling of the Universe ($E_0 \approx 0$). During the relaxation of the Higgs field, when $\mu_0 \propto \partial_0\phi^2 \neq 0$, the Universe produces most of the lepton asymmetry. As we mentioned, this time is generally insufficient for the system to reach equilibrium, and so the asymmetry produced is about $n_{\rm rlx} \simeq n_{L,eq}\left(t_{\rm rlx}\right) \times \frac{2}{\pi^2}\sigma_R T_{\rm rlx}^3 t_{\rm rlx}$, where $t_{\rm rlx}$ is the time period during which the Higgs field relaxes (or the time that the Higgs VEV first crosses zero), and $T_{\rm rlx} = T\left(t_{\rm rlx}\right)$. The equilibrium lepton asymmetry can be approximated by its value at $t_{\rm rlx}$ as

$$n_{L,eq}\left(t_{\rm rlx}\right) \simeq \frac{2}{\pi^2} E_0 T_{\rm rlx}^2 = \frac{2}{\pi^2} T_{\rm rlx}^2 \frac{\partial_0\phi^2}{\Lambda_n^2} \simeq \frac{2}{\pi^2}\frac{T_{\rm rlx}^2}{t_{\rm rlx}}\left(\frac{\phi_0}{\Lambda_n}\right)^2, \tag{2.30}$$

where ϕ_0 is the initial VEV of Higgs, and Λ_n is the new scale in the $\mathcal{O}_6$ operator. From this, we find the approximate lepton number density at $t_{\rm rlx}$ to be

$$n_{L,\,\rm rlx} \simeq \frac{2}{\pi^2}\frac{T_{\rm rlx}^2}{t_{\rm rlx}}\left(\frac{\phi_0}{\Lambda_n}\right)^2 \min\left(1,\, \frac{2}{\pi^2}\sigma_R T_{\rm rlx}^3 t_{\rm rlx}\right) \simeq \frac{4}{\pi^4}\sigma_R T_{\rm rlx}^5\left(\frac{\phi_0}{\Lambda_n}\right)^2, \tag{2.31}$$

where the thermally averaged cross section $\sigma_R = \langle\sigma v\rangle_0$ can be estimated by its value at $T = T_{\rm rlx}$, and is about 10^{-31} GeV^{-2}.

As we discussed in Sec. 1.2, the temperature before and after the reheating completes ($t_{RH} \equiv 1/\Gamma_I$) is given by

$$T(t) \approx \begin{cases} T_{RH}\left(\frac{t_{RH}}{t}\right)^{1/4} & t < t_{RH} \\ \left(\frac{45}{16\pi^3 g_*}\right)^{1/4}\sqrt{\frac{m_{pl}}{t}} & t > t_{RH}. \end{cases} \tag{2.32}$$

Depending on the scenario and the reheating process, the relaxation time of the Higgs can be either $t_{\rm rlx} \approx 6.9/\sqrt{\lambda_{\rm eff}}\phi_0$ if the $\lambda\phi^4$ term dominates the effective potential, or $t_{\rm rlx} \approx t_{RH}\,(7.6/T_{RH}t_{RH})^{4/3}$ if the thermal mass term dominates in IC-2 (see discussion in Appendix D.1). For IC-1, the relxation time is typically determined by the time when thermal correction destabilizes the metastable vacuum.

After the Higgs relaxation is completed at $t_{\rm rlx}$, the generated lepton asymmetry can be partially washed out by heavy neutrino exchanges, until these go out of equilibrium. During washout, Eq. (2.28) can be rewritten as

$$\frac{dN_L(t)}{dt} \simeq -\frac{2}{\pi^2}T^3\sigma_R N_L(t), \tag{2.33}$$

where $N_L \equiv n_L a^3$ is the lepton number per comoving volume. By solving Eq. (2.33) in terms of temperature given in (2.32), one find the following scaling for the lepton number before and after reheating ends (at $T = T_{RH}$ and $t = t_{RH} = 1/\Gamma_I$),

$$\frac{N_L(T)}{N_L(T_0)} = \begin{cases} \exp\left[-\frac{8}{\pi^2}\frac{\sigma_R T_{RH}^4}{\Gamma_I}(T^{-1} - T_0^{-1})\right] & T \text{ and } T_0 \geq T_{RH} \\ \exp\left[-\frac{\sqrt{15}}{\pi^2}\frac{\sigma_R T_{RH}^2}{\Gamma_I}(T_0 - T)\right] & T \text{ and } T_0 \leq T_{RH}. \end{cases} \tag{2.34}$$

The resulting asymptotic value of N_L at low temperature is

$$N_L\left(T\to 0\right)=N_L\left(T_{\rm rlx}\right)\exp\left\{-\frac{\sigma_R T_{RH}^3}{\pi^2\Gamma_I}\left[8\left(1-\frac{T_{RH}}{T_{\rm rlx}}\right)+\sqrt{15}\right]\right\} \tag{2.35}$$

$$\approx N_L\left(T_{\rm rlx}\right)\exp\left(-\frac{8+\sqrt{15}}{\pi^2}\frac{\sigma_R T_{RH}^3}{\Gamma_I}\right) \tag{2.36}$$

for $t_{\rm rlx}<t_{RH}$, and

$$N_L\left(T\to 0\right)=N_L\left(T_{\rm rlx}\right)\exp\left(-\frac{\sqrt{15}}{\pi^2}\frac{\sigma_R T_{RH}^2 T_{\rm rlx}}{\Gamma_I}\right) \tag{2.37}$$

for $t_{\rm rlx}>t_{RH}$, where $N_L\left(T_{\rm rlx}\right)$ can be found using (2.31). We note that depending on the strength of the lepton-number-violating potential, it may be advantageous to arrange for a comparatively rapid decay of the ϕ condensate, so that the oscillation amplitude of the scalar VEV is significantly damped.

The asymmetry is also further diluted by $\left(a_{\rm rlx}/a_{RH}\right)^3\approx\left(t_{\rm rlx}/t_{RH}\right)^2$ for the case that $t_{\rm rlx}<t_{RH}$ due to the entropy production from the decay of inflaton. Thus, at the end of reheating (assuming the oscillation of the scalar field has ended), the Universe obtains the the ratio of the lepton asymmetry to entropy

$$Y_L\equiv\frac{n_L}{s}=\frac{45}{2\pi^2 g_{*S}}\frac{n_L}{T^3} \tag{2.38}$$

$$\simeq\frac{45}{2\pi^2 g_*}\frac{n_{L,\,\rm rlx}}{T_{RH}^3}\frac{N_L\left(T\to 0\right)}{N_L\left(T_{\rm rlx}\right)}\left(\frac{a_{\rm rlx}}{a_{RH}}\right)^3 \tag{2.39}$$

$$\simeq\frac{90}{\pi^6 g_{*S}}\left(\frac{\phi_0}{\Lambda_n}\right)^2\frac{\sigma_R T_{\rm rlx}^5}{T_{RH}^3}\left(\frac{t_{\rm rlx}}{t_{RH}}\right)^2\exp\left(-\frac{8+\sqrt{15}}{\pi^2}\sigma_R T_{RH}^3 t_{RH}\right) \tag{2.40}$$

for $t_{\rm rlx}<t_{RH}$, and

$$Y_L\simeq\frac{45}{2\pi^2 g_*}\frac{n_{L,\,\rm rlx}}{T_{\rm rlx}^3}\frac{N_L\left(T\to 0\right)}{N_L\left(T_{\rm rlx}\right)} \tag{2.41}$$

$$\simeq\frac{90}{\pi^6 g_*}\left(\frac{\phi_0}{\Lambda_n}\right)^2\sigma_R T_{\rm rlx}^2\exp\left(-\frac{\sqrt{15}}{\pi^2}\sigma_R T_{RH}^2 T_{\rm rlx} t_{RH}\right) \tag{2.42}$$

for $t_{\rm rlx}>t_{RH}$. This estimation formula agrees within one order of magnitude with the numerical result.

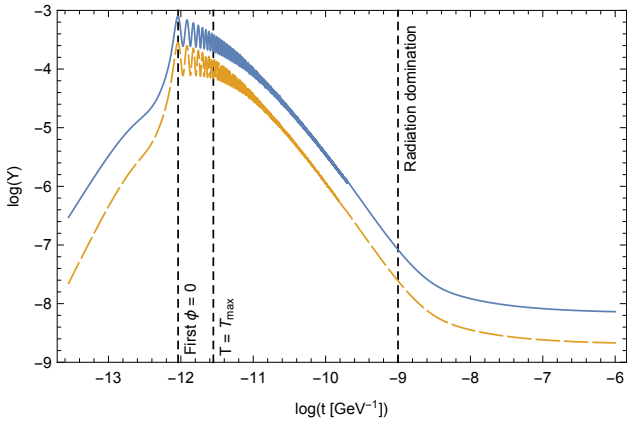

Figure 2.3: Plot of the resulting asymmetry for IC-1, for $\Lambda_n = T$ (blue, solid) and $\Lambda_n = M_n = 10^{14}$ GeV (yellow, dashed). Both scenarios have $\Lambda_I = 10^{15}$ GeV, and $\Gamma_I = 10^9$ GeV. The vertical lines designate the first time the Higgs VEV crosses zero, time of maximum reheating, and the beginning of the radiation dominated era, from left to right. $t = 0$ corresponds to the beginning of inflaton oscillations.

2.5.2 Four Numerical Examples

The precise time-evolution of the lepton asymmetry can be obtained by solving the Boltzmann equation (2.28) numerically. In this subsection, we present the numerical result for the four scenarios mentioned above. First, we consider two scenarios for IC-1 in Fig. 2.3, one with $\Lambda_n = T$ (blue, solid) and one with $\Lambda_n = M_n = 10^{14}$ (yellow, dashed) for the relevant scales in the $\mathcal{O}_6$ operator. Both scenarios have a maximum temperature of 6×10^{13} GeV, since they share the inflationary parameters $\Lambda_I = 10^{15}$ GeV and $\Gamma_I = 10^9$ GeV. As in Fig. 1.10, the initial Higgs VEV is 10^{15} GeV in both cases, which is set by the location of the second minimum in the Higgs potential. Although the asymmetry Y oscillates during the first few oscillations of the Higgs VEV, it relatively quickly settles into a steady state, and approaches a constant value around the beginning of the radiation dominated era. Note that the Higgs field begins to oscillate before the time of maximum reheating.

As mentioned above, the cross section depends primarily on y^2/M_R which is fixed by the light neutrino masses. As mentioned above, we require $T \ll M_R$ in order to suppress

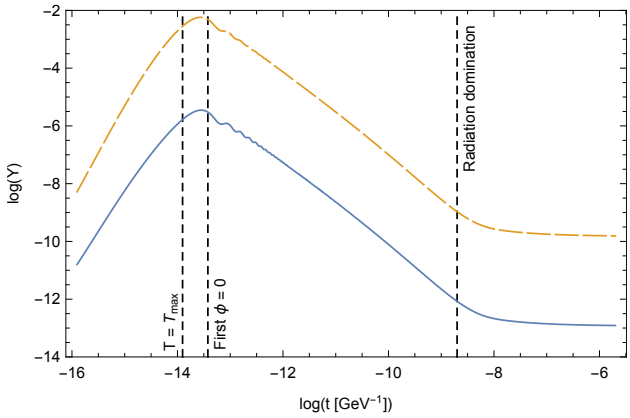

Figure 2.4: Plot of the resulting asymmetry for IC-2, for $\Lambda_n = T$ (blue, solid) and $\Lambda_n = M_n = 5 \times 10^{12}$ GeV (yellow, dashed). Both scenarios have $\Lambda_I = 1.5 \times 10^{16}$ GeV and $\Gamma_I = 5 \times 10^8$ GeV. From left to right, the vertical dashed lines correspond to the time of maximum reheating, the first time the Higgs VEV crosses zero, and the beginning of the radiation dominated era.

the thermal production of right-handed neutrinos; we found that it was sufficient to set $M_R = 6 \times 10^{14}$ GeV, which results in $y \sim 1.5$ using equation (2.21). (This gives $y^2/4\pi \sim 0.16$, within the perturbative regime.)

The late time asymptotic asymmetry is $Y \simeq 10^{-8}$ for $\Lambda_n = T$ and $Y \simeq 10^{-9}$ for $\Lambda_n = M_n = 10^{14}$ GeV; this is expected as the temperature is lower than M_n. We discuss the variation of the final asymmetry over parameter space below.

Next, we present similar results for the IC-2 scenario, again for the two cases $\Lambda_n = T$ (blue, solid) and $\Lambda_n = M_n = 5 \times 10^{12}$ GeV (yellow, dashed). Both plots have the inflationary parameters $\Lambda_I = 1.5 \times 10^{16}$ GeV and $\Gamma_I = 5 \times 10^8$ GeV, which results in a maximum temperature of 2×10^{14} GeV during reheating. We again take $N_{\rm last} = 48$ to determine the Higgs VEV at the end of inflation; this results in $\phi_0 = 6 \times 10^{13}$ GeV for the Higgs VEV as the start of Higgs relaxation. (We emphasize that this choice, with $M_n < \phi_0$ and $M_n < T$, raises questions regarding the use of effective field theory, which we address below.)

In order to suppress the thermal production of right-handed neutrinos, we have taken $M_R = 5T_{\rm max} = 10^{15}$ GeV; in order to produce left-handed neutrino masses on the scale of

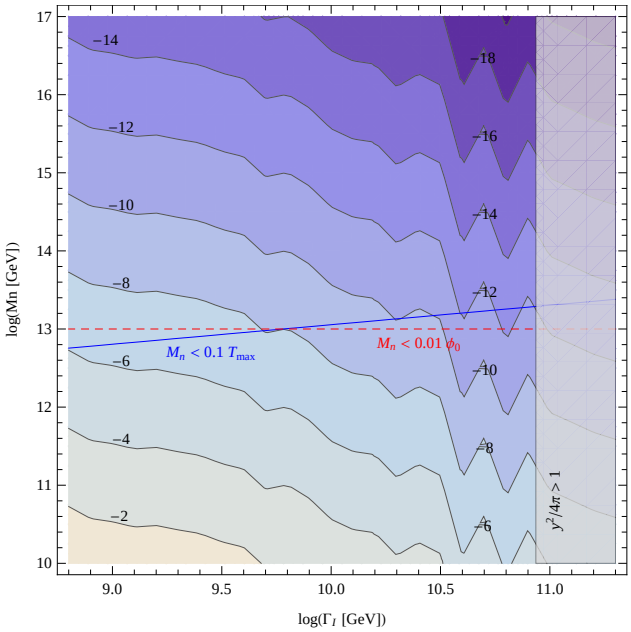

Figure 2.5: The resulting asymmetry ($\log|Y|$) at the end of reheating for IC-1, for $\Lambda_n = M_n$, with $\Lambda_I = 10^{15}$ GeV.

0.1 eV, the neutrino Yukawa coupling must be ~ 1.9. (This gives $y^2/4\pi \approx 0.3$.)

The final asymmetries here are of order 10^{-12} (for $\Lambda_n = T$) and 10^{-10} (for $\Lambda_n = M_n = 5\times10^{12}$ GeV). As M_n is generally smaller than the temperature, it is not surprising that this results in a larger asymmetry. The value for the $\Lambda_n = T$ case is insufficient to account for the observed matter-antimatter asymmetry; this motivates a search of the available parameter space.

2.5.3 Parameter Space

In three of the four scenarios above, the resulting lepton asymmetry is $\mathcal{O}(10^{-10})$ or larger, which is sufficient to explain the observed baryon asymmetry. However, it is interesting to explore the resulting asymmetry as a function of parameter space; results are shown in Figures 2.5, 2.6, 2.7, and 2.8.

As above, we handle the initial conditions with the operator and scale given in 2.1.1 for the IC-1 plots, and as discussed in 2.1.2 with $N_{\rm last} = 48$ for the IC-2 plots. We emphasize again

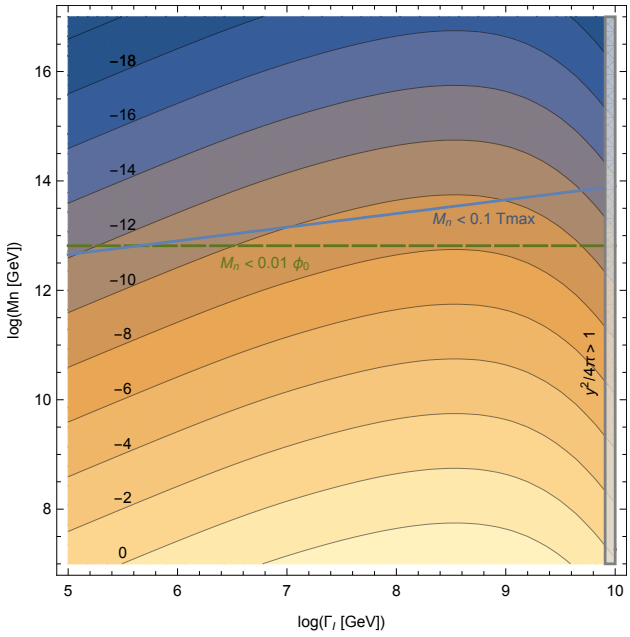

Figure 2.6: The resulting asymmetry ($\log|Y|$) at the end of reheating for IC-2, for $\Lambda_n = M_n$ with $\Lambda_I = 5 \times 10^{16}$ GeV, which gives $\phi_0 = 6.5 \times 10^{14}$ GeV.

that the resulting asymmetry is sensitive to y^2/M_R, which is set by the left-handed neutrino mass scale, and not on the specific value of M_R. However, to suppress thermal production of right-handed neutrinos, we have chosen $M_R = 10T_{\max}$ (for IC-1) and $M_R = 5T_{\max}$ (for IC-2). We have then set the neutrino Yukawa coupling y by the scale of the left-handed neutrino masses [Eq. (2.21)]. We have noted in gray the regions in which the perturbativity condition $y^2/4\pi < 1$ fails.

For the IC-1 plots, the post-inflationary Higgs VEV ϕ_0 is determined entirely by the operator which lifts the second minimum to generate the quasistable vacuum; for the operator and scale in 2.1.1, the Higgs VEV relaxes from $\phi_0 = 10^{15}$ GeV. For IC-2, ϕ_0 is determined by the Hubble parameter during inflation, which is in turn fixed by the energy density in the inflation field [see Eq. (2.6)].

First, we remark on some general features. The asymmetries generated in the IC-2 scenario are smaller than those generated in the IC-1 scenario. This is because in IC-1, the Higgs VEV does not evolve until the temperature is sufficiently large to destabilize the false

vacuum; consequently, the initial evolution of the VEV to zero occurs at higher temperatures. (Compare the vertical lines significantly the first Higgs VEV crossing and maximum reheating in Figures 2.3 and 2.4.) As a result of the higher temperature, the system is driven towards equilibrium at a faster rate [through the Boltzmann equation (2.28)]; furthermore, in the $\Lambda_n = T$ scenario, the larger temperature also means that the equilibrium charge density is larger.

Figs. 2.5 and 2.6 show the lepton asymmetry Y as a function of parameter space, in the case in which the scale of the $\mathcal{O}_6$ operator is a constant $\Lambda_n = M_n$. To reach comparable asymmetries in the IC-2 scenario, we must decrease the scale M_n significantly, such that throughout this plot, $M_n < \phi_0$ and $M_n < T_{\rm max}$. In the IC-1 plot, these conditions fail below the red dashed line and blue solid line respectively. In these regions, the use of effective field theory in generating the operator (2.11) is questionable. An ultraviolet completion of the model is necessary to obtain a reliable description of the dynamics in the regime where the temperature exceeds the scale M_n. We leave such a completion, which would also elucidate the nature of the new physics leading to the appearance of the $\mathcal{O}_6$ operator, for a future work.

We focus on the region of Fig. 2.5 for which the asymmetry Y is larger than 10^{-10} and $M_n > 0.1 T_{\rm max}$. We see that this favors smaller values of Γ_I. However, for a given Λ_I, there is a minimum Γ_I, for which the maximum temperature is insufficient to destabilize the second vacuum. For the parameters considered here ($\Lambda_I = 10^{15}$ GeV and the lift operator given in 2.1.1), this occurs for $\Gamma_I = 6.3 \times 10^8$ (the left boundary of the Fig. 2.5).

Next, we consider the case in which the scale of the $\mathcal{O}_6$ operator is set by the temperature, $\Lambda_n = T$, in Figs. 2.7 and 2.8. This parameter space has one fewer parameters, and so we allow Λ_I to also vary, which changes the Hubble parameter during inflation. For IC-2, increasing H_I results in a larger value of ϕ_0, as described by Eq. (2.6), which increases the resulting asymmetry. This also increases the temperature scale, resulting in a larger asymmetry, as is evident in both figures. (We also note that for IC-1, we must take care that quantum fluctuations during inflation do not destabilize the second vacuum; this is shown in orange

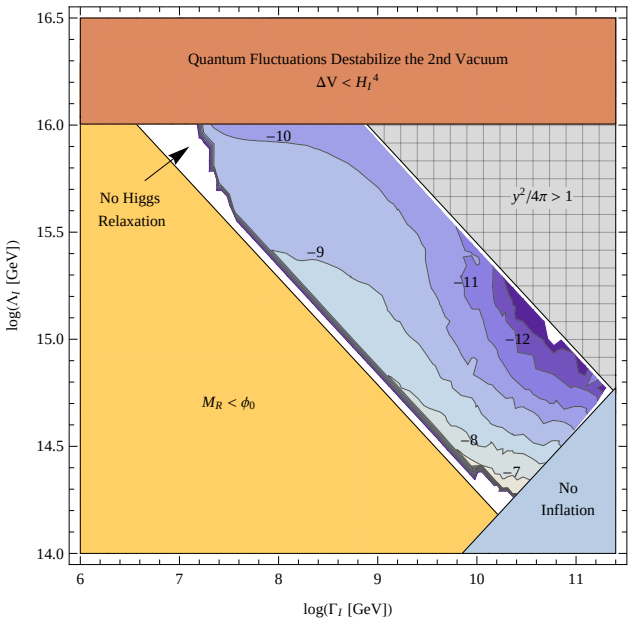

Figure 2.7: The resulting asymmetry ($\log|Y|$) at the end of reheating for IC-1, for $\Lambda_n = T$.

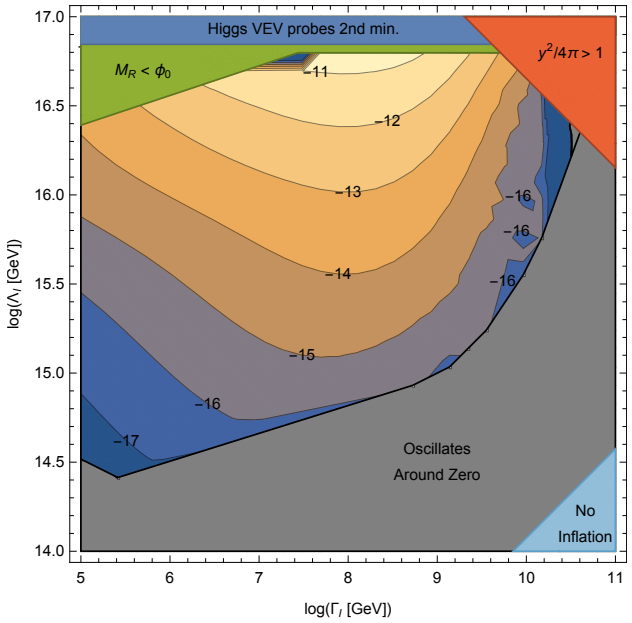

Figure 2.8: The resulting asymmetry ($\log|Y|$) at the end of reheating for IC-2, for $\Lambda_n = T$.

in Fig. 2.7.)

As mentioned above, if the reheat temperature is sufficiently small, thermal corrections are unable to destabilize the second vacuum, and therefore this is no relaxation of the Higgs VEV. This region is denoted in white in Fig. 2.7. Furthermore, in the region in which $M_R < \phi_0$, right-handed neutrinos can be copiously produced by the decay of the Higgs condensate, which is not desirable (as concerns the lepton asymmetry production scenario presented here); this region is denoted in yellow in Fig. 2.7 and green in Fig. 2.8. Furthermore, if Λ_I is too small such that $\Gamma_I > 3H_I$, the inflation period of the universe doesn't start; this region is shown in light blue on both figures.

In IC-2, there is a further concern that the Higgs VEV can probe the second, deeper minimum at large VEVs. This may not be a phenomenological problem [76], but would require a refinement of the analysis presented here. (Alternatively, $N_{\rm last}$ could be decreased, such that ϕ_0 remains below the instability scale.) This region is shown in dark blue in Fig. 2.8. Also, in the gray region of Fig. 2.8, washout is sufficiently large to cause the lepton asymmetry to oscillate around zero at the end of our numerical analysis; the final value will be quite small.

We see that for IC-1, it is possible to find parameter space in which a sufficiently large asymmetry is generated, but this is not possible for IC-2. For IC-1, smaller Γ_I values are favored (and consequently, slower reheating), as for constant Λ_n.

2.5.4 Converting the Lepton Asymmetry into a Baryon Asymmetry

Thus far, we have analyzed the production of the lepton asymmetry; here we discuss how this is converted into a baryon asymmetry. This process has produced a net density of $(B - L)$ charge, which is unchanged once these processes are negligible. However, the $(B + L)$ $U(1)$ symmetry is anomalous, and electroweak sphalerons will redistribute the excess between

leptons and baryons[1] as in standard leptogenesis [74], at a rate per unit volume

$$\Gamma_{\rm sp} \sim (\alpha_W T)^4 \exp\left[-g_W \phi(t)/T\right]. \tag{2.43}$$

At small vacuum expectation values, the B and L densities approach their equilibrium values, $n_B = (28/79) n_{B-L}$. This produces a baryon asymmetry of about the same order of magnitude as the lepton asymmetry found above. Consequently, the regions of parameter space that generate $Y \gtrsim 10^{-10}$ in the analysis above give a final baryon asymmetry matching the observed value of $\mathcal{O}(10^{-10})$.

2.6 Conclusions for Chapter 2

In this chapter, we introduced a novel leptogenesis possibility in which the lepton asymmetry is as a consequence of an effective chemical potential induced by the post-inflationary relaxation of the Higgs field. Although right-handed neutrinos participate in the lepton-number-violating interactions as a mediator, this is different from the typical leptogenesis scenario in which the asymmetry is produced via the decay of right-handed neutrinos. Even though the heavy right-handed neutrino suppresses the cross section which produces the asymmetry, we have shown parameters for which a sufficiently large the asymmetry is generated.

We have derived the relevant Boltzmann equation which governs lepton number, and we have computed the tree-level scattering cross section between Higgs bosons and neutrinos which violates the lepton number in the thermal plasma. Furthermore, we have considered the evolution of the lepton asymmetry for four combinations of producing the large Higgs VEV during inflation (IC-1 and IC-2) and the scale of the $\mathcal{O}_6$ operator (a fermion mass scale M_n and the temperature T); we then presented an analysis of the asymmetry as a function of parameter space. We demonstrated regions which produces a baryonic asymmetry that meets or exceeds observational limits.

[1] Since the electroweak sphalerons violates $B + L$ while conserving $B - L$, to produce positive B through sphaleron processes, the initial lepton asymmetry actually needs to be negative.

We note that in this work we consider an asymmetry produced via the scattering of neutrinos and Higgs bosons in the plasma produced by the decays of the inflaton, and therefore this scenario requires a relatively fast reheating. This is in contrast to Ref. [3], which similarly considered the same $\mathcal{O}_6$ operator but produced the matter asymmetry via the decay of the Higgs condensate.

While we present the relaxation leptogenesis via the standard model Higgs field, one can also extend this framework to other scalar fields. It has been observed that the axion field can undergo a similar post-inflationary relaxation, and provide a possible scenario for relaxation leptogenesis [77, 78]. In the following sections of this thesis, we will discus two leptogenesis models based on this similar idea.

CHAPTER 3

Baryogenesis via Elementary Goldstone Higgs Relaxation

In this chapter, we extend the relaxation mechanism to the Elementary Goldstone Higgs framework. Besides studying the allowed parameter space of the theory we add the minimal ingredients needed for the framework to be phenomenologically viable. The very nature of the extended Higgs sector allows to consider very flat scalar potential directions along which the relaxation mechanism can be implemented. This fact translates into wider regions of applicability of the relaxation mechanism when compared to the Standard Model Higgs case.

Our results show that, if the electroweak scale is not fundamental but radiatively generated, it is possible to generate the observed matter-antimatter asymmetry via the relaxation mechanism. This chapter is based on Ref. [4], joint work done with Helene Gertov, Lauren Pearce, and Francesco Sannino.

3.1 Introduction

The discovery of the Higgs boson crowns the Standard Model (SM) of particle interactions as one of the most successful description of physical phenomena below or at around the electroweak (EW) scale. However, several puzzles remain unexplained such as the nature of dark matter, neutrino masses and mixing as well as the cosmological matter-antimatter asymmetry of the universe. Solutions to any of these puzzles generically requires introduction of new physics beyond the SM.

Here we focus our attention on the important cosmological mystery of how the observable

universe came to be dominated by an excess of matter over antimatter. The necessary conditions for baryogenesis are well-known [49] and several models of baryogenesis exist (for a review, see e.g. [79]). Among these, an appealing scenario involves the relaxation of a scalar or pseudo scalar field in the post-inflationary universe. Such fields can acquire large vacuum expectation values due to flat potentials [10–12] or by being trapped in a quasi-stable minimum. After inflation, such fields relax to their equilibrium values via a coherent motion, and higher dimensional operators can couple the time-dependent condensate to baryon and/or lepton number [62, 65]. This can be done with the Higgs field [1–3] or an axion field [78, 80]. Similar models have been constructed using quintessence fields [81, 82] and MSSM flat directions [77, 83, 84]. A novel feature of the Higgs scenario is that the chemical potential depends on the time-derivative of the VEV-squared, which as we discuss, resolves some difficulties with producing an asymmetry of the correct sign throughout the observable universe. An additional advantage of this scenario is that it makes use of fields whose existence is either known or well-motivated.

However, the SM Higgs sector is far from established and could hide new exciting physics. In fact, several alternative paradigms have been put forward that are not only as successful as the SM in reproducing the experimental results, but also can simultaneously address some of the remaining experimental puzzles.

The Elementary Goldstone Higgs (EGH) paradigm established in [85, 86] allows one to disentangle the vacuum expectation of the *e*lementary Higgs sector from the EW scale [85]. Here the Higgs sector symmetry is larger than the minimally required symmetry needed to spontaneously break the EW gauge symmetry. Furthermore, the physical Higgs emerges as a pseudo Nambu Goldstone Boson (pNGB). A welcome feature is that once the SM gauge and fermion sectors are embedded in the larger symmetry, one discovers that calculable radiative corrections automatically induce the proper breaking of the EW symmetry by naturally aligning the vacuum in the pNGB Higgs direction. In this way the EW scale is not fundamental but radiatively induced[1]. The template Higgs sector leading to the

[1]The EGH setup is profoundly different from the composite (Goldstone) Higgs scenario [87–89]. The main differences being: i) the elementary case is amenable to perturbation theory; ii) it is straightforward

SU(4) $\to$ Sp(4) pattern of chiral symmetry breaking was first introduced in [91–93].

In this work, we successfully marry the EGH paradigm and the relaxation leptogenesis scenario [1, 2]. There are at least two motivations for this marriage: first, we observe that in a model such as the EGH scenario, which has an extended scalar sector, there are naturally new scalar-field directions along which one can implement the relaxation mechanism; secondly, the relative freedom in the overall potential flatness translates into a wider region of applicability of the approximations and effective theory used to derive successful baryogenesis (as compared to the SM Higgs case).

The structure of this chapter is as follows: we begin by reviewing the EGH model, as introduced in [85, 86], with particular emphasis on the scalar sector and the Yukawa sector. We then review the Higgs relaxation scenario, focusing on the modifications necessary due to the extended Higgs sector. Finally, we present an analysis of the available parameter space in which Higgs relaxation leptogenesis occurs when marrying it to the EGH paradigm.

Although we use a specific template to perform our analysis, the general results and features are expected to hold for generic realizations of successful baryogenesis via EGH driven leptogensis scenarios.

3.2 Elementary Goldstone Higgs: A Brief Review

The EGH scenario [85, 86] necessarily extends the SM Higgs sector symmetry. A working template uses a linear realization with SU(4) symmetry breaking spontaneously to Sp(4). The SM Higgs doublet is now part of the SU(4)/Sp(4) coset, while the EW symmetry, $\mathrm{SU}(2)_L \times \mathrm{U}(1)_Y$, is embedded in SU(4).

The relaxation leptogenesis mechanism [1–3] uses the scalar sector of the theory at very high energies. We therefore start by reviewing the scalar sector of the theory.

The SM Higgs boson is identified with one of the Goldstone bosons which acquires mass

to endow the SM fermions with mass terms; iii) it is possible to immediately consider Grand Unified Theory extensions [90].

via a slight vacuum misalignment mechanism induced by quantum corrections. The misalignment is due mostly to top-induced quantum corrections [85, 86] and therefore we will neglect here the EW gauge sector corrections.

The most general vacuum structure of the theory can be parametrised by an angle $0 \leq \theta \leq \pi/2$ [85] and

$$E_\theta = \cos\theta\, E_B + \sin\theta\, E_H = -E_\theta^T\,, \tag{3.1}$$

where the two independent vacuum directions E_B and E_H are

$$E_B = \begin{pmatrix} i\sigma_2 & 0 \\ 0 & -i\sigma_2 \end{pmatrix}, \quad E_H = \begin{pmatrix} 0 & 1 \\ -1 & 0 \end{pmatrix}. \tag{3.2}$$

The alignment angle θ is determined by radiative corrections after having constrained the model to reproduce the experimental results. It was found in [86] that the model naturally prefers small values of θ, privileging a pNGB nature of the Higgs.

We note that because SU(4) is broken radiatively through corrections from top and gauge interactions, the strength of SU(4) breaking increases at higher scales. Therefore, there is no high scale in which it is appropriate to neglect SU(4) breaking.

3.2.1 Scalar and Fermionic Sector

In the minimal scenario described above, the scalar sector is codified by

$$M = \left[\frac{1}{2}\left(\sigma + i\,\Theta\right) + \sqrt{2}\left(\Pi_i + i\,\tilde{\Pi}_i\right) X_\theta^i\right] E_\theta\,, \tag{3.3}$$

where X_θ^i $(i = 1, \ldots, 5)$ are the broken generators associated to the breaking of SU(4) to Sp(4), reported in Appendix A of [86], and the five Π_i are the five Goldtone bosons of the theory, where after symmetry breaking, the first three become the longitudinal components of the gauge bosons, the fourth is the observed Higgs, and the last is a dark matter candidate. The full SU(4) invariant (tree-level) scalar potential can be found in [86].

Having introduced the scalar sector of the model, we turn our attention to the fermionic sector. Our focus here is two-fold: first, we have explained above how the top-sector is

responsible for setting θ, and therefore indirectly affects the vacuum and the scalar sector more generally, and secondly, the leptogenesis scenario produces the asymmetry through the excess production of neutrinos, which involves electroweak interactions between fermions.

We construct the Yukawa sector of the theory by introducing EW gauge invariant operators that explicitly break the SU(4) global symmetry and correctly reproduce the SM fermion masses and mixing. First, we formally accommodate each one of the SM fermion families in the fundamental representation of SU(4), namely

$$\mathbf{L}_\alpha = \left(L, \quad \tilde{\nu}, \quad \tilde{\ell}\right)^T_{\alpha L} \sim \mathbf{4}, \qquad \mathbf{Q}_i = \left(Q, \quad \tilde{q}^u, \quad \tilde{q}^d\right)^T_{i\,L} \sim \mathbf{4}, \tag{3.4}$$

where $\alpha = e, \mu, \tau$ and $i = 1, 2, 3$ are generation indices and the tilde indicates the charge conjugate fields of the Right Handed (RH) fermions, that is, for instance, $\tilde{\nu}_{\alpha L} \equiv (\nu_{\alpha R})^c$, $\tilde{\ell}_{\alpha L} \equiv (\ell_{\alpha R})^c$, $L_{\alpha L} \equiv (\nu_{\alpha L}, \ell_{\alpha L})^T$ and similarly for the quark fields. Notice that a RH neutrino $\nu_{\alpha R}$ for each family must be introduced in order to define $\mathbf{L}_\alpha$ which transforms according to the fundamental irrepresentation of SU(4).

Given the embedding of quarks and leptons in SU(4), we now construct a Yukawa mass term for the SM fermions. For this we make use of SU(4) spurion fields [94] P_a and $\overline{P}_a$, where $a = 1, 2$ is an $\mathrm{SU}(2)_L$ index. They transform as ${}^{(}\overline{P}^{)}_a \to (u^\dagger)^T {}^{(}\overline{P}^{)}_a\, u^\dagger$, with $u \in \mathrm{SU}(4)$. We have

$$P_1 = \frac{1}{\sqrt{2}} \begin{pmatrix} \mathbf{0}_2 & \tau_3 \\ -\tau_3 & \mathbf{0}_2 \end{pmatrix}, \quad P_2 = \frac{1}{\sqrt{2}} \begin{pmatrix} \mathbf{0}_2 & \tau^- \\ -\tau^+ & \mathbf{0}_2 \end{pmatrix}, \tag{3.5}$$

$$\overline{P}_1 = \frac{1}{\sqrt{2}} \begin{pmatrix} \mathbf{0}_2 & \tau^+ \\ -\tau^- & \mathbf{0}_2 \end{pmatrix}, \quad \overline{P}_2 = \frac{1}{\sqrt{2}} \begin{pmatrix} \mathbf{0}_2 & \overline{\tau}_3 \\ -\overline{\tau}_3 & \mathbf{0}_2 \end{pmatrix}, \tag{3.6}$$

with

$$\tau^\pm = \frac{\sigma_1 \pm i\,\sigma_2}{2}, \; \tau_3 = \frac{\mathbf{1}_2 + \sigma_3}{2}, \quad \text{and} \quad \overline{\tau}_3 = \frac{\mathbf{1}_2 - \sigma_3}{2}\,. \tag{3.7}$$

Then, using $P_{1,2}$ and $\overline{P}_{1,2}$, we may write Yukawa couplings for the SM fermions which

preserve the $SU(2)_L$ gauge symmetry:

$$\begin{aligned} -\mathcal{L}^{\text{Yukawa}} &= \frac{Y^u_{ij}}{\sqrt{2}} \left(\mathbf{Q}_i^T\, P_a\, \mathbf{Q}_j\right)^\dagger \text{Tr}\left[P_a\, M\right] + \frac{Y^d_{ij}}{\sqrt{2}} \left(\mathbf{Q}_i^T\, \overline{P}_a\, \mathbf{Q}_j\right)^\dagger \text{Tr}\left[\overline{P}_a\, M\right] \\ &+ \frac{Y^\nu_{\alpha\beta}}{\sqrt{2}} \left(\mathbf{L}_\alpha^T\, P_a\, \mathbf{L}_\beta\right)^\dagger \text{Tr}\left[P_a\, M\right] + \frac{Y^\ell_{\alpha\beta}}{\sqrt{2}} \left(\mathbf{L}_\alpha^T\, \overline{P}_a\, \mathbf{L}_\beta\right)^\dagger \text{Tr}\left[\overline{P}_a\, M\right] + \text{h.c.} \end{aligned} \tag{3.8}$$

with the Yukawa matrices of quarks and leptons chosen in agreement with experimental measurements. This Lagrangian explicitly breaks the SU(4) global symmetry mentioned above, and therefore, it also contributes fixing the parameter θ which interpolates between the otherwise equivalent vacuum structures. In fact, in terms of the SM quark and lepton fields, Eq. (3.8) can be written as

$$\begin{aligned} -\mathcal{L}^{\text{Yukawa}} &= Y^u_{ij} \left(Q_{iL}\, \tilde{q}^u_{jL}\right)^\dagger_a \text{Tr}\left[P_a\, M\right] + Y^d_{ij} \left(Q_{iL}\, \tilde{q}^d_{jL}\right)^\dagger_a \text{Tr}\left[\overline{P}_a\, M\right] \\ &+ Y^\nu_{\alpha\beta} \left(L_{\alpha L}\, \tilde{\nu}_{\beta L}\right)^\dagger_a \text{Tr}\left[P_a\, M\right] + Y^\ell_{\alpha\beta} \left(L_{\alpha L}\, \tilde{\ell}_{\beta L}\right)^\dagger_a \text{Tr}\left[\overline{P}_a\, M\right] + \text{h.c.} \end{aligned} \tag{3.9}$$

where

$$\text{Tr}\left[P_1 M\right] = \frac{-1}{\sqrt{2}} \left(\sigma \sin\theta + \Pi_4 \cos\theta + i\Theta \sin\theta - i\tilde{\Pi}_4 \cos\theta + i\Pi_3 + \tilde{\Pi}_3\right), \tag{3.10}$$

$$\text{Tr}\left[P_2 M\right] = \frac{1}{\sqrt{2}} \left(i\Pi_1 + \Pi_2 + \tilde{\Pi}_1 - i\tilde{\Pi}_2\right). \tag{3.11}$$

Therefore, after EW symmetry breaking, the SM fermions acquire the masses

$$m_F = y_F \frac{f \sin\theta}{\sqrt{2}}\,, \tag{3.12}$$

with $f = \langle\sigma\rangle$ at low energies and y_F being the SM Yukawa coupling of quarks and leptons in the fermion mass basis. Comparing this expression with the corresponding SM prediction $m_{F,SM} = \frac{y_F}{\sqrt{2}} v_{EW}$ we see that f and θ must satisfy the phenomenological constraint

$$f \sin\theta \;=\; v_{EW} \;\simeq\; 246 \text{ GeV}\,. \tag{3.13}$$

Notice that a Dirac mass for neutrinos is generated as well. Ref. [86] also investigated the parameter space at low energy and found that (when keeping the masses of the scalars below five TeV) the most frequent value for f is $\overline{f} \;=\; 13.9^{+2.9}_{-2.1}$ TeV corresponding to $\overline{\theta} \;=\; 0.018^{+0.004}_{-0.003}$. Although these are the most common values that give the appropriate

electroweak phenomenology, the points of parameter space which satisfy the electroweak constraints vary significantly in values for f and $\sin(\theta)$. This is because there are quite a few couplings in the SU(4) potential. To generate an acceptable electroweak phenomenology at values of f and $\sin(\theta)$ significantly different than these, it is likely necessary to fine-tune at least some of the parameters in the SU(4) potential.

This model does not naturally generate a Majorana mass term for the RH neutrino fields; however, one can be explicitly added. This provides an explicit breaking of the SU(4) symmetry, but preserves the EW gauge group and gives the standard seesaw mechanism. Although this is not strictly speaking necessary for the EGH boson model, we include it in our analysis here. This is because a successful leptogenesis model must involve lepton-number violating terms, and following [1–3], we will make use of the neutrino-sector Majorana mass term.

In this case, the most general mass Lagrangian for the leptons is

$$-\mathcal{L}^{\text{lep}} = Y^{\ell}_{\alpha\beta}\,\frac{f\sin\theta}{\sqrt{2}}\;\bar{\ell}_{\alpha L}\ell_{\beta R} + Y^{\nu}_{\alpha j}\frac{f\sin\theta}{\sqrt{2}}\;\overline{\nu}_{\alpha L}\nu_{jR} + \frac{1}{2}\,(M_R)_{jk}\,\overline{\nu}_{jR}\,(\nu_{kR})^c \;+\; \text{h.c.} \tag{3.14}$$

where M_R is the Majorana mass term of the three RH neutrinos. The couplings in Eq. (3.14) allow to generate at tree-level a Majorana mass term for the LH neutrinos, in a manner similar to the standard type I seesaw extension of the SM [70, 72, 73, 95]. This yields

$$\mathcal{L}^{\nu}_{\text{mass}} \;=\; -\frac{1}{2}\,(m_\nu)_{\alpha\beta}\;\overline{\nu}_{\alpha L}\,(\nu_{\beta L})^c \;+\; \text{h.c.} \tag{3.15}$$

with

$$m_\nu \;=\; -m_D\,M_R^{-1}\,m_D^T \quad \text{and} \quad m_D \;=\; Y^\nu\,\frac{f\sin\theta}{\sqrt{2}} \;=\; Y^\nu\,\frac{v_{EW}}{\sqrt{2}}\,. \tag{3.16}$$

One can hope that this Majorana mass term would be generated by embedding the EGH model into a larger model, perhaps a Grand Unified Theory.

3.2.2 Radiative Corrections

Next we return our attention to the scalar sector. The one-loop correction $\delta V(\Phi)$ to the scalar potential takes the general expression

$$\delta V(\Phi) = \frac{1}{64\pi^2}\mathrm{Str}\left[\mathcal{M}^4(\Phi)\left(\log\frac{\mathcal{M}^2(\Phi)}{\mu^2} - C\right)\right] \tag{3.17}$$

where in this case $\Phi \equiv (\sigma,\, \Pi_4)$ denotes the background scalar fields that we expect to lead to the correct vacuum alignment of the theory and $\mathcal{M}(\Phi)$ is the corresponding tree-level mass matrix. The supertrace, Str, is defined as

$$\mathrm{Str} = \sum_{\text{scalars}} -2\sum_{\text{fermions}} +3\sum_{\text{vectors}} . \tag{3.18}$$

We have $C = 3/2$ for scalars and fermions and $C = 5/6$ for the gauge bosons, and μ_0 is a reference renormalization scale. As explained above, the Yukawa sector terms explicitly break the global SU(4) symmetry and gauge interactions will also provide explicit symmetry breaking. This explicit breaking will generate a nonzero mass term for the Goldstone bosons at the quantum level and a mass mixing term between the Π_4 and the σ fields.

At very high energy scales the background-dependent masses of all the scalars are the same, namely, $m \approx \sqrt{\lambda}\sigma$, where λ is a linear combination of several quartic couplings. The renormalization scale is fixed as a constant at the energy scale of inflation. Taking only the top and scalar corrections into account, the one-loop corrections to the potential take the simple form

$$\delta V \;=\; \frac{\sigma^4}{64\pi^2}\left[7\lambda^2\left(\log\frac{\lambda\sigma^2}{\mu^2} - \frac{2}{3}\right) - 3y_t^4\sin^4\theta\left(\log\frac{y_t^2\sin^2\theta\sigma^2}{2\mu^2} - \frac{3}{2}\right)\right]. \tag{3.19}$$

in the direction of σ. Thus the effective potential to one-loop order can be written as

$$V(\sigma) = \frac{\lambda_{\text{eff}}(\sigma)}{4}\sigma^4 \tag{3.20}$$

where the effective quartic coupling is

$$\lambda_{\text{eff}}(\sigma) = \lambda + \frac{4}{64\pi^2}\left[7\lambda^2\left(\log\left(\frac{\lambda\sigma^2}{\mu^2}\right) - \frac{3}{2}\right) - 3y_t^4\sin^4\theta\left(\log\left(\frac{y_t^2\sin^2\theta\sigma^2}{2\mu^2}\right) - \frac{3}{2}\right)\right] . \tag{3.21}$$

Here y_t is the top quark Yukawa and λ is not yet experimentally constrained. At lower energy, the one-loop potential is more involved and a detailed analysis of the one-loop potential at low energy can be found in [86]. In that paper the authors found that for θ around 0.018 and λ around 0.007 there is a region of parameter space with the most "EW-favorable points", but that it is by no means required for good EW behavior for theta and lambda to take these values. In this work we will be primarily interested in the high energy regime since the scalar field will acquire a comparatively large vacuum expectation value. Below, we will find that in order to produce a baryon asymmetry of the appropriate size, it is desirable to have a small coupling λ_{eff}. In order to ensure the stability of the potential at large σ, it may be necessary to tune both λ and θ to be small, by choosing the parameters in the SU(4) potential appropriately. This is not a problem since, unlike in the SM, λ_{eff} is not set by the observed Higgs mass because of the enlarged scalar sector.

3.2.3 The Physical Higgs

For maximum clarity, we here pause to identify the physical Higgs boson states. At low energy there is a mass mixing between the σ and the Π_4 fields as mentioned earlier. The mass eigenstates of this mixing are the two Higgs particles, h and H, given by

$$\begin{pmatrix} \sigma \\ \Pi_4 \end{pmatrix} = \begin{pmatrix} \cos\alpha & -\sin\alpha \\ \sin\alpha & \cos\alpha \end{pmatrix} \begin{pmatrix} h \\ H \end{pmatrix}, \tag{3.22}$$

where α is the scalar mixing angle, chosen in the interval $[0, \pi/2]$. The observed Higgs boson will be the lightest eigenstate with a mass

$$m_h = 125.7 \pm 0.4 \text{ GeV} \tag{3.23}$$

which in [86] was found that α is preferred to be very close to $\pi/2$; that is, the observed Higgs is mostly a pNGB.

As noted, though, at high energies these states are nearly degenerate in mass.

3.3 Relaxation-Leptogenesis Framework

Having introduced the EGH model, with particular attention to the scalar and fermionic sectors, we now introduce the Higgs relaxation leptogenesis framework, which has been explored in the SM context in [1–3].

We outline the important steps of relaxation leptogenesis as follows: First, we need a scalar (or pseudo-scalar) field with a large vacuum expectation value (VEV). This can occur through quantum fluctuations during inflation, or the field may be trapped in a quasi-stable minimum. Afterwards, the field relaxes to its equilibrium value.

During this relaxation, a chemical potential for lepton number may be induced via higher dimensional operators. This lowers the energy of leptons and raises the energy of antileptons. Lepton-number-violating processes, such as those mediated by the neutrino Majorana masses introduced above, produce an excess of leptons over antileptons. These interactions can occur within the particle plasma produced during reheating [1, 2], or during the decay of the Higgs condensate itself [3]. Here we focus on the first scenario as an illustrative example.

While we specifically consider the scalar sector here (which is of the most interest due to the extended scalar sector in the EGH model), we acknowledge that similar considerations apply to axion-like degrees of freedom, which have been explored in [78, 80].

In our previous realisations of Higgs-relaxation leptogenesis, the relaxing field was identified with the SM Higgs, although we allowed for a modified potential at high scales. The recent observation of the Higgs boson at the LHC sets the quartic coupling, although it is significantly modified at large scales (as described by the renormalization group equations) [9]. However, the EGH model has additional freedom as can be seen in Eq. (3.21). We will show below that in order to generate the observed baryonic asymmetry, while remaining in the regime in which certain approximations are valid, the quartic coupling must be significantly smaller than the value preferred in the SM. This is not phenomenologically problematic in the EGH scenario because the extended Higgs sector allows for additional flat directions.

3.3.1 Large Initial Vacuum Expectation Value (VEV) of σ

As we mentioned above, during inflation, scalar fields may acquire large vacuum expectation values (VEVs) through quantum fluctuations: because relaxation via a coherent motion is a classical process, its time-scale may be significantly longer than those typical of quantum fluctuations (see [10–12]). Concretely, quantum fluctuations occur on a scale such that $V(\sigma_I) \sim H_I^4$ where $\sigma_I = \sqrt{\langle\sigma^2\rangle}$ is the scalar field vacuum expectation value and $H_I \equiv \sqrt{8\pi/3}\Lambda_I^2/m_{pl}$ is the Hubble parameter during inflation. The VEV rolls down classically to its minimum with the characteristic time scale

$$\tau_{\rm roll} \sim 1/m_{\sigma,\rm eff} \sim \left[\frac{d^2V(\sigma)}{d\sigma^2}\right]^{-1/2}. \tag{3.24}$$

However, if $\tau_{\rm roll} \gg H_I^{-1}$, there is insufficient time between quantum fluctuations for the generated field VEV to roll down. In this case, the scalar field would develop a large VEV $\sim \sigma_I$ during inflation.

An alternative scenario for starting with a large scalar vacuum expectation value is that the scalar field may be trapped in a quasi-stable minimum in the early universe; this is particularly well-motivated in scenarios in which the initial scalar VEVs are distributed stochastically (provided the scalar potential does, indeed, have a high-scale quasi-stable minimum).

The SM potential provides motivation for both scenarios: recent measurements of the Higgs mass suggest a rather flat potential, before turning over (and potentially becoming negative) [9]. The flat potential makes it easier for quantum fluctuations to generate a large VEV in the early universe; on the other hand, if the potential does turn over, higher-dimensional operators can stabilize the potential in such a way as to produce a quasi-stable minimum.

Here, though, we are interested in the EGH model, which has a different potential shape. As noted, the physical Higgs boson h and H are mixtures of the σ and Π_4 degrees of freedom, although there is an approximate rotational symmetry at high energies. We will consider the case in which the field σ acquires a large VEV during inflation within the effective potential

given in Eq. (3.20). In fact at high energies σ can be seen as simply the modulus of the scalar field and therefore it would not matter which direction one selects. Furthermore, as already explained, the effective quartic potential in this case is not fixed at low energies, because the mass of the pNGB Higgs emerges radiatively via top corrections and there are no sufficient experimental constraints yet to fix this overall coupling.

Next, we address an issue which affects all relaxation leptogenesis models, which is discussed in more detail in [1, 2]. Namely, in both ways of generating large scalar VEVs, different patches of the Universe generically have different values of σ_I at the end of inflation. If the lepton asymmetry is linked to the initial VEV of σ, each patch of the Universe could have a different final asymmetry. This would result in unacceptably large baryonic isocurvature perturbations [50–54], which are constrained by the cosmic microwave background (CMB) observations [24, 25].

One solution to this problem, which was proposed in [1], is to couple the Higgs sector to the inflaton in such a way as to suppress the growth of the VEV until the end of slow-roll inflation. The resulting isocurvature perturbations are then on scales smaller than those which have been experimentally probed. In the EGH model, we adapt this solution by coupling the σ field to the inflaton I via operators of the form

$$\mathcal{L}_{\sigma I} = c\frac{I^n}{m_{pl}^{m+n-4}}\mathrm{Tr}\left[M^+M\right]^{m/2}. \tag{3.25}$$

Such a non-renormalizable operator can be generated by integrating out heavy states in loops; we can envision that these states arise by heavy SU(4)-preserving multiplets which arise when the EGH model is embedded into larger (perhaps grand unified) models. In the early stages of inflation, the VEV of the inflaton $\langle I\rangle$ can be large (superplanckian) and gives a large effective mass $m_{\sigma,\mathrm{eff}}\left(\langle I\rangle\right)$ to σ; this suppresses the quantum fluctuations of the σ field. In the later stages of inflation, $\langle I\rangle$ decreases to a value such that $m_{\sigma,\mathrm{eff}}\left(\langle I\rangle\right) \ll H_I$, allowing a large VEV for σ to develop. If the development of the VEV occurs during the last N_{last} e-folds of inflation, the VEV reaches the average value

$$\sigma_0 = \min\left(\sigma_I,\ \frac{H_I}{2\pi}\sqrt{N_{\mathrm{last}}}\right). \tag{3.26}$$

The resulting isocurvature perturbations appear only at the smallest angular scales, and are not yet constrained for $N_{\rm last} \lesssim 8$.

While other solutions to this isocurvature problem were noted in [1], we consider this one as an illustrative example which also allows the most freedom in parameter space.

3.3.2 Relaxation of the σ Field

When the inflation is over, the inflaton begins oscillating coherently as it decays; consequently, the universe behaves as if it is matter dominates. During this epoch, the σ field also relaxes from its starting value of σ_0 and oscillates around $\sigma = 0$ (the minimum of Eq. (3.20)) with diminishing amplitude. The equation of motion for $\sigma(t)$ (where by an abuse of notation we use $\sigma(t)$ for the VEV of the σ field) is

$$\ddot{\sigma} + 3H(t)\,\dot{\sigma} + \frac{dV(\sigma)}{d\sigma} = 0. \tag{3.27}$$

The Hubble parameter $H(t)$ is determined by the system of differential equations

$$H(t) \equiv \frac{\dot{a}}{a} = \sqrt{\frac{8\pi}{3m_{pl}^2}(\rho_r + \rho_I)}, \tag{3.28}$$

$$\dot{\rho_r} + 4H(t)\,\rho_r = \Gamma_I \rho_I, \tag{3.29}$$

where Γ_I is the decay rate of inflaton, and $\rho_I = \Lambda_I^4 e^{-\Gamma_I t}/a(t)^3$ and $\rho_r = (g_*\pi^2/30)\,T^4$ are the energy densities of the inflaton field and the produced radiation respectively. We ensure that the energy density of the σ condensate never dominates the universe, so as to preserve that standard cosmological picture. Note that the maximum temperature during reheating and the reheat temperature can be estimated as [96] $T_{\rm max} \approx 0.618\,(\Lambda_I^2\,\Gamma_I\,m_{pl}/g_*)^{1/4}$ and [27] $T_{RH} \simeq (3/\pi^3 g_*)^{1/4}\sqrt{\Gamma_I m_{pl}}$, respectively.

3.3.3 Effective Chemical Potential

We consider the following couplings between the lepton current and the σ field

$$\mathcal{L}_6 = -\frac{1}{M_n^2}{\rm Tr}\left[M^+M\right]\partial_\mu j_B^\mu = -\frac{1}{M_n^2}\sigma^2\partial_\mu j_B^\mu, \tag{3.30}$$

where M_n is a potentially new scale. This coupling does not break SU(4) symmetry, and is therefore consistent with the EGH picture. As this is a higher-dimensional operator, it may be generated by integrating out heavy states; one obvious method is to expand the minimal EGH model introduced above with heavy RH states that couple to a gauge boson anomaly, as discussed in some detail in [2]. Other possibilities for generating this operator, unique to EGH models, may exist. We note that, to generate this effective operator, CP-violation is necessary [58, 59].

While this operator preserves SU(4), when the scalar VEV is evolving it breaks CPT; in fact, it is similar in form to the one considered in spontaneous baryogenesis scenarios [62, 65]. An integration by parts gives

$$\mathcal{L}_6 = \frac{1}{M_n^2} \left(\partial_\mu \sigma^2\right) j_L^\mu. \tag{3.31}$$

For a patch of the Universe where the σ field is approximately spatially homogeneous, the operator becomes

$$\mathcal{L}_6 = \frac{1}{M_n^2} \left(\partial_0 \sigma^2\right) j_L^0. \tag{3.32}$$

When σ is decreasing, this operator effectively raises the energy of antiparticles, while lowering it for particles. Within the equation of motion for the fermions, this term plays a role similar to that of an effective external chemical potential

$$\mu_0 = -\frac{\partial_0 \sigma^2}{M_n^2}. \tag{3.33}$$

In the presence of lepton-number-violating processes, the system will favor the production of particles over antiparticles.

We emphasize that because the operator (3.30) depends on the VEV squared, a positive lepton number is produced everywhere as the Higgs field relaxes. This is in contrast to many spontaneous baryogenesis models in which the effective chemical potential depends on $\partial_0 S$ (where S is the scalar VEV), and in which the sign of the asymmetry depends on the initial sign of the VEV. Consequently, in this model it is not necessary for the observable universe to be enclosed within a single patch of constant σ; instead we need only satisfy the isocurvature constraints mentioned above. (We also note that the spatial variation in the field does not contribute to the charge asymmetry.)

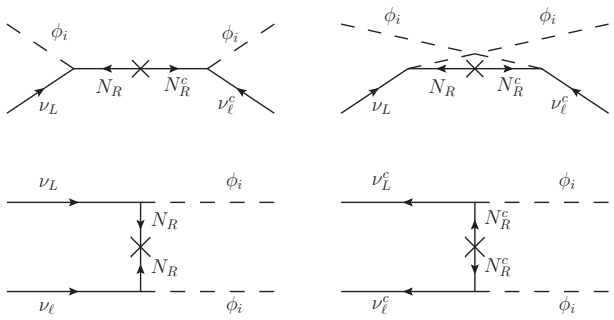

Figure 3.1: Some diagrams that contribute to lepton number violation via exchange of a heavy Majorana neutrino, where ϕ_i can be Π_4, Θ, $\tilde{\Pi}_4$, Π_3, $\tilde{\Pi}_3$, or σ, depending on which fields are in thermal equilibrium.

3.3.4 Lepton Number Violating Processes

This chemical potential alone will not yield any lepton asymmetry; successful leptogenesis additionally requires some lepton-number-violating process. This was addressed above when we introduced Majorana masses in the neutrino sector. Therefore, we consider the standard seesaw mass matrix in Eq. (3.14) for neutrinos (which requires a small breaking of SU(4), as discussed in [86]). The L violating processes are (i) a left-handed neutrino converting into an anti-left-handed neutrino through exchange of a heavy Majorana neutrino; (ii) pair production or annihilation of neutrinos or antineutrinos. These processes are shown in the diagram in Fig. 3.1.

With the introduction of the neutrino Majorana mass, several leptogenesis mechanisms become possible within the EGH model, beyond the Higgs relaxation leptogenesis considered here. These include thermal leptogenesis [74, 75], resonant leptogenesis [97, 98], and ARS-type leptogenesis [99]. We consider a regime of parameter space in which these leptogenesis mechanisms are insufficient to generate the observed baryon asymmetry, but the asymmetry produced through the Higgs relaxation mechanism can account for the observed asymmetry. In particular, we consider large Majorana mass M_R; in the Higgs relaxation mechanism, the smallness of the Majorana mass can be counteracted by a large $\partial_t \sigma^2$. We also do not arrange the neutrino sector parameters so as to have resonant production of neutrinos.

The thermally averaged cross section of these processes $\langle \sigma v \rangle_0$ can be found in [2]. This calculation can be easily extended to the EGH case, which will be discussed in Appendix C. Due to the additional scalar fields that participate in these processes, the cross section is enhanced by a factor of 16 if all scalar fields are in thermal equilibrium,

$$\langle \sigma v \rangle_0 = 16 \left[\langle \sigma \left(\nu_L \phi \leftrightarrow \bar{\nu}_L \phi \right) v \rangle_0 + \langle \sigma \left(\nu_L \nu_L \leftrightarrow \phi \phi \right) v \rangle_0 \right], \tag{3.34}$$

where ϕ stands for a scalar field that couples to ν_L with the Yukawa coupling Y^ν. We emphasize that all processes which violate lepton number contribute to producing the asymmetry in the presence of the nonzero chemical potential. If heavier, weakly-interacting fields such as the σ and the Θ are not in thermal equilibrium, then the cross section is scaled by $\left[1 - \sin^2(\theta)/2\right]^2 \approx 1$.

For the $\nu_L \phi \leftrightarrow \bar{\nu}_L \phi$ process, the s-channel process has a resonance at $E \sim M_R$, which is generally ineffective because, in order to suppress standard leptogenesis, we ensure that M_R is well above the energy scales probed by the VEV (and also above the reheat temperature). The center-of-mass cross section is

$$\begin{aligned} \sigma_{CM} \left(\nu_L \phi \leftrightarrow \bar{\nu}_L \phi \right) = \frac{1}{16\pi} \frac{|Y^\nu|^4}{4} \left(M_R^2 + \frac{\Gamma_R}{4} \right) \int_{-s}^{0} dt \, (s+t) \\ \times \left[\frac{1}{A^2 + C^2} + \frac{1}{B^2 + C^2} + \frac{2(AB + C^2)}{(AB + C^2)^2 + C^2 (A - B)^2} \right] \end{aligned} \tag{3.35}$$

where

$$\begin{aligned} A &= s - M_R^2 + \Gamma_R^2/4, \\ B &= t - M_R^2 + \Gamma_R^2/4, \\ C &= \Gamma_R M_R, \end{aligned} \tag{3.36}$$

and the decay rate of the RH neutrino is approximated by $\Gamma_R \approx |Y^\nu|^2 M_R / 16\pi$. The thermally averaged cross section for massless particles to the CM cross section can be obtained as [100]

$$\langle \sigma v \rangle_0 = \frac{1}{32 T^5} \int_0^\infty ds \, s^{3/2} K_1(\sqrt{s}/T) \sigma_{CM}(s). \tag{3.37}$$

For the $\nu_L\nu_L \leftrightarrow \phi\phi$ process, the thermally averaged cross section can be approximated as

$$\langle \sigma \left(\nu_L\nu_L \leftrightarrow \phi\phi\right) v \rangle_0 \approx \frac{|Y^\nu|^4}{16\pi M_R^2}, \tag{3.38}$$

in the limit $T \ll M_R$. To account for the $\sim 0.1\,\text{eV}$ left-handed neutrino mass, the sum from two channels gives about $\langle \sigma v \rangle_0 \sim 5 \times 10^{-30}\,\text{GeV}^{-2}$ for the EGH scenario.

3.3.5 Boltzmann Transport Equation

The lepton number violating processes described above are usually not fast enough to reach chemical equilibrium, due to the suppression from the large Majorana mass. Nevertheless, the relaxation of the system toward its equilibrium can be described by the Boltzmann transport equation. To the first order in μ_0/T, we have

$$\dot{n}_L + 3Hn_L = -2n_0^{eq} \langle \sigma v \rangle_0 \left(n_L - \frac{2\mu_0}{T} n_0^{eq} \right) \tag{3.39}$$

where $n_L = n_\nu - n_{\overline{\nu}}$ is the total asymmetry of neutrinos, and $n_0^{eq} = T^3/\pi^2$. If the interaction were fast enough, the system would yield the lepton asymmetry $n_{L,\,eq} = \frac{2}{\pi^2}\mu_0 T^2$ in equilibrium. The derivation of this equation is discussed in Ref. [2].

3.3.6 Resulting Lepton Asymmetry

As in [1], the evolution of the lepton asymmetry can be analyzed in two regimes: during the relaxation of the σ field ($\mu_0 \neq 0$) and during the subsequent cooling of the Universe ($\mu_0 \approx 0$). During the relaxation of the σ field, when $\mu_0 \propto \partial_0\sigma^2 \neq 0$, the Universe produces most of the lepton asymmetry; as mentioned this time is generally insufficient for the system to reach equilibrium, and so the asymmetry produced is of the order $n_{L,\text{eq}} \times \sigma_R T_{\text{rlx}}^3 t_{\text{rlx}}$, where t_{rlx} is the time period during which the Higgs field relaxes, and $T_{\text{rlx}} = T(t_{\text{rlx}})$. The equilibrium lepton asymmetry can be approximated by its value at t_{rlx} as

$$n_{L,\text{eq}} \simeq \frac{2}{\pi^2}\mu_0 T_{\text{rlx}}^2 = \frac{2}{\pi^2}\frac{\partial_0\sigma^2}{M_n^2} T_{\text{rlx}}^2 \simeq \frac{2}{\pi^2}\frac{\sigma_0^2}{M_n^2 t_{\text{rlx}}} T_{\text{rlx}}^2, \tag{3.40}$$

where σ_0 is the initial VEV of σ given by Eq. (3.26), and M_n is the new scale. From this, we find the approximate number density

$$n_{L,\,\mathrm{rlx}} \simeq \frac{2\sigma_0^2 T_{\mathrm{rlx}}^2}{\pi^2 M_n^2 t_{\mathrm{rlx}}} \min\left\{1,\ \frac{2}{\pi^2}\sigma_R T_{\mathrm{rlx}}^3 t_{\mathrm{rlx}}\right\}, \tag{3.41}$$

where σ_R is the thermally averaged cross section given by Eq. (3.34).

Note the temperature before and after the reheating completes ($t_{RH} \equiv 1/\Gamma_I$) is given by

$$T(t) \approx \begin{cases} T_{RH}\left(t_{RH}/t\right)^{1/4} & t < t_{RH} \\ \left(\dfrac{45}{16\pi^3 g_*}\right)^{1/4} \sqrt{\dfrac{m_{pl}}{t}} & t > t_{RH}. \end{cases} \tag{3.42}$$

We note that because we consider a pure ϕ^4 potential, the relaxation time is $t_{\mathrm{rlx}} \approx 7/\sqrt{\lambda_{\mathrm{eff}}}\sigma_0$. (This holds within a factor of two even for quartic couplings of the order $\lambda \sim 10^{-20}$.)

After the initial relaxation, the produced asymmetry can be partially washed out. This is due either to subsequent oscillations, during which the sign of the chemical potential oscillates, or due to ongoing lepton-number-violating interactions in the plasma after the chemical reaction has become small. As computed in [1, 5], the effect of washout can be approximated by

$$N_{L,\,f} = N_{L,\,\mathrm{rlx}} \exp\left\{-\frac{\sigma_R T_{RH}^3}{\pi^2 \Gamma_I}\left[8\left(1 - \frac{T_{RH}}{T_{\mathrm{rlx}}}\right) + \sqrt{15}\right]\right\} \tag{3.43}$$

$$\approx N_{L,\,\mathrm{rlx}} \exp\left(-\frac{8+\sqrt{15}}{\pi^2}\frac{\sigma_R T_{RH}^3}{\Gamma_I}\right) \tag{3.44}$$

for $t_{\mathrm{rlx}} < t_{RH}$, and

$$N_{L,\,f} = N_{L,\,\mathrm{rlx}} \exp\left(-\frac{\sqrt{15}}{\pi^2}\frac{\sigma_R T_{RH}^2 T_{\mathrm{rlx}}}{\Gamma_I}\right) \tag{3.45}$$

for $t_{\mathrm{rlx}} > t_{RH}$. We note that depending on the strength of the lepton-number-violating potential, it may be advantageous to arrange for a comparatively rapid decay of the σ condensate, so that the oscillation amplitude of the scalar VEV is significantly damped.

The asymmetry is also further diluted by $(a_{\mathrm{rlx}}/a_R)^3 \approx t_{\mathrm{rlx}}^2 \Gamma_I^2$ for the case that $t_{\mathrm{rlx}} < t_{RH}$. Thus at the end of reheating (assuming the oscillation of the scalar field has ended), the

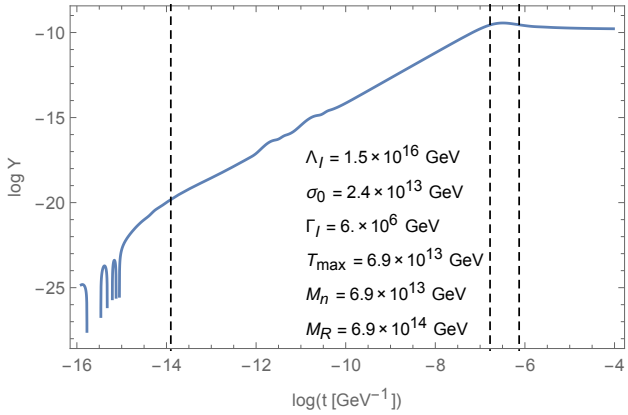

Figure 3.2: Evolution of the lepton asymmetry $Y = n_L/\left(2\pi^2 g_{*S} T^3/45\right)$ for $\lambda_{\rm eff} = 10^{-13}$, with the parameters $\Lambda_I = 1.5 \times 10^{16}$ GeV, $\Gamma_I = 6 \times 10^6$ GeV, $M_n = 6.9 \times 10^{13}$ GeV, and $M_R = 6.9 \times 10^{14}$ GeV. The initial VEV of the σ field is $\sigma_0 = 2.4 \times 10^{13}$ GeV. The maximum temperature during reheating is $T_{\rm max} = 6.9 \times 10^{13}$ GeV. The vertical dashed lines denote the time of maximum reheating, the beginning of the radiation-dominated era, and the first time the σ VEV crosses zero, form left to right.

Universe obtains the the ratio of the lepton asymmetry to entropy

$$\begin{aligned} Y \equiv \frac{n_L}{s} &= \frac{45}{2\pi^2 g_{*S}} \frac{n_L}{T^3} \\ &\simeq \frac{45}{2\pi^2 g_{*S}} \frac{2\sigma_0^2}{\pi^2 M_n^2} \frac{T_{\rm rlx}^2 t_{\rm rlx} \Gamma_I^2}{T_{RH}^3} \min\left\{1, \frac{2}{\pi^2}\sigma_R T_{\rm rlx}^3 t_{\rm rlx}\right\} \exp\left(-\frac{8+\sqrt{15}}{\pi^2}\frac{\sigma_R T_{RH}^3}{\Gamma_I}\right) \end{aligned} \tag{3.46}$$

for $t_{\rm rlx} < t_{RH}$, and

$$Y \simeq \frac{45}{2\pi^2 g_{*S}} \frac{2\sigma_0^2}{\pi^2 M_n^2} \frac{1}{T_{\rm rlx} t_{\rm rlx}} \min\left\{1, \frac{2}{\pi^2}\sigma_R T_{\rm rlx}^3 t_{\rm rlx}\right\} \exp\left(-\frac{\sqrt{15}}{\pi^2}\frac{\sigma_R T_{RH}^2 T_{\rm rlx}}{\Gamma_I}\right) \tag{3.47}$$

for $t_{\rm rlx} > t_{RH}$. This estimation formula agrees within one order of magnitude with the numerical result.

One can obtain the evolution of the lepton asymmetry more precisely by solving Eq. (3.39) numerically. In Fig. 3.2, we present a numerical example for $\lambda_{\rm eff} = 10^{-13}$ with the inflationary parameters $\Lambda_I = 1.5 \times 10^{16}$ GeV, and $\Gamma_I = 6 \times 10^6$ GeV. The RH neutrino mass scale is set at $M_R = 10 T_{\rm max}$ to suppress the thermal production of RH neutrinos during reheating, and we verify that the resulting neutrino Yukawa coupling is within the perturbative regime

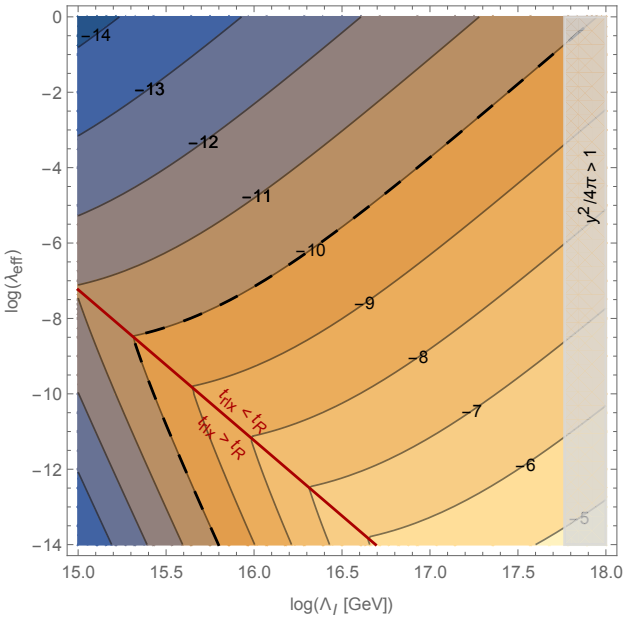

Figure 3.3: The approximate late time asymptotic asymmetry ($\log|Y|$) using Eqs. (3.46) and (3.47) with $\Gamma_I = 3\times10^6\,\mathrm{GeV}$, $M_R = 10T_{\max}$, and $M_n = 0.1T_{\max}$. The red line indicates where $t_{\rm rlx} = t_{RH}$. The dashed line denotes the required asymmetry to explain the observed baryonic matter-antimatter asymmetry.

($|Y^\nu|^2/4\pi = 0.18 < 1$). This example gives a late time asymptotic asymmetry about $Y \sim 10^{-10}$.

We explored the parameter space of the model using the approximate formula [Eqs. (3.46) and (3.47)]. In Fig. 3.3, we show the approximate late time asymmetry ($\log|Y|$) as a function of $\lambda_{\rm eff}$ and Λ_I with mass scales $M_R = 10T_{\max}$ and $M_n = 0.1T_{\max}$. We have checked that this value of M_R is sufficient to ensure that standard leptogenesis does not produce a sufficiently large asymmetry. The decay rate of the inflaton is set to $\Gamma_I = 3.7\times10^6\,\mathrm{GeV}$ so that it gives the maximum asymmetry for each $\lambda_{\rm eff}$ and Λ_I. The requirement of the neutrino coupling being perturbative ($|Y^\nu|^2/4\pi < 1$) imposes an upper bound on the inflationary energy scale $\Lambda_I \lesssim 7\times10^{17}\,\mathrm{GeV}$, which is weaker than the bound $\Lambda_I \lesssim 1-2\times10^{16}\,\mathrm{GeV}$ from CMB observations [24, 25].

In Fig. 3.3 we see that the generated asymmetry increases as $\lambda_{\rm eff}$ decreases in the region

where $t_{\rm rlx} < t_{RH}$. This can be understood as follows: the initial VEV is set by inflationary parameters, since by construction, the VEV is permitted only to grow during the last $N \approx 8$ e-folds of inflation. The relaxation time though scales as $1/\sqrt{\lambda_{\rm eff}}$; therefore, as $\lambda_{\rm eff}$ decreases the system has more time to approach the equilibrium asymmetry.

The dashed line in the figure indicates $Y = 10^{-10}$, which matches the observed value. The region of most interest is the lower left side, in which a sufficiently large asymmetry is generated with $\Lambda_I \lesssim 10^{16}\,\text{GeV}$, which is required by observations of the tensor-to-scalar ratio in the CMB [24, 25].

From this figure, we see the effective quartic coupling is restricted to $\lambda_{\rm eff} \lesssim 10^{-8}$, which corresponds to a relatively flat effective potential for the σ field. Such flat directions can develop in models with multi-field scalar sectors, such as the EGH model considered here.

We note that in all of this parameter space, $M_n < T_{\rm max}$, and in much of it, $M_n < \sigma_0$. Because M_n is not the largest scale in the analysis, the use of effective field theory to derive Eq. (3.30) is questionable. Consequently, the exact asymmetry would depend on the details of the UV-complete theory considered; however, Eq. (3.30) is likely to give a reasonable approximation.

In order to compare with our earlier work using the SM Higgs boson, it is convenient to consider the asymmetry as a function of the new scale M_n and the decay rate of the inflaton, Γ_I. This is shown in Fig. 3.4, where we have fixed the inflationary scale Λ_I and coupling $\lambda_{\rm eff}$. As above, we also take $M_R = 10 T_{\rm max}$. Therefore, the inflaton decay rate Γ_I, which fixes $T_{\rm max}$, also effectively fixes M_R and therefore, when combined with observational limits on the left-handed neutrino masses, the neutrino coupling Y^ν. Demanding that the coupling Y^ν be in the perturbative regime eliminates the parameter space shown in grey on the right-hand side of the plots.

In these plots, we additionally illustrate the regime in which $\text{Max}(\sigma_0, T_{\rm max}) > M_n$ using cross-hatching. As noted above, in this regime the exact asymmetry would depend on the details of the UV-complete theory considered; however, Eq. (3.30) is a reasonable estimate. We see that if one fine-tunes $\lambda_{\rm eff}$ to extremely small values [$\mathcal{O}(10^{-13})$ or smaller], an asymme-

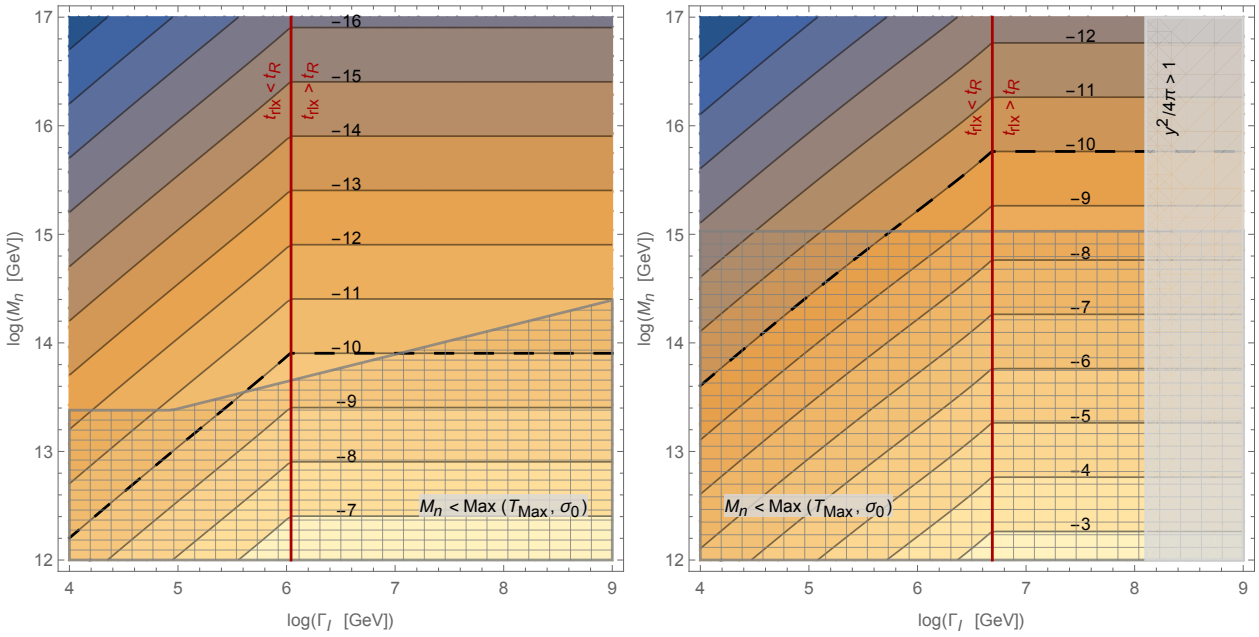

Figure 3.4: An exploration of parameter space as a function of M_n and Γ_I, for $\Lambda_I = 1.5 \times 10^{16}$ GeV and $\lambda_{\text{eff}} = 10^{-13}$ (left) and $\Lambda_I = 10^{17}$ GeV and $\lambda_{\text{eff}} = 10^{-15}$ (right). The grey area on the right indicates where the theory is not under perturbative control, and the cross hatched region denotes the regime in which the effective field theory used to derive Eq. (3.30) is unreliable. The red lines indicate where $t_{\text{rlx}} = t_{RH}$. The dashed lines denote the required asymmetry to explain the observed baryonic matter-antimatter asymmetry.

try $Y \sim 10^{-10}$ can be generated in the regime in which effective field theory is reliable. For $\Lambda_I = 1.5 \times 10^{16}\,\text{GeV}$, near the upper limit allowed by CMB observations, this region is near $M_n \sim 10^{14}\,\text{GeV}$ and $\Gamma_I \sim 10^{6}\,\text{GeV}$. If Λ_I is increased to $10^{17}\,\text{GeV}$ (and the quartic coupling decreased), then the parameter space is significantly larger, as illustrated by the plot on the right. For so small values of λ_{eff} the value of θ is also small and hence the value of the VEV f is large. In fact for $\lambda_{\text{eff}} = 10^{-13}$ the mode of θ is $\bar{\theta} = 2.216^{+0.704}_{-0.200} \times 10^{-13}$ (the plot on the left) and for $\lambda_{\text{eff}} = 10^{-15}$ (the plot on the right) the mode of θ is $\bar{\theta} = 8.359^{+2.621}_{-0.487} \times 10^{-8}$.

The plots in Fig. 3.4 illustrate the freedom available in this model. While the quartic coupling of the SM has a minimum value set by the recently observed Higgs boson, no such constraint restricts the effective EGH self-coupling λ_{eff} yet. By decreasing λ_{eff} one can

enhance the asymmetry; alternatively, one may say that lower inflationary scales Λ_I and Γ_I are permitted in the EGH model. Furthermore, such small values of λ_{eff} allow us to generate a sufficiently large asymmetry in the regime in which effective field theory is reliable; in order to accomplish this withing the SM Higgs boson, significant modifications to the Higgs potential (using non-renormalizable operators) at large scales were necessary [2].

As noted above, at small couplings we must be concerned about corrections to the potential. We note that using the full running coupling (3.21) alters the final asymmetry at the level of about 1%. One may also be concerned that finite temperature corrections could significantly affect the potential. However, the finite temperature corrections to the potential scale as $\lambda_{\text{eff}} T^2 \sigma^2$, and so are also suppressed by the small quartic coupling. For the parameters in Fig. 3.2, this correction only affects the asymmetry by 0.1%. Couplings to the Standard Model fermions are suppressed by the $\sin(\theta)$ factor, which as indicated by Eq. (3.21), is necessarily small when the quartic coupling is small.

As mentioned above, we can only tune the quartic coupling λ_{eff} to be this small in models with an extended Higgs sector, as the observed Higgs boson mass suggests a quartic coupling $\mathcal{O}(10^{-2})$ at high scales. Therefore, we have shown that in an extension of the SM with an extended Higgs sector (included but not limited to the EGH paradigm) it is possible for Higgs-relaxation leptogenesis to generate the observed baryonic asymmetry, although it requires a small self-coupling if the potential in the direction of the VEV has a ϕ^4 form (and one wishes to remain in the regime in which effective field theory is reliable). Furthermore, although the parameter space is not large, this can be accomplished for inflationary scales consistent with CMB measurements.

3.4 Conclusions and Outlook for Chapter 3

In this work, we have successfully extended the baryogenesis scenario using the relaxation mechanism to the EGH framework. Our results show that if the electroweak scale is not fundamental but radiatively generated and consequently the Higgs particle a quasi elemen-

tary Goldstone Boson it is possible to generate the baryon asymmetry by marrying the EGH framework to the relaxation mechanism. In particular, we showed that in order to accommodate baryogenesis the only necessary extensions to the model is to include RH neutrinos and furthermore the operator in Eq. (3.30) is generated.

Because of the nature of the EGH new Higgs sector one can consider very flat scalar potential directions along which the relaxation mechanism can be implemented. This further translates into achieving a wider region of applicability of the approximations, particularly regarding the regime in which the use effective theory used to derive Eq. (3.30), as compared to the SM Higgs case. Specifically baryogenesis can be achieved even from an unmodified ϕ^4 potential and within a regime in which the effective field theory interpretation of Eq. (3.30) is justified, unlike in the SM case. Observed limits on the inflationary scale Λ_I restrict, but do not eliminate, this parameter space.

CHAPTER 4

Leptogenesis via the 750 GeV Pseudoscalar

In December 2015, the ATLAS and CMS Collaborations have reported signal of a diphoton excess which may be interpreted as a pseudoscalar boson S with a mass around 750 GeV. To explain the diphoton excess, such a boson is coupled to the Standard Model gauge fields via $SF\tilde{F}$ operators. In this chapter, we consider the implications of this state for early universe cosmology; in particular, the S field can acquire a large vacuum expectation value due to quantum fluctuations during inflation. During reheating, it then relaxes to its equilibrium value, during which time the same operators introduced to explain the diphoton excess induce a nonzero chemical potential for baryon and lepton number. Interactions such as those involving right-handed neutrinos allow the system to develop a nonzero lepton number and, therefore, this state may also be responsible for the observed cosmological matter-antimatter asymmetry. This chapter is based on the work [5] done with Alexander Kusenko and Lauren Pearce.

4.1 Introduction

In December 2015, the ATLAS and CMS Collaborations have reported signal of a diphoton excess at an invariant mass of $m_S \approx 750\,\text{GeV}$ [101, 102]. One possible explanation for the excess is the resonant process $pp \to S \to \gamma\gamma$, where S is a new scalar or pseudoscalar field with mass m_S [103–105]. To produce the signal, this field should couple to the $\text{SU}(3)_\text{C}$ field strength tensor $G^a_{\mu\nu}$ (for production from gluons) and to the $\text{U}(1)_\text{QED}$ field strength tensor $F_{\mu\nu}$ (to enable decays to two photons).

The discovery of beyond-the-Standard-Model physics may have implications for unre-

solved issues such as the nature of dark matter [106–113] and the matter-antimatter asymmetry of the Universe [114, 115]. While Ref. [114, 115] considered the impact of a 750 GeV scalar for electroweak scale baryogenesis, we here show that a 750 GeV pseudoscalar can produce the observed cosmological matter excess during an epoch of relaxation in the early Universe, similar to the Higgs- and axion-relaxation leptogenesis scenarios discussed in [1–4, 63, 78, 80, 116–120].

The structure of this chapter is as follows: In the subsequent section, we introduce a concrete model with a pseudoscalar field with a mass of 750 GeV. We then discuss how the very operators introduced to explain the LHC diphoton excess can also produce an effective chemical potential in the early Universe, if the pseudoscalar field acquire a time-dependent vacuum expectation value (VEV). Then in Sec. 4.3, we discuss how a large VEV can be produced during the inflationary epoch in the early Universe, which will subsequently relax to its equilibrium value. In Sec. 4.4 we discuss the lepton-number-violating processes in the early Universe which, in the presence of the chemical potential, result in a lepton asymmetry. The model parameters are restricted by isocurvature constraints and the fact that the entire observable Universe is a domain of baryon excess (as opposed to anti-baryonic excess). These constraints are discussed in Sec. 4.5. Finally, we present a numerical analysis of the available parameter space in 4.6.

4.2 The Model and Effective Chemical Potential

In order to explain the observed diphoton excess, we supplement the Standard Model (SM) with a real singlet S which interacts via the terms [103–105]:

$$\mathcal{L} \supset \tilde{\lambda}_g \frac{\alpha_s}{12\pi v_{EW}} S G^a_{\mu\nu} \tilde{G}^{\mu\nu}_a + \tilde{\lambda}_W \frac{\alpha}{\pi \sin^2\theta_W v_{EW}} S W^a_{\mu\nu} \tilde{W}^{\mu\nu}_a + \tilde{\lambda}_B \frac{\alpha}{\pi \cos^2\theta_W v_{EW}} S B_{\mu\nu} \tilde{B}^{\mu\nu}, \quad (4.1)$$

where θ_W is the weak mixing angle, and W and B are the $\mathrm{SU(2)_L}$ and $\mathrm{U(1)_Y}$ field strength tensors, respectively. After the Higgs boson acquires a nonzero vacuum expectation value, the Lagrangian contains the couplings

$$\mathcal{L} \supset \tilde{\lambda}_g \frac{\alpha_s}{12\pi v_{EW}} S G^a_{\mu\nu} \tilde{G}^{\mu\nu}_a + \tilde{\lambda}_\gamma \frac{\alpha}{\pi v_{EW}} S F_{\mu\nu} \tilde{F}^{\mu\nu}, \quad (4.2)$$

where $F^{\mu\nu}$ is the $\mathrm{U(1)_{QED}}$ field strength tensor, and $\tilde{\lambda}_\gamma = \tilde{\lambda}_W + \tilde{\lambda}_B$. Ref. [105] has explored the parameter space in which this model reproduces the observed excess, finding $\tilde{\lambda}_\gamma = 0.48 \pm 0.08$, although the lower values are in some tension with dijet resonance searches. Production via gluon interaction is controlled by $\tilde{\lambda}_g \sim 0.1$ to 1. For leptogenesis, we will make use of the operators with the $\mathrm{SU(2)_L}$ and $\mathrm{U(1)_Y}$ gauge fields. These are $\mathcal{O}_5$ operators with an effective scale of $\pi v_{\mathrm{EW}}/\alpha\tilde{\lambda}_\gamma \sim 10^5\,\mathrm{GeV}$, although as discussed in Ref. [105], these operators are generally constructed from fermions with masses on the TeV scale.

Next, we show that these operators can lead to an effective chemical potential for baryon and lepton number when the S field has a time-dependent vacuum expectation value (VEV). In the Standard Model, the baryon number and lepton number currents (j_B^μ and j_L^μ) are not conserved; baryon and lepton number can be violated by sphaleron processes. The divergence of these currents is given by the electroweak anomaly equation

$$\partial_\mu j_B^\mu = \partial_\mu j_L^\mu = \frac{N_f}{32\pi^2}\left(-g^2 W^a_{\mu\nu}\tilde{W}_a^{\mu\nu} + g'^2 B_{\mu\nu}\tilde{B}^{\mu\nu}\right), \tag{4.3}$$

where $N_f = 3$ is the number of families in the Standard Model.

Using the anomaly equation, the terms in Eq. (4.1) generate a coupling between the pseudoscalar S and the divergence of the $(B+L)$ current,

$$\mathcal{L} \supset -\tilde{\lambda}_W \frac{8}{N_f v_{EW}} S \partial_\mu j^\mu_{B+L} = \tilde{\lambda}_W \frac{8}{N_f v_{EW}} \left(\partial_\mu S\right) j^\mu_{B+L}, \tag{4.4}$$

where we have integrated by parts and dropped a total derivative in the second step. This effective operator is valid when electroweak sphalerons to be in thermal equilibrium; in the early Universe, this occurs for temperatures below $T \lesssim 10^{12}\,\mathrm{GeV}$ [64, 121].

For a patch of the Universe where the VEV $\langle S \rangle$ is approximately spatially homogeneous but evolves in time, this operator becomes

$$\mathcal{L}_{O_5} = \tilde{\lambda}_W \frac{8}{N_f v_{EW}} \left(\partial_0 \langle S \rangle\right) j^0_{B+L}. \tag{4.5}$$

which acts as an effective chemical potential

$$\mu_0 = \tilde{\lambda}_W \frac{8}{N_f v_{EW}} \left(\partial_0 \langle S \rangle\right) \tag{4.6}$$

for the $B + L$ charge j^0_{B+L}.

We assume that the axion-like couplings in Eq. (4.1), which are nonrenormalizable operators, are effective couplings. These may be generated by integrating out a loop of fermions which are heavy compared to 750 GeV. As noted above, we expect these effective operators to break down around the TeV scale. In the scenario outlined here, we will consider temperatures in the early Universe above this. If this operator is generated by a fermionic loop, these degrees of freedom will typically acquire thermal corrections to their masses, proportional to their coupling times the temperature. For temperatures $T \gg 10^5\,\mathrm{GeV}$, the thermal masses will dominate. Similar finite temperature considerations will apply to other mechanisms of generating the $\mathcal{O}_5$ operators in Eq. (4.1). Therefore, we will use the effective chemical potential

$$\mu_0 \sim \frac{1}{T}\left(\partial_0 \langle S \rangle\right). \tag{4.7}$$

The interpretation of the term in Eq. (4.5) as a chemical potential [65, 122] simplifies the analysis of the asymmetry generation. However, in some cases, such an interpretation may fail [123, 124]. The effective chemical potential is a valid approximation when there is a separation of scales: the plasma interactions at temperature T are very rapid on the time scales on which the scalar field is moving. In this regime, one can introduce two Wilsonian cutoffs, one at some high energy scale Λ_h and one at an energy scale Λ_l, such that $\left(\partial_0 \langle S \rangle / \langle S \rangle\right) \ll \Lambda_l \ll T$. One can then integrate out all degrees of freedom outside these two cutoffs and construct an effective theory for the scales between Λ_l and Λ_h. In this effective theory, the field S and its time derivative are not propagating degrees of freedom, but slowly varying external parameters. From the remaining degrees of freedom, describing plasma at temperature T, one can construct the Hamiltonian in the usual manner. The term in Eq. (4.5) becomes $\mu_0 n_{B+L}$, where $\mu_0 \propto \partial_0 S$ is the effective chemical potential.

We observe that this chemical potential, generated by the relaxation of a scalar field, is similar to that in the models considered in Refs. [1–3, 78]; however, in this model μ_0 depends on the time-derivative of $\langle S \rangle$ rather than the time-derivative of $\langle S^2 \rangle$. Consequently, the sign of $\langle S \rangle$ is important to determining whether an excess of particle or antiparticles is produced;

this will lead to constraints discussed in Sec. 4.5 below.

4.3 Vacuum Expectation Value during Inflation

In the previous section, we demonstrated how the terms between the 750 GeV pseudoscalar field and SM field strengths introduced to explain the observed LHC excess can themselves lead to an effective chemical potential for baryon and lepton number in the early Universe, provided that the pseudoscalar field acquired a time-dependent vacuum expectation value. In this section, we explain how this can naturally occur during inflation.

In addition to the $\mathcal{L}_{O_5}$ operator discussed above, the scalar S must have the canonical kinetic term, quadratic coupling, and quartic self-coupling

$$\mathcal{L}_S = \frac{1}{2}\partial_\mu S\,\partial^\mu S - \frac{1}{2}m_S^2 S^2 - \frac{1}{4}\lambda_S S^4 \tag{4.8}$$

for the theory to be renormalizable. The LHC data suggested that $m_S \approx 750\,\text{GeV}$. During inflation, the scalar field S can acquire a nonzero vacuum expectation value (VEV), of magnitude $S_0 \equiv \sqrt{\langle S^2\rangle}$ due to quantum fluctuations. The average initial VEV can be computed through the Hawking-Moss instanton or via a stochastic approach [10, 11, 14, 15, 21]. In the massive noninteracting limit ($\lambda_S = 0$), the average initial VEV has magnitude [12]

$$S_0 = \sqrt{\frac{3}{2}}\frac{H_I^2}{2\pi m_S} \approx 0.19\frac{H_I^2}{m_S}, \tag{4.9}$$

where $H_I \equiv \sqrt{8\pi/3}\Lambda_I^2/m_{pl}$ is the Hubble parameter during inflation. For the massless interacting limit ($m_S = 0$), the VEV is [12]

$$S_0 = \sqrt{\frac{\Gamma\left(\frac{3}{4}\right)}{\Gamma\left(\frac{1}{4}\right)}}\left(\frac{3}{2\pi^2\lambda_S}\right)^{1/4} H_I \approx 0.36\frac{H_I}{\lambda_S^{1/4}}. \tag{4.10}$$

At the end of inflation, the field rolls down classically to the minimum of its potential. The relaxation of the VEV after inflation provides the time-dependence in the chemical potential (4.6). The evolution of the VEV is governed by the equation of motion,

$$\ddot{S} + 3H\dot{S} + \Gamma_S\dot{S} + V'(S) = 0, \tag{4.11}$$

where $V(S)$ is the potential from Eq. (4.8), and Γ_S is the decay width of the S boson. The total decay width has been explored in the parameter space for the diphoton excess in Ref. [105]; it is constrained from below by

$$\begin{aligned}\Gamma(S \to gg) &= 47\,\text{MeV} \times \tilde{\lambda}_g^2 \left(\frac{m_S}{750\,\text{GeV}}\right)^3, \\ \Gamma(S \to \gamma\gamma) &= 3.4\,\text{MeV} \times \tilde{\lambda}_\gamma^2 \left(\frac{m_S}{750\,\text{GeV}}\right)^3,\end{aligned} \tag{4.12}$$

although additional couplings between the S boson and other fields can enhance the decay width. Ref. [105] found that in the preferred region of parameters, a decay width between $\mathcal{O}(0.1)$ and $\mathcal{O}(0.01)$ GeV is preferred. As in the case of the Higgs relaxation, the evolution of the condensate can be treated as classical coherent motion as long as the condensate decay width is not too large [48, 125].

We note that this potential is invariant under $S \to -S$, and therefore when a nonzero vacuum expectation value develops, domains with either sign generally occur, separated by domain walls. In regions where $\langle S \rangle$ has different signs, the chemical potential given by (4.6) also has different signs, which means that whether production particles or antiparticles are biased depends on the sign of the initial vacuum expectation value $\langle S \rangle$.

We note that the potential implied by (4.8) will also generally acquire finite temperature corrections, generally of the form $\lambda_S S^2 T^2$. We will focus below on the case in which λ_S is small, and therefore these corrections are not significant.

4.4 Lepton-Number-Violating Process— The Standard Seesaw Mass Matrix

The results of the previous two sections establish that in the early Universe, the pseudoscalar field S naturally acquires a vacuum expectation value and subsequently relaxes to its equilibrium value; furthermore, the very terms introduced to account for the LHC diphoton excess lead to a nonzero chemical potential which can bias the production of particles or antiparticles. However, this can only occur if the model also includes a lepton-number-

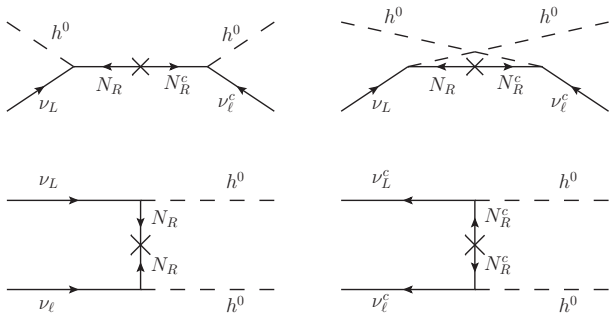

Figure 4.1: Lepton-number-violating processes mediated by right-handed neutrinos which generate a lepton asymmetry in the early Universe.

violating process. While there are myriad possibilities for this, we here consider processes mediated by neutrino Majorana mass. This is motivated by the well-known neutrino seesaw mechanism [70, 72, 73, 126].

Interactions mediated by a massive right-handed Majorana fermion can violate lepton number, including those shown in Fig. 4.1. These processes are suppressed by the right-handed Majorana mass, which is required to be large in the standard seesaw mechanism. In the scenario considered here, this is advantageous: if the right-handed Majorana mass is significantly larger than the reheat temperature, then the production of a lepton asymmetry via the production and decay of right-handed neutrinos (as in [74, 127]) is suppressed. We also note that we ensure that $\max(m_S = 750\,\mathrm{GeV}, \sqrt{\lambda_S} S_0)$ is smaller than M_R, so that decays of the condensate into right-handed neutrinos is also suppressed.

The thermally averaged cross section for these processes is [2]

$$\sigma_R \sim m_\nu^2 / 16\pi v_{\mathrm{EW}}^4 \sim 10^{-31}\,\mathrm{GeV}^{-2}, \tag{4.13}$$

provided that the effective Higgs mass is less than the temperature. Like the pseudoscalar S field, the Higgs field can acquire a vacuum expectation value during inflation such that $m_{\mathrm{H,eff}} \sim H_I$, and it will subsequently also relax to its equilibrium position. This relaxation may occur before or after the relaxation of the pseudoscalar field; however, we will show in Sec. 4.6 that the asymmetry is generated when the temperature $T \gg H_I$ and so this

expression for the cross section is valid.

The heavy Majorana mass does suppress lepton-number-violating processes in this model as well; however, this is counterbalanced by the chemical potential (4.6), which can be large if the pseudoscalar field relaxes to equilibrium rapidly. We observe that the scattering processes can even be out of thermal equilibrium ($\langle\sigma v\rangle\, n < H$). The small probability for a single particle to undergo a lepton-number-violating interaction is counterbalanced by the fact that we only need to generate a final asymmetry $\mathcal{O}(10^{-10})$ (and the number density remains significant).

In this analysis, we consider these lepton-number-violating processes occurring in the plasma of particles produced during reheating. (We note that because the VEV is trapped at large values until the end of inflation, the relaxation of the pseudoscalar field will generally occur during reheating, without any fine-tuning necessary.) This is similar to the processes considered in Higgs relaxation analyses such as [1, 2, 4] and for axion relaxation in [78]. An additional asymmetry is produced by the decay of the condensate itself, as analyzed for Higgs relaxation in [3] and axion relaxation in [80, 116].

With the inclusion of the right-handed Majorana neutrinos, we have all of the necessary ingredients for relaxation-generated leptogenesis: an effective chemical potential for lepton number, which is generated by a field which acquires a large VEV during inflation that subsequently relaxes to equilibrium, and lepton-number-violating processes which can occur during this relaxation.

4.5 Domain Size and Baryonic Isocurvature Constraint

Equations (4.9) and (4.10) give the magnitude of the average vacuum expectation value of the S field; however, as the vacuum expectation value is produced via quantum fluctuations, different patches of the Universe will generally have different VEVs. In relaxation leptogenesis scenarios, the lepton asymmetry depends on the initial VEV of the field, and therefore, each patch of the Universe could have a different final asymmetry. As discussed above, not

only the magnitude, but also the sign of the final lepton/baryon asymmetry of the Universe is determined by the VEV. Consequently, in this model the Universe would be divided between domains with a matter excess and domains with an antimatter excess. Therefore, the observable Universe must fit inside a patch with a single sign of the VEV. Similar concerns apply to many models of spontaneous baryogenesis [65, 122].

We note that Z_2 symmetry of the potential Eq. (4.8) is broken by the interactions in Eq. (4.1). Through renormalization group equations, these interactions could produce linear or cubic terms in the potential. Consequently, one of the two vacua could have a lower energy. If the energy difference is larger than the inflationary Hubble parameter, this vacuum would dominate during inflation, which would suppress the production of domain walls.

In this section, we will first calculate the constraint from avoiding domain walls in the limit of an exact Z_2 symmetry, which is the most constraining scenario. Then we will discuss baryonic isocurvature, and show that this leads to stronger constraints than concerns about domain walls.

The characteristic size of one domain can be estimated by the correlation length of the field S during de Sitter expansion. The spatial physical correlation radius R_c is given by [12]

$$R_c = H_I^{-1} \exp\left(\frac{H_I t_c}{2}\right), \tag{4.14}$$

where t_c is the correlation time. For the massive noninteracting limit ($\lambda_S = 0$),

$$t_c = 3\,(\ln 2)\,\frac{H_I}{m_S^2}. \tag{4.15}$$

For the massless interacting limit ($m_S = 0$),

$$t_c \approx \frac{7.62}{H_I\sqrt{\lambda_S}}. \tag{4.16}$$

To avoid domain walls, our observable patch of the Universe has to be within one domain. This patch has a physical radius

$$R_{RH} \simeq R_{\rm now}\frac{T_{\rm now}}{T_{RH}} \sim 5\times 10^{29} T_{RH}^{-1} \tag{4.17}$$

at the end of reheating. During reheating, the patch grows by a factor of

$$\frac{R_{RH}}{R_0} \simeq \left(\frac{\Lambda_I^4}{T_{RH}^4}\right)^{1/3}. \tag{4.18}$$

Thus, the patch of our observable Universe corresponds to a patch with radius

$$\begin{aligned} R_0 &\simeq R_{\rm now} T_{\rm now} \left(\frac{T_{RH}}{\Lambda_I^4}\right)^{1/3} \simeq R_{\rm now} T_{\rm now} \left(\frac{3}{\pi^3 g_*}\right)^{1/12} \frac{m_{pl}^{1/6} \Gamma_I^{1/6}}{\Lambda_I^{4/3}} \\ &= H_I^{-1} R_{\rm now} T_{\rm now} \sqrt{\frac{8\pi}{3}} \left(\frac{3}{\pi^3 g_*}\right)^{1/12} \left(\frac{\Lambda_I^4 \Gamma_I}{m_{pl}^5}\right)^{1/6} \\ &\sim 8 \times 10^{29} \left(\frac{\Lambda_I^4 \Gamma_I}{m_{pl}^5}\right)^{1/6} H_I^{-1} \\ &\approx 2 \times 10^{23} \left(\frac{\Lambda_I}{10^{13}\,{\rm GeV}}\right)^{2/3} \left(\frac{\Gamma_I}{10^4\,{\rm GeV}}\right)^{1/6} H_I^{-1} \end{aligned} \tag{4.19}$$

at the end of inflation, where Γ_I is the inflaton decay rate parameter. For our observable Universe to be within one domain, the correlation radius has to be $R_c \gtrsim R_0$, which gives

$$\frac{H_I t_c}{2} \gtrsim 53.8 + \frac{2}{3} \ln\left(\frac{\Lambda_I}{10^{13}\,{\rm GeV}}\right) + \frac{1}{6} \ln\left(\frac{\Gamma_I}{10^4\,{\rm GeV}}\right). \tag{4.20}$$

This imposes constraints

$$\frac{H_I}{m_S} \gtrsim 7.19 + 0.05\, \ln\left(\frac{\Lambda_I}{10^{13}\,{\rm GeV}}\right) + 0.01\, \ln\left(\frac{\Gamma_I}{10^4\,{\rm GeV}}\right) \tag{4.21}$$

for the massive noninteracting case, and

$$\lambda_S \lesssim 5.02 \times 10^{-3} \left[1 - 0.09\, \ln\left(\frac{\Lambda_I}{10^{13}\,{\rm GeV}}\right) - 0.02\, \ln\left(\frac{\Gamma_I}{10^4\,{\rm GeV}}\right)\right] \tag{4.22}$$

for the massless interacting case.

Furthermore, baryonic isocurvature perturbations are constrained by the observations of cosmic microwave background [50–54]. The upper bound on the baryonic isocurvature perturbation imposed by observations by the Planck satellite is [24, 54, 128]

$$|\mathcal{S}_{b\gamma}| = \left|\frac{\delta Y_B}{Y_B}\right| \lesssim 5.0 \times 10^{-5}. \tag{4.23}$$

To satisfy baryonic isocurvature constraints, and to protect against matter-antimatter domain walls, we require that the observable Universe be contained within a single matter domain in which the initial VEV $\langle S \rangle$ does not vary significantly.

We will show in Sec. 4.6 below that the baryon asymmetry $Y_B = n_B/s \propto S$ in this particular model where we generate the asymmetry through operator (4.5). The isocurvature constraint leads to a condition on the variation of the initial VEV of S,

$$\left|\frac{\delta S}{S_0}\right| = \left|\frac{\delta Y_B}{Y_B}\right| \lesssim 5.0 \times 10^{-5}. \tag{4.24}$$

The variation of $\langle S \rangle$ about S_0 is $\delta S = H_I/2\pi$ in a de Sitter space. Thus, this constraint gives

$$\frac{m_S}{H_I} \lesssim 6.1 \times 10^{-5} \tag{4.25}$$

for the massive noninteracting scenario, and

$$\lambda_S \lesssim 1.7 \times 10^{-16} \tag{4.26}$$

for the massless interacting scenario. As expected, these are stronger than the requirement that the observable Universe be contained within a domain of the same sign.

We note that in Higgs relaxation scenarios, such as those in Ref. [1–4], it was necessary to introduce new nonrenormalizable couplings to evade the baryonic isocurvature constraints. That is not necessary here, because of the large amount of freedom in the quartic coupling.

4.6 Resulting Asymmetry

In the model introduced, we have shown how a chemical potential is generated, and with the lepton-number-violating interactions, the system will approach its equilibrium state of nonzero lepton number. In general, the system will not reach its equilibrium state during the rapid relaxation of the S field, and so we analyze the generation of the nonzero lepton number with the Boltzmann equation (see the derivation in Sec. 2.4),

$$\frac{dn_L}{dt} + 3Hn_L = -\frac{2T^3\sigma_R}{\pi^2}\left(n_L - \frac{2}{\pi^2}\mu_0 T^2\right), \tag{4.27}$$

where σ_R is the thermally averaged cross section given by Eq. (4.13).

Following the analysis in Sec. 2.5.1 (setting $M_n = T_{\rm rlx}$), we derive an analytic approximation for the resulting asymmetry. During the S field relaxation, we approximate the chemical

potential as

$$\mu_0 \sim \frac{S_0}{T_{\rm rlx} t_{\rm rlx}}, \tag{4.28}$$

using Eq. (4.7). This gives the approximate lepton number density at time $t_{\rm rlx}$ as

$$n_{L,\,\rm rlx} \sim \frac{2 S_0 T_{\rm rlx}}{\pi^2 t_{\rm rlx}} \min\left\{1,\, \frac{2}{\pi^2}\sigma_R T_{\rm rlx}^3 t_{\rm rlx}\right\}. \tag{4.29}$$

The largest asymmetry is produced during the initial relaxation of the $\langle S\rangle$ field. If the oscillations of the $\langle S\rangle$ field are not significantly damped, there will be substantial washout (as the chemical potential changes sign during the oscillations). Furthermore, even after the oscillations end and the chemical potential goes to zero, ongoing lepton-number-violating processes will equilibrate the system towards zero lepton number until they go out of equilibrium. Therefore, we see that a large Majorana mass M_R is again desirable. During this washout, the system satisfies the approximate Boltzmann equation,

$$\frac{dN_L}{dt} = -\frac{2T^3\sigma_R}{\pi^2} N_L, \tag{4.30}$$

which leads the following scaling for the lepton number $N_L \equiv n_L a^3$ before and after reheating ends (at $T = T_{RH}$ and $t = t_{RH} \equiv 1/\Gamma_I$),

$$\frac{N_L(T)}{N_L\left(T_0\right)} = \begin{cases} \exp\left[-\frac{8}{\pi^2}\frac{\sigma_R T_{RH}^4}{\Gamma_I}\left(T^{-1} - T_0^{-1}\right)\right] & T \text{ and } T_0 \geq T_{RH} \\ \exp\left[-\frac{\sqrt{15}}{\pi^2}\frac{\sigma_R T_{RH}^2}{\Gamma_I}\left(T_0 - T\right)\right] & T \text{ and } T_0 \leq T_{RH}. \end{cases} \tag{4.31}$$

The asymptotic value of N_L at late times is

$$N_L(T \to 0) \approx N_L(T_{\rm rlx}) \exp\left(-\frac{8+\sqrt{15}}{\pi^2}\frac{\sigma_R T_{RH}^3}{\Gamma_I}\right), \tag{4.32}$$

for $t_{\rm rlx} < t_{RH}$, and

$$N_L(T \to 0) \approx N_L(T_{\rm rlx}) \exp\left(-\frac{\sqrt{15}}{\pi^2}\frac{\sigma_R T_{RH}^2 T_{\rm rlx}}{\Gamma_I}\right) \tag{4.33}$$

for $t_{\rm rlx} > t_{RH}$, where $N_L(T_{\rm rlx})$ can be found using Eq. (4.29). From this, we find the final

ratio of the lepton asymmetry to entropy,

$$Y = \frac{n_L}{s} \tag{4.34}$$

$$\approx \frac{45}{2\pi^2 g_*} \frac{n_{L,\,\mathrm{rlx}}}{T_{RH}^3} \frac{N_L\left(T \to 0\right)}{N_L\left(T_{\mathrm{rlx}}\right)} \left(\frac{a_{\mathrm{rlx}}}{a_{RH}}\right)^3 \tag{4.35}$$

$$\approx \frac{45}{2\pi^2 g_*} \left(\frac{2}{\pi^2}\right)^2 \sigma_R \frac{S_0}{M_n} \frac{T_{\mathrm{rlx}}^5 t_{\mathrm{rlx}}^2 \Gamma_I^2}{T_{RH}^3} \exp\left(-\frac{8+\sqrt{15}}{\pi^2} \frac{\sigma_R T_{RH}^3}{\Gamma_I}\right) \tag{4.36}$$

for $t_{\mathrm{rlx}} < t_{RH}$, and

$$Y \approx \frac{45}{2\pi^2 g_*} \frac{n_{L,\,\mathrm{rlx}}}{T_{\mathrm{rlx}}^3} \frac{N_L\left(T \to 0\right)}{N_L\left(T_{\mathrm{rlx}}\right)}$$

$$\approx \frac{45}{2\pi^2 g_*} \left(\frac{2}{\pi^2}\right)^2 \sigma_R \frac{S_0}{M_n} T_{\mathrm{rlx}}^2 \exp\left(-\frac{\sqrt{15}}{\pi^2} \frac{\sigma_R T_{RH}^2 T_{\mathrm{rlx}}}{\Gamma_I}\right) \tag{4.37}$$

for $t_{\mathrm{rlx}} > t_{RH}$ at the end of reheating when the oscillation of the scalar field has ended.

In general, the asymmetry is larger for the massive noninteracting case than the massless interacting case, that is, when the S^2 term dominates the potential instead of the S^4 term. This may require fine-tuning the quartic coupling to small values, which we discuss below. For the massive noninteracting case, one can approximate $t_{\mathrm{rlx}} \approx \pi/m_S$, provided that $m_S \ll H_I$ [12]. T_{rlx}, the temperature when the field relaxes at time t_{rlx}, is

$$T_{\mathrm{rlx}} \approx \begin{cases} T_{RH} \left(\frac{m_S}{\pi \Gamma_I}\right)^{1/4} & t_{\mathrm{rlx}} < t_{RH} \\ \left(\frac{45}{16\pi^3 g_*}\right)^{1/4} \sqrt{\frac{m_{pl} m_S}{\pi}} & t_{\mathrm{rlx}} > t_{RH}. \end{cases} \tag{4.38}$$

The reheat temperature is $T_{RH} \approx \left(3/\pi^3\right)^{1/4} g_*^{-1/4} \sqrt{m_{pl}\Gamma_I}$ where m_{pl} is the Planck mass. Using these, the lepton asymmetry can be expressed as

$$Y \approx \frac{45}{\sqrt{2\pi^9 g_*}} \sigma_R H_I^2 \frac{T_{RH}^3}{m_{pl} m_S^2} \exp\left(-\frac{8+\sqrt{15}}{\pi^{7/2}} \sqrt{\frac{3}{g_*}} \sigma_R m_{pl} T_{RH}\right) \tag{4.39}$$

$$\approx 8 \times 10^{-8} \left(\frac{\sigma_R}{10^{-31}\,\mathrm{GeV}^{-2}}\right) \left(\frac{H_I}{5 \times 10^{10}\,\mathrm{GeV}}\right)^2 \left(\frac{T_{RH}}{5 \times 10^{9}\,\mathrm{GeV}}\right)^3 \left(\frac{750\,\mathrm{GeV}}{m_S}\right)^2$$

$$\times \exp\left[-7 \times 10^{-4} \left(\frac{\sigma_R}{10^{-31}\,\mathrm{GeV}^{-2}}\right) \left(\frac{T_{RH}}{5 \times 10^{9}\,\mathrm{GeV}}\right)\right] \tag{4.40}$$

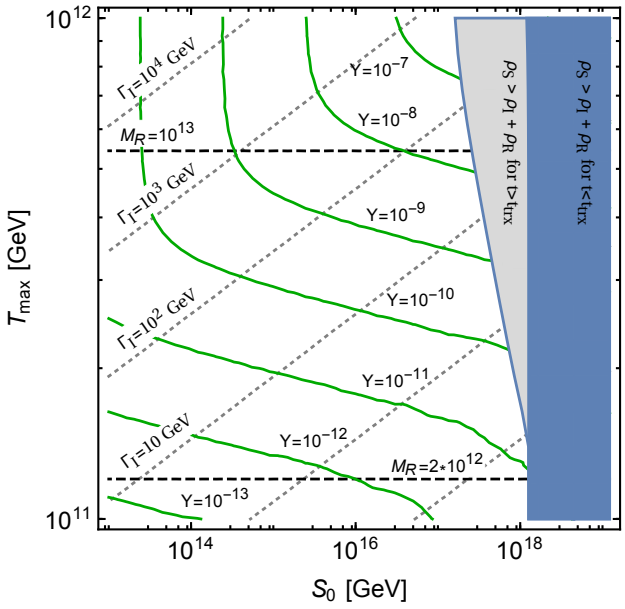

Figure 4.2: The final lepton asymmetry as a function of parameter space for the massive noninteracting scenario. The dashed lines indicate contours of constant right-handed neutrino mass M_R and the dashed lines indicate contours of constant Γ_I (the decay rate of the inflaton). In the shaded region on the right, the pseudoscalar condensate comes to dominate the energy density of the Universe.

for $t_{\rm rlx} < t_{RH}$, and

$$Y \approx \left(\frac{45}{\pi^3 g_*}\right)^{5/4} \sqrt{\frac{3}{8\pi^9}} \sigma_R H_I^2 \sqrt{\frac{m_{pl}}{m_S}} \exp\left[-\left(\frac{45}{\pi^3 g_*}\right)^{3/4} \frac{\sigma_R}{2\pi^{5/2}} \sqrt{m_{pl}^3 m_S}\right] \tag{4.41}$$

$$\approx 2 \times 10^{-8} \left(\frac{\sigma_R}{10^{-31}\,\mathrm{GeV}^{-2}}\right) \left(\frac{H_I}{10^{10}\,\mathrm{GeV}}\right)^2 \left(\frac{750\,\mathrm{GeV}}{m_S}\right)^{1/2}$$
$$\times \exp\left[-1.3 \times 10^{-4} \left(\frac{\sigma_R}{10^{-31}\,\mathrm{GeV}^{-2}}\right) \left(\frac{m_S}{750\,\mathrm{GeV}}\right)^{1/2}\right] \tag{4.42}$$

for $t_{\rm rlx} > t_{RH}$. These estimation formulas agree within 1 order of magnitude with the numerical results.

While these are useful analytic approximations, we can also solve the full Boltzmann equation numerically (using the exact cross section σ_R given in Ref. [2]). We have done this to explore the available parameter space as a function of S_0 and $T_{\rm max}$, which is shown in Fig. 4.2. We note that the initial VEV of the pseudoscalar field fixes the inflationary scale

by Eq. (4.9) and the relation

$$H_I = \sqrt{\frac{8\pi}{3}} \frac{\Lambda_I^2}{m_{pl}}. \tag{4.43}$$

The inflaton decay parameter Γ_I is the fixed by the maximum temperature reached during reheating via [96]

$$T_{\max} = \left[\frac{30}{\pi^2} \left(\frac{3}{8} \right)^{8/5} \frac{2}{3} \sqrt{\frac{3}{8\pi}} \frac{\Lambda_I^2 \Gamma_I M_{\rm pl}}{g_*} \right]^{1/4}, \tag{4.44}$$

where $g_* \approx 107$ is the total number of effectively massless degrees of freedom; we assume that the 750 GeV boson and related fields do not significantly alter this from the Standard Model value.

As noted above, the right-handed neutrinos enable the production of a lepton asymmetry via thermal leptogenesis, with a lepton-to-photon ratio

$$\eta_{th} = \frac{n_{L,th}}{n_\gamma} \approx \epsilon \left(\frac{M_R T_{\max}}{2\pi} \right)^{3/2} \frac{e^{-M_R/T_{\max}}}{T_{\max}^3}, \tag{4.45}$$

where we have taken $\epsilon \approx 3 M_R M_\nu / 16\pi v_{EW}^2$ for the CP asymmetry parameter in the lepton sector [129]. (This estimate is found by multiplying the asymmetry parameter by the ratio of nonrelativistic right-handed neutrinos to photons at the temperature $T_{\max}$.) We note that this is an optimistic estimate for the asymmetry from the thermal decay of right-handed neutrinos, as washout effects and small CP-violating phases can further suppress this. This will be suppressed by a factor ~ 30 due to the entropy production resulting with the Standard Model particles go out of thermal equilibrium. For the results shown in Fig. 4.2, we have fixed M_R by setting $\eta_{th} = 10^{-10}$, so that the mechanism discussed here dominates the lepton asymmetry. (We have verified that for these values, the neutrino coupling constant $y = M_R M_\nu / v_{EW}^2$ is in the perturbative regime, taking $M_\nu \approx 0.1\,\text{eV}$.) We have shown some contours of M_R on Fig. 4.2.

Over the parameter space of interest, the inflationary scale Λ_I ranges from $10^{13}\,\text{GeV}$ (at $S_0 = 10^{14}\,\text{GeV}$) to $10^{14}\,\text{GeV}$ (at $S_0 = 10^{18}\,\text{GeV}$). Using Eq. (4.43), we see that $T_{\max} \gg H_I$, which validates the use of the cross section (4.13). Contours for Γ_I, which is significantly smaller, are shown on the plot.

The blue region on the right of Fig. 4.2 is excluded because the energy density of the pseudoscalar condensate comes to dominate the energy density of the Universe. This can be understood as follows: Before the pseudoscalar field S relaxes, its energy density is approximately constant and equal to $V_S = m_S^2 S_0^2/2$. However, the energy density in the inflaton field and in radiation is decreasing. The relaxation time, $t_{\rm rlx} = \pi/m_S$, is less than $1/\Gamma_I$, and therefore the energy density of the inflaton field still dominates the potential, with $\rho_I \approx m_{pl}^2/6\pi t^2$. Imposing $V_S < \rho_I(t_{\rm rlx})$ constrains $S_0 < m_{pl}/\sqrt{3\pi^3} \approx 10^{18}\,\text{GeV}$.

We note that constraint (4.25) imposes $S_0 \gtrsim 4 \times 10^{10}\,\text{GeV}$, which does not eliminate any of the parameter space in which a sufficiently large asymmetry is generated.

In Fig. 4.2, we have set the decay width of the S boson to 0.1 GeV, near the upper bound of the range suggested by LHC data [105]. Γ_I is less than 0.1 GeV only beneath the dashed line in the lower right, which means that for much of the parameter space $\Gamma_S < \Gamma_I$, and the S condensate is relatively long lived. While the condensate is oscillating its energy density is diluted like matter, while after reheating has ended, the plasma loses energy as a^{-4}. Consequently, it is possible for the condensate to come to dominate the energy-momentum density during oscillations, and its decay would significantly re-reheat the Universe. We have excluded this region in gray in the plot (under the approximation that coherent oscillations of the S condensate begin instantly at $t_{\rm rlx}$).

We note that finite temperature corrections may affect Γ_S. Decay widths to light Standard Model fermions will be suppressed as T^{-3} due to temperature corrections to the fermionic masses. However, decay widths to dark sector particles may or may not be similarly affected, depending on the strength of their coupling to electrically charged Standard Model fields. If the decay width Γ_S is further suppressed in the early Universe, the pseudoscalar field undergoes coherent oscillations for longer and the bound represented by the gray region becomes more severe.

In Fig. 4.2, we have restricted our maximum temperature to $10^{12}\,\text{GeV}$. As noted above, at this temperature electroweak sphalerons go out of thermal equilibrium, and therefore, the replacement of the couplings in Eq. (4.1) with the baryon and lepton current in (4.4) is

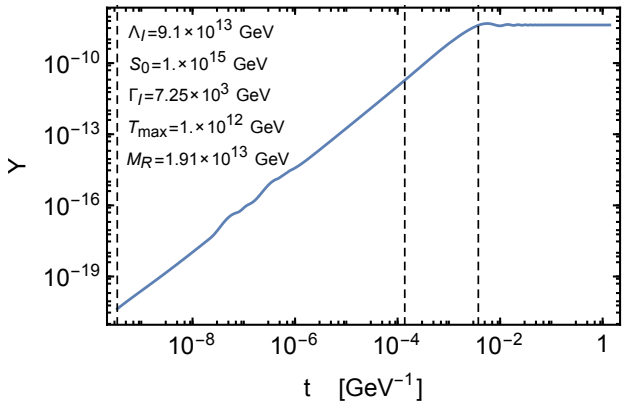

Figure 4.3: The evolution of the lepton asymmetry as a function of time for the parameters indicated. The dashed vertical lines indicate the time of maximum temperature, the beginning of the radiation dominated era, and the first time the S VEV crosses zero, from left to right.

invalid. However, as shown in Fig. 4.3, most of the lepton asymmetry is produced after the temperature has reached its maximum value. Therefore, there should be some parameter space available at larger temperatures. However, a complete analysis of the situation in which the electroweak sphalerons are in thermal equilibrium during only part of the evolution of the pseudoscalar condensate is beyond the scope of this thesis.

As we mentioned above, this analysis is for the massive noninteracting scenario, in which the potential is dominated by the quadratic term. This is valid for quartic terms $\lambda_S < 2m_S^2/S_0^2$. For this hold to $S_0 = 10^{18}\,\mathrm{GeV}$ requires $\lambda_S < 10^{-30}$, or to hold to $S_0 = 10^{15}\,\mathrm{GeV}$ requires $\lambda_S < 10^{-24}$. It would be difficult to arrange such small couplings without some degree of fine-tuning, unless the S boson is embedded in a larger scalar sector, such that the potential has a flat direction. (Note that in contrast to Affleck-Dine baryogenesis [130, 131], such a flat direction would not need to carry lepton or baryon number.)

In the massless interacting scenario, we have an additional degree of freedom corresponding to λ_S. To explore the parameter space, we set $T_{\max} = 10^{12}\,\mathrm{GeV}$, since in the massive case a significant asymmetry was produced only near this limit. Fixing $\eta_{th} = 10^{-10}$ sets $M_R \approx 2 \times 10^{13}\,\mathrm{GeV}$, and as before, we have taken $\Gamma_S = 0.1\,\mathrm{GeV}$.

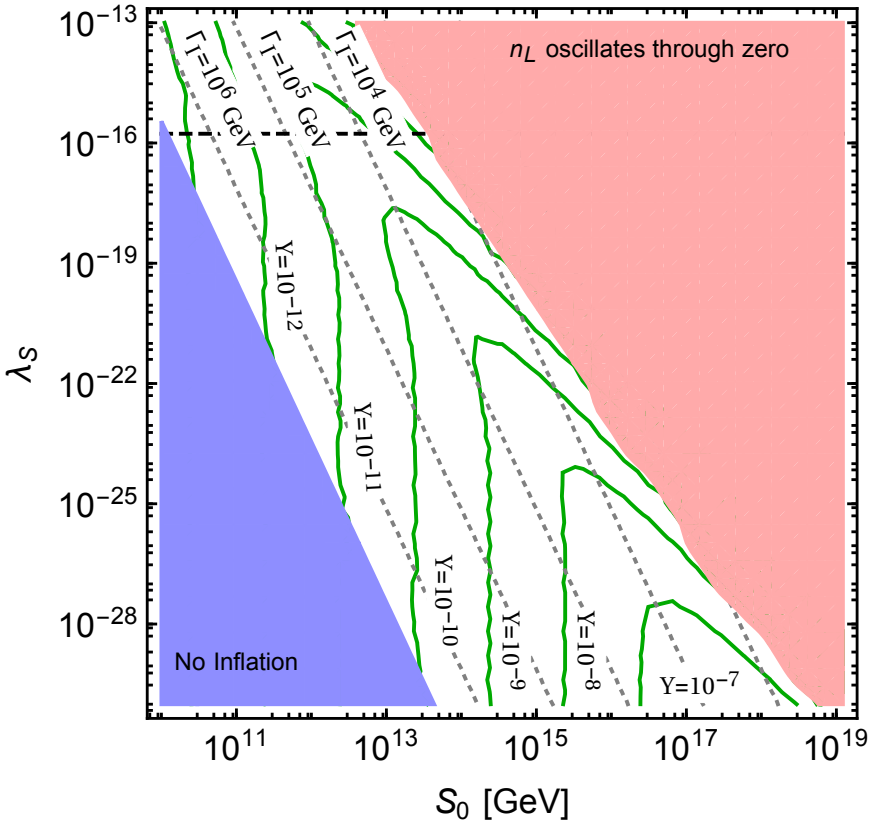

Figure 4.4: The final lepton asymmetry as a function of parameter space for the quartic potential and $T_{\max} = 10^{12}\,\text{GeV}$. In the lower left section, $\Gamma_I > H_I$, and so there would be no inflationary epoch. In the upper right section, n_L oscillates through zero. The black dashed line shows the constraint (4.26), while the gray dotted lines show contours of constant Γ_I.

The results are shown in Fig. 4.4. The scale of inflation is set by

$$\Lambda_I^2 = m_{pl} S_0 \sqrt{\frac{3\Gamma(1/4)}{8\pi\Gamma(3/4)}} \left(\frac{2\pi^2 \lambda_S}{3}\right)^{1/4}, \tag{4.46}$$

In this plot, it ranges from $\mathcal{O}(10^{12}\,\mathrm{GeV})$ near $S_0 = 10^{10}\,\mathrm{GeV}$ and $\lambda_S = 10^{-13}$ to $\mathcal{O}(10^{15}\,\mathrm{GeV})$ near $S_0 = 10^{18}\,\mathrm{GeV}$ and $\lambda_S = 10^{-30}$. Contours of constant Γ_I are shown; we have marked the region in which no inflation occurs because $\Gamma_I > H_I$ in the lower left.

In the upper right, washout is strong enough that the lepton asymmetry n_L oscillates through zero. We note that the quartic potential is steeper than the quadratic potential; consequently, the pseudoscalar VEV relaxes to its equilibrium value faster. This increases μ_0 given by Eq. (4.7), but the system has less time in which to generate the asymmetry. Furthermore, the VEV continues to evolve quickly during its oscillation, leading to relatively large chemical potentials during this epoch. Therefore, washout is a more severe problem in the quartic potential. This can be alleviated if the pseudoscalar field S were to acquire a larger decay width Γ_S; this increases the effective friction which decreases the amplitude of the oscillation (in addition to slowing the relaxation).

We see that generating a sufficiently large asymmetry generally requires a small λ_S, although not quite a small as required for the quadratic term to dominate the potential. A sufficiently large asymmetry can be generated with $\lambda_S \sim 10^{-20}$ if $S_0 \sim 10^{15}$. This is more stringent than limit (4.26), which is shown by the black dashed line.

As mentioned above, a larger asymmetry can be generated if we consider higher temperatures. We note, however, that Eq. (4.45) would imply a nonperturbative coupling for the neutrino sector for $T_{\max} > 1.4 \times 10^{13}\,\mathrm{GeV}$. However, a small CP-violating phase in the neutrino can relax this.

4.7 Result Update in 2016

In August 2016, ATLAS and CMS have reported on the search for resonant production of high mass diphoton signals [132, 133]. No significant excess over the background expectation is

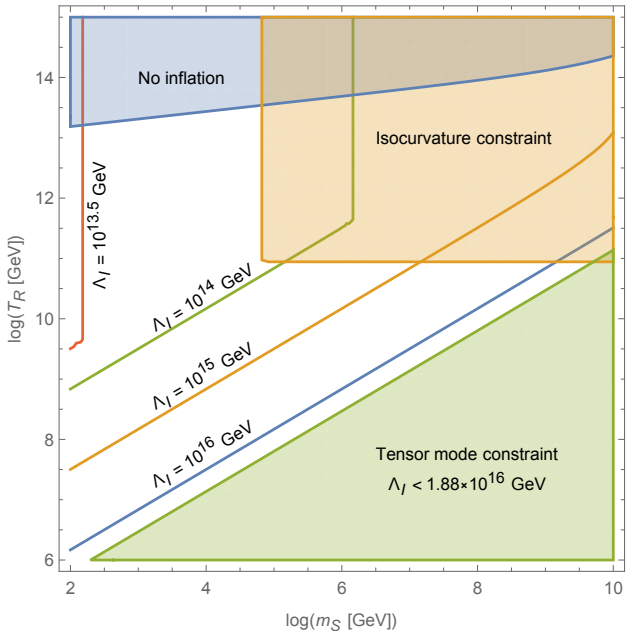

Figure 4.5: Parameter space for $m_S \gtrsim 750$ GeV with massive non-interacting potential.

observed in the mass range of 0.5 to 4.5 TeV in the 2016 data. Nevertheless, the leptogenesis model we discuss here remains viable for pseudoscalar mass m_S much higher than 4.5 TeV.

In Fig. 4.5, we shows the parameter space in the scalar mass m_S and the reheat temperature T_R for the massive non-interacting scenario. Solid lines denote the required mass m_S and T_R at each inflation scale Λ_I in order to produce sufficient lepton asymmetry $Y \sim 10^{-10}$ matching the observed value. In the upper blue region of the plot, high reheat temperature results in $\Gamma_I > 3H_I$ so the inflation is not successful. In the upper right orange region, the produced baryon asymmetry has large isocurvature perturbation and is constrained by CMB observations. The lower left green region denotes the maximum allowed inflation scale Λ_I coming from non-detection of the tensor mode fluctuation from CMB. We see the model with $m_S \gtrsim 10^3$ GeV remains viable for inflation scale $\Lambda_I \gtrsim 10^{14}$. The upper bound on m_S is $\sim 10^{10}$ GeV.

4.8 Conclusions for Chapter 4

Observations of the 750 GeV diphoton excess at the LHC has motivated the consideration of a pseudoscalar field which couples to the electromagnetic field strength [103–105]. To generate this operator, the pseudoscalar field S should couple to the fundamental $\mathrm{SU}(2)_\mathrm{L}$ and/or $\mathrm{U}(1)_\mathrm{Y}$ field strengths. The first of these couplings generates a chemical potential for lepton and baryon number in the early Universe, as the pseudoscalar field relaxes from a large vacuum expectation value naturally generated by quantum fluctuations during inflation. In the presence of lepton-number-violating interactions, such as those mediated by heavy right-handed neutrinos, a nonzero lepton asymmetry is produced, which is transferred to baryons via electroweak sphalerons.

We have explored the parameter space in which a sufficiently large asymmetry is generated via this mechanism for both a quadratic and quartic potential. In particular, there are regions of parameter space in which a sufficiently large asymmetry is generated through this mechanism while the asymmetry generated by thermal leptogenesis is insufficient. We have also considered constraints from the condition that the entire observable Universe have a particle excess (in contrast to an antiparticle excess) and baryonic isocurvature observations. These do not restrict the available parameter space. This is in contrast to the Higgs relaxation models [1, 2, 4], in which additional nonrenormalizable couplings were required to satisfy isocurvature constraints.

CHAPTER 5

Relaxation Leptogenesis, Isocurvature Perturbations, and the Cosmic Infrared Background

Observations of cosmic infrared background (CIB) radiation exhibit significant fluctuations on small angular scales. A number of explanations have been put forth, but there is currently no consensus on the origin of these large fluctuations. We consider the possibility that small-scale fluctuations in matter-antimatter asymmetry could lead to variations in star formation rates which are responsible for the CIB fluctuations. We show that the recently proposed Higgs relaxation leptogenesis mechanism can produce such small-scale baryonic isocurvature perturbations which can explain the observed excess in the CIB fluctuations. This chapter is based on work done with Masahiro Kawasaki, Alexander Kusenko, and Lauren Pearce [6].

5.1 Introduction

Observations of near-infrared cosmic infrared background (CIB) radiation by the AKARI and Spitzer space telescopes both have a consistent excess at the subdegree scale [134–138]. In particular, the integrated CIB fluctuation at 5 arcminutes, between 2 and 5 μm, is $\delta F_{2-5\,\mu\mathrm{m}}\,(5') \simeq 0.09\,\mathrm{nW\,m^{-2}sr^{-1}}$ [139, 140]. This measurement of the anisotropic CIB entails that the power in the fluctuations is $F_{\mathrm{CIB}} \approx \delta F_{\mathrm{CIB}}/\Delta_{5'} \sim 1$ nW m^{-2} sr^{-1}. The origin of this excess has not been clearly identified, but one plausible source is the first (population III) stars, which form at redshifts $z \gtrsim 10$ [139, 140]. While the AKARI observations can be explained by faint galaxies, the Spitzer observations are not consistent with this explanation [141]. (The Spitzer space telescope is able to resolve fainter point sources and does

not observe a sufficiently large faint galaxy population to explain the excess [141].) Zodiacal light is unable to account for the excess [142].

The star formation rate depends on the distribution of halos, seeded by cosmological density perturbations. It was recently pointed out that, if primordial black holes account for dark matter, then isocurvature density perturbations arising from fluctuations in the distribution of black holes can explain the CIB measurements [139, 140, 143, 144]. In this scenario, the increase in the power of dark matter density perturbations on the small scales leads to a larger fraction of collapsed halos at redshift $z > 10$. This results in a higher F_{CIB}, which can explain the CIB observations [144].

We here explore a different possibility. Depending on its origin, the baryonic asymmetry of the universe can exhibit small-scale fluctuations. These fluctuations can have the same effect on the CIB as the fluctuations produced by the black holes; namely, they can also increase the number of collapsed halos. Models of inhomogeneous baryogenesis have been considered [145, 146]. In particular, the recently proposed Higgs relaxation leptogenesis models [1–3] are expected to produce small-scale baryonic isocurvature perturbations. A similar scenario can be constructed with other scalar fields, such as axions, or in models with an extended Higgs sector [4, 5, 78].

This leptogenesis model is motivated by the observation that the Higgs field will generically undergo a postinflationary relaxation epoch [23]. Higgs relaxation leptogenesis uses an effective dimension 6 operator in the scalar sector to produce an effective chemical potential during the Higgs relaxation epoch, which distinguishes matter from antimatter. In the presence of a lepton-number-violating or baryon-number-violating interaction, the system relaxes toward its equilibrium state with nonzero asymmetry.

In the Higgs relaxation leptogenesis scenario, the final baryon asymmetry depends on the magnitude of the postinflationary, prerelaxation vacuum expectation value (VEV) of the Higgs field. This can be produced by quantum fluctuations during inflation [1, 2]. Therefore this initial VEV, and consequently the produced asymmetry, will generically vary spatially. In this work, we illustrate how these variations give rise to matter isocurvature

perturbations. Isocurvature perturbations are not affected by Silk or Landau damping, and baryonic isocurvature perturbations cannot be converted into adiabatic perturbations prior to the decoupling of baryons and photons [147]. Therefore, such perturbations can cause massive regions to reach the nonlinear regime earlier, enhancing star-formation at $z \simeq 10$. This provides an elegant resolution to the problem of excess CIB radiation.

This chapter is organized as follows: In Sec. 5.2, we review the relevant features of the Higgs relaxation model and illustrate how it generates matter isocurvature perturbations. Subsequently, in Sec. 5.3, we calculate the spectrum of these baryonic isocurvature perturbations; we then consider how these modes evolve in Sec. 5.4. The main results of this work are contained in Sec. 5.5, in which we show that these isocurvature modes cause sufficiently many halos large enough to support star formation to collapse around $z = 10$ to explain the CIB observations. Finally, we present the parameter space in which Higgs relaxation leptogenesis can both account for the observed matter-antimatter asymmetry of the universe and explain the CIB observations in Sec. 5.6.

5.2 The Higgs Relaxation Leptogenesis Model as a Source of Isocurvature Perturbations

In this section, we review the Higgs relaxation leptogenesis model, following the discussion in [1, 2], and then explain how it generates baryonic isocurvature perturbations.

During inflation, any scalar field ϕ, including the Higgs field, with mass $m_\phi < H_I$ will develop a vacuum expectation value (VEV) $\sqrt{\langle\phi^2\rangle}$ through quantum fluctuations [11, 14, 15]. Due to Hubble friction, the field is unable to efficiently relax to its equilibrium value. The average VEV can be computed via a stochastic approach, which we discuss in detail below. At the end of inflation, the Hubble parameter decreases, and the scalar field will relax to its equilibrium value.

For successful Higgs relaxation leptogenesis, we additionally assume that the Higgs field

is coupled to the $(B+L)$ fermion current, j^{μ}_{B+L}, through an operator of the form

$$\mathcal{O}_6 = -\frac{1}{\Lambda_n^2}\left(\partial_\mu |\phi|^2\right) j^{\mu}_{B+L}, \tag{5.1}$$

which can be arranged by coupling ϕ^2 to $-g^2 W^a_{\mu\nu}\tilde{W}^{\mu\nu}_a + g'^2 B_{\mu\nu}\tilde{B}^{\mu\nu}$ and using the electroweak anomaly equation, among other possibilities [1–3]. As the VEV of ϕ evolves in time, this operator acts as an effective chemical potential,

$$\mu_{\text{eff}} = \frac{1}{\Lambda_n^2}\partial_t |\phi|^2, \tag{5.2}$$

for the fermion current j^{μ}_{B+L}. In the presence of a B or L-violating interaction (such as those mediated by heavy right-handed neutrinos), the system will acquire a nonzero $B+L$ charge. The available parameter space was described in Ref. [2]; here we simply emphasize that this included regions of parameter space in which the right-handed neutrino is too heavy to thermalize, thus suppressing thermal leptogenesis. The final lepton-number-to-entropy ratio is in general determined by the initial VEV ϕ_0 at the end of inflation, $Y \propto \phi_0^2$, as explained in Appendix D.1.

We emphasize that since the effective chemical potential $\propto \partial_t|\phi|^2$, it is independent of the phase of $\langle\phi\rangle$, and therefore, the same sign asymmetry is generated in all Hubble patches. Consequently, it is not necessary for the observable universe to be contained within one Hubble patch. Due to quantum fluctuations, these different regions of the universe will generically have different initial VEVs ϕ_0 right after the inflation. Since the asymmetry is proportional to the initial VEV, different patches in the universe will end up with different baryon asymmetries after the above-described leptogenesis mechanism is completed. As time progresses, different scales will reenter the horizon; as baryons become nonrelativistic, these baryonic density fluctuations will evolve, and some may collapse. The observable universe today consists of many Hubble patches, and therefore we expect enhanced baryonic fluctuations in the Higgs relaxation leptogenesis model.

Since the Higgs field ϕ is not the inflaton, and we ensure that it does not dominate the energy density of the universe, the baryonic fluctuations generated in this manner are

isocurvature (entropy) perturbations. They are independent from the adiabatic (curvature) perturbations produced during reheating by the decay of the inflaton.

This production of baryonic isocurvature perturbations in Higgs relaxation leptogenesis was noted in Refs. [1, 2], where it was observed that these perturbations have the potential to exceed observational bounds from the cosmic microwave background radiation (CMB) [24]. Therefore, these isocurvature perturbations must be suppressed at scales probed by the CMB. This led to the construction of the "IC-2" initial condition in those references, in which the Higgs field ϕ is massive ($m_\phi > H_I$) at the beginning of the inflation, due to a coupling to inflaton via one or several operators of the form

$$\mathcal{L}_{\phi I} = c\frac{\left(\phi^\dagger\phi\right)^{m/2}\left(I^\dagger I\right)^{n/2}}{M_{pl}^{m+n-4}}. \tag{5.3}$$

While the inflaton VEV $\langle I\rangle$ is large, these operators provide a large effective mass to the scalar field ϕ, suppressing the growth of its VEV due to quantum fluctuation. As inflation proceeds and $\langle I\rangle$ decreases, the Higgs field ϕ becomes effectively massless ($m_\phi < H_I$), and the vacuum expectation value starts to grow. As we discuss below, the initial VEV, and therefore the resulting asymmetry, depends on $N_{\rm last}$, the number of e-folds (measured from the end of inflation) that the Higgs VEV developed during. In Refs. [1, 2, 4], we set $N_{\rm last} \sim 8$ out of an abundance of caution; next, we discuss more precisely the exact observational constraint.

5.3 Spectrum of Primordial Baryonic Isocurvature Perturbations

Having explained how the Higgs relaxation leptogenesis model produces baryonic isocurvature perturbations, we now proceed in this section to determine the spectrum of these primordial baryonic isocurvature perturbations. We will also apply observational constraints to the spectrum, and we will determine how this constrains $N_{\rm last}$, the number of e-folds the Higgs VEV grows during.

We will first need to calculate the spectrum of the fluctuations in the Higgs vacuum expectation value, since this sources the fluctuations in the baryon density. As mentioned above, in Higgs relaxation leptogenesis models, the Higgs field is coupled to the inflaton in

such a way that the vacuum expectation value grows during only the last $N_{\rm last}$ e-folds of inflation. If the effective mass turns off sufficiently fast, then the average VEV of ϕ at the end of inflation in a completely flat potential is

$$\phi_0 \equiv \sqrt{\langle \phi^2 \rangle} \approx \sqrt{\int_{H_I e^{-N_{\rm last}}}^{H_I} \frac{dk}{k} \left(\frac{H_I}{2\pi}\right)^2} = \sqrt{N_{\rm last}} \frac{H_I}{2\pi}. \tag{5.4}$$

This ignores curvature in the potential; a more accurate determination of the VEV is found by first solving the Fokker-Planck equation [12]

$$\frac{\partial P(\phi,t)}{\partial t} = \frac{\partial^2}{\partial \phi^2}\left[\frac{H_I^3 P(\phi,t)}{8\pi^2}\right] + \frac{\partial}{\partial \phi}\left[\frac{P(\phi,t)}{3H_I}\frac{dV(\phi)}{d\phi}\right], \tag{5.5}$$

for $P(\phi,t)$, the probability distribution function of observing the VEV equal to ϕ at time t. [$V(\phi)$ is the potential for the scalar ϕ; in this case, our scalar is the Higgs boson.] The time evolution of the average VEV of ϕ can then be computed through

$$\left\langle \phi^2(t) \right\rangle = \int d\phi\, \phi^2 P(\phi,t), \tag{5.6}$$

with the initial condition $P(\phi, t=0) = \delta(\phi)$. In our analysis, we make use of the Higgs potential at one loop, with running couplings where the RG equations are calculated at two loops, following [9]. We use the same potential, with thermal corrections, to evaluate the postinflationary relaxation of this vacuum expectation value, as in [1–3]. ϕ_0 denotes the vacuum expectation value at the end of inflation, which is the initial VEV for the Higgs relaxation epoch.

This vacuum expectation value is produced by quantum fluctuations, and therefore it is not constant in space, as was mentioned above. Perturbations are produced on all physical spatial scales inside the horizon $l \lesssim H_I^{-1}$, where the Hubble parameter is evaluated when the VEV begins to grow (that is, $N_{\rm last}$ e-folds before the end of inflation). Therefore, perturbations exists in all of the subhorizon modes which have physical momentum $p = k/a > H_I$. As the modes exit the horizon ($p = k/a \lesssim H_I$), these perturbations become classical and are frozen with the amplitude

$$\delta\phi_k \equiv \Delta_\phi \approx \frac{H_I}{2\pi} \tag{5.7}$$

per unit interval in $\ln p/H_I$ [13]. The isocurvature perturbations are approximately conserved in the superhorizon regime because the Higgs field does not contribute significantly to the energy density.

We define $k_s = a(N_{\rm last})p_s \sim a(N_{\rm last})H_I$, the comoving wave number corresponding to the mode which leaves the horizon as the fluctuations in the Higgs field are first produced. The power spectrum of ϕ is then approximately

$$\mathcal{P}_\phi(k) \approx \begin{cases} 0 & \text{for } k < k_s, \\ \left(\frac{H_I}{2\pi}\right)^2 & \text{for } k \geq k_s. \end{cases} \tag{5.8}$$

In principle, one can further determine the details of the power spectrum from the transition from the Higgs field from an effectively massive field to an effectively massless field, which depends on the specific form of the operators (5.3) which couple the Higgs to the inflaton, generating the large effective mass during the early stages of inflation.

As discussed in Sec. 5.2, these perturbations in the Higgs VEV ϕ generate isocurvature perturbations in the baryon asymmetry Y_B. These perturbations have a spectrum

$$\left.\frac{\delta Y_B}{Y_B}\right|_k = \frac{\delta(\phi^2)_k}{\langle\phi^2\rangle} \approx \frac{2\ln^{1/2}(k/k_s)}{N_{\rm last}}\theta(k-k_s), \tag{5.9}$$

up to a large scale cutoff; see Appendix D.2. This makes use of the improved analytical estimates in Ref. [4]; see the discussion in Appendix D.1. We note here that the CIB signal will be dominated by $k \approx 1.4k_s$, as we will discuss in Sec. 5.5. As the universe cools, this induces a baryon energy density perturbation with the same spectrum

$$\delta_B(k) \equiv \left.\frac{\delta\rho_B}{\rho_B}\right|_k = \left.\frac{\delta Y_B}{Y_B}\right|_k. \tag{5.10}$$

Having determined the spectrum, we now consider observational constraints. For scales $k \lesssim 0.1\,\text{Mpc}^{-1}$, measurements of the cosmic microwave background radiation (CMB) from the Planck and WMAP collaborations constrain the baryonic isocurvature perturbation [24]. The measured upper bound on the completely uncorrelated isocurvature fraction is given by

$$\beta_{\rm iso} = \frac{\mathcal{P}_{\mathcal{SS}}(k_{*p})}{\mathcal{P}_{\mathcal{SS}}(k_{*p}) + \mathcal{P}_{\mathcal{RR}}(k_{*p})} \tag{5.11}$$

where $\mathcal{P}_{\mathcal{RR}}$ is the power spectrum of the adiabatic fluctuation, $\mathcal{P}_{\mathcal{SS}}$ is the power spectrum of the isocurvature fluctuation, and k_{*p} is the pivot scale used by the Planck collaboration. Planck reports bounds evaluated at three momentum scales for a variety of models (see Table 15 of Ref. [25]). To constrain our model, we use the most conservative bound from the CDI general model, making use of TT, TE, EE, low P, and WP data:

$$\begin{aligned}
\beta_{\rm iso}(k_{*p} = 0.002\,{\rm Mpc}^{-1}) &\lesssim 0.021, \\
\beta_{\rm iso}(k_{*p} = 0.050\,{\rm Mpc}^{-1}) &\lesssim 0.034, \\
\beta_{\rm iso}(k_{*p} = 0.100\,{\rm Mpc}^{-1}) &\lesssim 0.031.
\end{aligned} \tag{5.12}$$

Since we are interested specifically in the baryonic isocurvature perturbation, we rescale the power spectrum by a factor of $(\Omega_b/\Omega_{DM})^2$. Thus the requisite bound is:

$$\left|\frac{\delta Y_B}{Y_B}\right| \lesssim \frac{\Omega_{DM}}{\Omega_b}(\beta_{\rm iso}\mathcal{P}_{\mathcal{RR}})^{1/2}, \tag{5.13}$$

where $\mathcal{P}_{\mathcal{RR}}^{1/2} \approx 2.2 \times 10^{-9}$ [25]. This gives constraints of $|\delta Y_B/Y_B| \lesssim 3.4 \times 10^{-5}$ at $k_{*p} = 0.002\,{\rm Mpc}^{-1}$, 4.3×10^{-5} at $k_{*p} = 0.050\,{\rm Mpc}^{-1}$, and 4.1×10^{-5} at $k_{*p} = 0.100$ Mpc^{-1}. However, these constraints may be evaded by taking $k_s > 0.100$ Mpc^{-1}, which corresponds to producing isocurvature perturbations on scales smaller than those probed by Planck. Observations of the primordial spectrum in the CMB data at these scales are limited by the Silk (photon diffusion) damping.

At smaller scales, $0.2\,{\rm Mpc}^{-1} \lesssim k \lesssim 10\,{\rm Mpc}^{-1}$, the Lyman-$\alpha$ forest provides information on the matter power spectrum, which strongly restricts isocurvature perturbations [148]. Again, we will evade this bound by taking $k_s \gtrsim 10\,{\rm Mpc}^{-1}$. We note that despite the large comoving momentum, these isocurvature perturbations remain cosmologically relevant as isocurvature perturbations are not affected by Silk damping [147].

Next, we connect k_s to $N_{\rm last}$, the number of e-folds during which the Higgs VEV grows. The results given below are exact in the limit that the curvature of the potential is negligible. In our parameter space plots in Sec. 5.6, we use similar reasoning with the exact calculation of the initial Higgs VEV in a curved potential, using Eq. (5.6).

The mode that is exiting the horizon $N_{\rm last}$ e-folds before the end of inflation (that is, the mode that corresponds to k_s) grows to a size of $l_{\rm EOI} \simeq e^{N_{\rm last}} H_I^{-1}$ at the end of inflation (EOI). Subsequently during reheating, the scale factor a grows by a factor of

$$\frac{a_{RH}}{a_{\rm EOI}} = \left(\frac{\Lambda_I}{T_{RH}}\right)^{4/3}, \tag{5.14}$$

where Λ_I is the energy scale of inflation and $T_{RH} \approx (3/\pi^3)^{1/4} g_*^{-1/4}(T_{RH})\sqrt{m_{pl}\Gamma_I}$ is the reheat temperature. After reheating, the entropy of the universe is conserved,

$$S = a^3 s = 2\pi^2 g_{*s}(T) a^3 T^3/45, \tag{5.15}$$

which allows us to relate the current scale factor to the scale factor at the end of reheating,

$$\frac{a_{\rm now}}{a_{RH}} = \frac{g_{*S}^{1/3}(T_{RH})}{g_{*S}^{1/3}(T_{\rm now})}\frac{T_{RH}}{T_{\rm now}}, \tag{5.16}$$

where $T_{\rm now} = 2.73\,{\rm K}$, the effective number of relativistic species is $g_{*S}(T_{RH}) = 106.75$ for $T > 300\,{\rm GeV}$, and $g_{*S}(T_{\rm now}) = 43/11$ for $T = T_{\rm now}$ (in the standard model). Combining these relations, the mode that exits the horizon $N_{\rm last}$ e-folds before the end of inflation corresponds to a perturbation mode with the comoving momentum

$$k \simeq 2\pi e^{-N_{\rm last}} H_I \left(\frac{T_{RH}}{\Lambda_I}\right)^{4/3} \frac{g_{*S}^{1/3}(T_{\rm now})}{g_{*S}^{1/3}(T_{RH})}\frac{T_{\rm now}}{T_{RH}}, \tag{5.17}$$

where we have set the scale $a_{\rm now} = 1$, so that the comoving wave number coincides with the physical wave number now; thus $k = 2\pi/\ell_{\rm now}$.

Therefore, the requirement that isocurvature perturbations are generated at scales $k_s \gtrsim k_* = 10\,{\rm Mpc}^{-1}$, which corresponds to a limit on $N_{\rm last}$ of

$$\begin{aligned} N_{\rm last} \lesssim 48.2 &- \ln\left(\frac{k_*}{10\,{\rm Mpc}^{-1}}\right) + \frac{2}{3}\ln\left(\frac{\Lambda_I}{10^{16}\,{\rm GeV}}\right) + \frac{1}{3}\ln\left(\frac{T_{RH}}{10^{12}\,{\rm GeV}}\right) \\ &+ \frac{1}{3}\ln\left(\frac{g_{*S,\,\rm now}}{3.91}\right) - \frac{1}{3}\ln\left(\frac{g_{*S,RH}}{106.75}\right) + \ln\left(\frac{T_{\rm now}}{2.73\,{\rm K}}\right), \end{aligned} \tag{5.18}$$

which is not very stringent. The allowed parameter space for baryonic isocurvature perturbations is illustrated in Fig. 5.1. The restrictions on k_s from the CMB and Lyman-α forest discussed above can be converted into limits on $N_{\rm last}$ through the use of (5.17); these are also shown in Fig. 5.1.

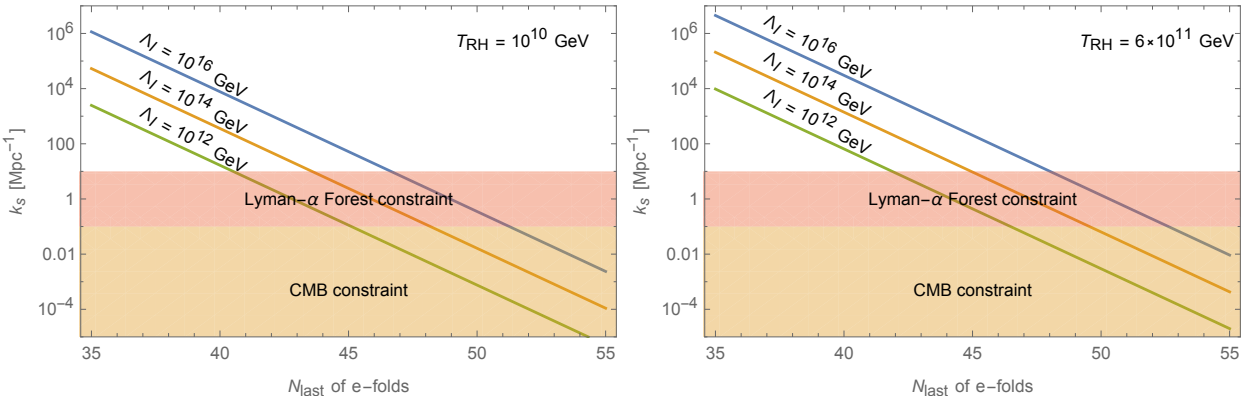

Figure 5.1: The solid lines show k_s as a function of $N_{\rm last}$, using Eq. (5.17), for various values of the inflationary scale Λ_I and reheat temperature T_{RH}. The orange (red) region indicates the constraints on k_s from the CMB (Lyman-α forest) observations.

We note that the Lyman-α forest constraints apply to the total contribution from both adiabatic and isocurvature perturbations. We recall that adiabatic perturbations have $\mathcal{R} = \sqrt{A_S} \cong 4.7 \times 10^{-5}$ if one assumes a flat spectrum. $N_{\rm last} \approx 40 \sim 50$ corresponds to an initial baryonic density contrast of $\delta_{B,0} \approx 0.02 \sim 0.03$ at $k = 1.4k_s$, using Eqs. (5.9) and (5.10). This entails that the baryonic isocurvature perturbations generally dominate the adiabatic perturbations in the range where both are present. Therefore, as Fig. 5.1 shows, it is indeed necessary to impose that $k_s \gtrsim 10\,\mathrm{Mpc}^{-1}$.

In fact, we will see in Sec. 5.5 that we best explain the CIB with $k_s \approx 65\,\mathrm{Mpc}^{-1}$. We note here that this corresponds to the perturbations beginning to grow around 46.5 e-folds before the end of inflation with $\Lambda_I = 10^{16}\,\mathrm{GeV}$ and $T_{RH} = 10^{12}\,\mathrm{GeV}$. From Eqs. (5.9) and (5.10), this corresponds to an initial baryonic density contrast of $\delta_{B,0} \approx 0.025$ at $k = 1.4k_s$. However, the second equality in Eq. (5.9), which was used with (5.10), holds in the limit of a flat potential. Accounting for the curvature in the potential, using (5.6), decreases ϕ_0, and so consequently increases $\delta Y_B/Y_B$ slightly. In Fig. 5.2, we have fixed $k_s = 65\,\mathrm{Mpc}^{-1}$ and used Eq. (5.17) to solve for the appropriate $N_{\rm last}$ and ϕ_0 at each point in parameter space. We then calculated $\delta_{B,0}$ at $k = 1.4k_s$ at each point. (We recall that, as mentioned above, this will be the scale most relevant to explaining the CIB excess.) As expected, $\delta_{B,0}$

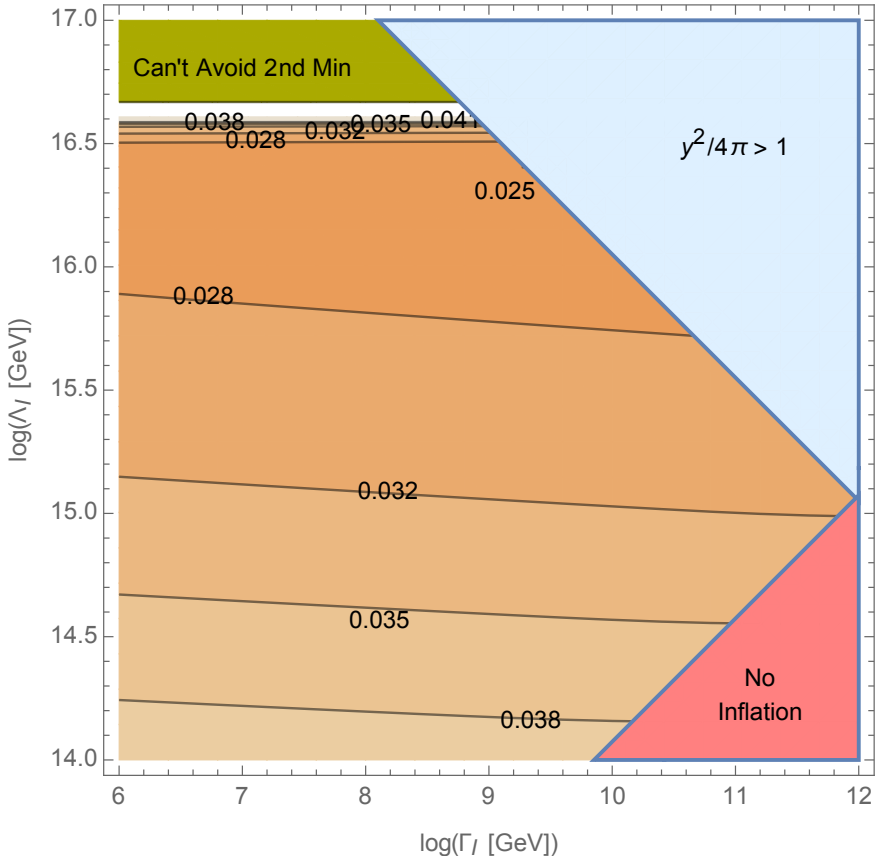

Figure 5.2: The variation of $\delta_{B,0}(k = 1.4k_s)$ in parameter space, with $k_s = 65\,\mathrm{Mpc}^{-1}$. In the green region on the upper left, the $N_{\rm last}$ given by Eq. (5.17) is large enough that the Higgs VEV probes the minimum of the Higgs potential at large VEVs. (Details on the parameters used in the calculation the potential can be found in [2].) In the red region on the lower right, $\Gamma_I > 3H_I$ so inflation doesn't happen. As in Ref. [2, 4] we set the neutrino Yukawa coupling such that right handed neutrino mass, inferred from the seesaw mechanism, is large enough that thermal leptogenesis is insufficient to explain the observed baryon asymmetry; in the upper right hand corner (light blue region), this would lead to a non-perturbative coupling. We see that there is a slight variation in $\delta_{B,0}$ over the available parameter space.

is slightly enhanced as compared to the flat potential case; this becomes more pronounced as Λ_I decreases.[1]

To summarize the results of this section, the Higgs relaxation model generates baryonic isocurvature perturbations with a spectrum given by Eq. (5.10). The single free parameter in the spectrum, k_s, can equivalently (for fixed Λ_I and Γ_I) be taken to be $N_{\rm last}$, the number of e-folds before the end of inflation during which the Higgs VEV grows. (However, since $N_{\rm last}$ affects the VEV ϕ_0, this then influences the final asymmetry produced by Higgs relaxation leptogenesis.) By taking $k_s > 10\,{\rm Mpc}^{-1}$, or (approximately) equivalently, $N_{\rm last} \lesssim 48$, the isocurvature perturbations evade all current observational bounds.

5.4 Evolution of the Baryonic Isocurvature Perturbations

In the previous sections, we explained how the Higgs relaxation model produces isocurvature perturbations, and we found the spectrum of these isocurvature perturbations. Next, we consider the evolution of the isocurvature perturbations during the subsequent evolution of the universe. We note that due to the tight coupling between photons and baryons, the amplitude of the isocurvature baryonic perturbations δ_B does not evolve before photon decoupling at $z \approx 1100$. (In fact, this was implicitly used above when we imposed constraints from the observations of the cosmic microwave background radiation and the Lyman-α forest.)

To study the late-time spectrum of the baryonic isocurvature perturbation, we calculate the evolution of the perturbations using the linearized Einstein equations and the linearized equation from conservation of the energy-momentum tensor. We work in the conformal Newtonian gauge, in which the scalar metric perturbation is parametrized as

$$ds^2 = a^2(\tau)\left[(1+2\Phi)\,d\tau^2 - (1-2\Phi)\,d\boldsymbol{x}^2\right]. \tag{5.19}$$

[1] As noted, in the green region at the top left, the Higgs VEV probes the global minimum at large VEV values (see [23]). As this region is approached, the Higgs VEV explores the "hilltop" that divides the two minima, where the potential becomes flat. Therefore, increasing Λ_I leads to a larger increase in ϕ_0, and consequently, the denominator of δ_B grows at a faster rate. It grows faster than the numerator, which scales as H_I. This accounts for the decrease in δ_B in the top left of the figure.

In our analysis, we consider the following components: radiation (denoted by $i = r$), dark matter ($i = DM$), and baryons ($i = B$). The equations of state are parametrized by $w_r = 1/3$ for radiation and $w_{DM} = w_B = 0$ for baryons and dark matter (that is, we consider cold dark matter). We assume that dark matter does not support sound waves, $u^2_{s,\,DM} = 0$, and we make the tight coupling limit that baryons and photons share the same velocity potential $v_B = v_r \equiv v_{Br}$ before decoupling. Therefore the effective speed of sound squared for the baryon and radiation fluids is $u^2_{s,\,Br} = 1/3\,(1 + R_B)$, where $R_B = 3\rho_B/4\rho_r$. However, we do not impose $4\delta_B = 3\delta_r$, which is appropriate only for adiabatic modes.

Therefore, the complete system of equations describing the evolution of the perturbations prior to recombination is [149]

$$k^2\Phi + 3\mathcal{H}\Phi' + 3\mathcal{H}^2\Phi = -\frac{a^2}{2M_{pl}^2}\sum_i \rho_i\delta_i, \tag{5.20}$$

$$\delta'_{DM} - k^2 v_{DM} = 3\Phi', \tag{5.21}$$

$$\delta'_B - k^2 v_{Br} = 3\Phi', \tag{5.22}$$

$$\delta'_r - \frac{4}{3}k^2 v_{Br} = 4\Phi', \tag{5.23}$$

$$v'_{DM} + \mathcal{H}v_{DM} = -\Phi, \tag{5.24}$$

$$v'_{Br} + \mathcal{H}\frac{R_B}{1+R_B}v_{Br} + \frac{3}{4}u^2_{s,\,Br}\delta_r = -\Phi, \tag{5.25}$$

where $\mathcal{H} \equiv a'/a$ and a prime denotes the derivative with respect to the conformal time defined via $d\tau = dt/a\,(t)$. The Hubble parameter in cosmic time, t, and in conformal time, τ, are related by $H(t) = \mathcal{H}(\tau)/a$, and the Hubble parameter can be well described by $H = H_0\sqrt{\Omega_m/a^3 + \Omega_r/a^4 + \Omega_\Lambda}$ with $a = 1/(1+z)$ after the universe enters radiation domination. The density perturbation spectra δ_i generically have both isocurvature and adiabatic contributions.

After recombination at $z \approx 1100$, photons and baryons decouple and so v_B and v_r evolve

separately. The perturbation equations for baryons and radiation are then replaced by

$$\delta_B' - k^2 v_B = 3\Phi', \tag{5.26}$$

$$\delta_r' - \frac{4}{3}k^2 v_r = 4\Phi', \tag{5.27}$$

$$v_B' + \mathcal{H} v_B = -\Phi, \tag{5.28}$$

$$v_r' + \frac{1}{4}\delta_r = -\Phi. \tag{5.29}$$

For large scales $k < k_s$, we assume the initial density perturbation spectra δ_i satisfy the adiabatic conditions

$$\delta_{DM,0} = \delta_{B,0} = \frac{3}{4}\delta_{r,0} = -\frac{3}{2}\Phi_0 = \mathcal{R}, \tag{5.30}$$

with a scale invariant spectrum. The Planck 2015 data set gives $A_S = e^{3.089}10^{-10}$ at $k = 0.05\,\mathrm{Mpc}^{-1}$ [25], which corresponds to the initial amplitude $\mathcal{R} = \sqrt{A_S} \cong 4.7 \times 10^{-5}$.

For small scales $k > k_s$, we include the baryonic isocurvature perturbations in addition to the adiabatic perturbations. For the parameters of interest, the isocurvature contribution to $\delta_{B,0}$ will generally dominate over the adiabatic contribution, and therefore $\delta_{B,0}(k)$ is given by Eq. (5.10). For the other components, we take $\delta_{DM,0} = \frac{3}{4}\delta_{r,0} = -\frac{3}{2}\Phi_0 = \mathcal{R}$ for $k > k_S$, since these have only the adiabatic contribution.

An example of the evolution of a single mode is shown in Fig. 5.3. We take $k_s = 65\,\mathrm{Mpc}^{-1}$, and consider the mode at $k = 1.4k_s = 91\,\mathrm{Mpc}^{-1}$. The baryon density contrast given by Eq. (5.10) is then 0.025. The evolution of the baryon, dark matter, and total matter perturbations are shown with solid lines. For completeness, we have also shown the evolution without the isocurvature modes in dashed lines (without accounting for Silk damping). We see that as expected the isocurvature perturbation does not evolve until decoupling; afterwards, it grows. Prior to decoupling, it enhances perturbations in dark matter and total matter.

In Fig. 5.4, we present the total matter power spectrum, which is given by

$$P(k,\,z) = \frac{2\pi^2}{k^3}\mathcal{P}_m(k,\,z) = \frac{2\pi^2}{k^3}\delta_m^2(k,\,z)\,. \tag{5.31}$$

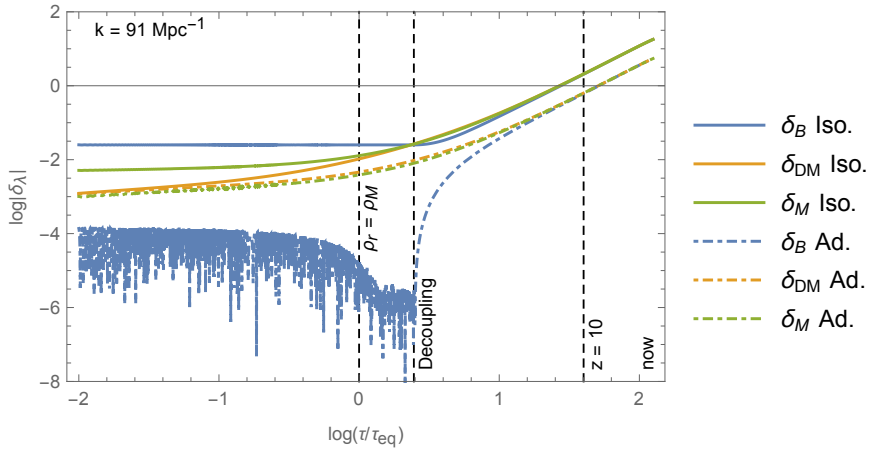

Figure 5.3: The evolution of baryon (blue), dark matter (orange), and total matter (green) perturbations at $k = 1.4k_s = 91\,\mathrm{Mpc}^{-1}$ with $\delta_{B,0}$ determined by: (1) (dashed lines) $\mathcal{R} = 4.7 \times 10^{-5}$, appropriate for a scenario with only primordial adiabatic perturbation, and (2) (solid lines) Including isocurvature perturbations; following Eq. (5.10), $\delta_B = 0.025$ for the $k = 91\,\mathrm{Mpc}^{-1}$ mode if $k_s = 65\,\mathrm{Mpc}^{-1}$. This scenario is appropriate to the Higgs relaxation scenario considered in this work.

By varying $\delta_{B,0}$, we have found that for $\delta_{B,0} \sim 0.025$, the total matter perturbation $\delta_m = (\Omega_B\delta_B + \Omega_{DM}\delta_{DM})/\Omega_m$ reaches the nonlinear regime ($\delta_m \gtrsim 1$) much earlier than it would if only the adiabatic fluctuation were present. Thus, in the Higgs leptogenesis model, structure formation begins earlier, which allows for earlier star formation. In the next section, we will use this modified history of structure formation to explain the cosmic infrared radiation excess.

5.5 Isocurvature Perturbations and the Cosmic Infrared Background Observations

In the above sections, we demonstrated that the Higgs relaxation leptogenesis scenario generates baryonic isocurvature perturbations and studied their evolution in the early universe. Now, we proceed to connect the above results to the observed CIB radiation. The isotropic flux (or absolute intensity) of the CIB is difficult to determine precisely due to the large

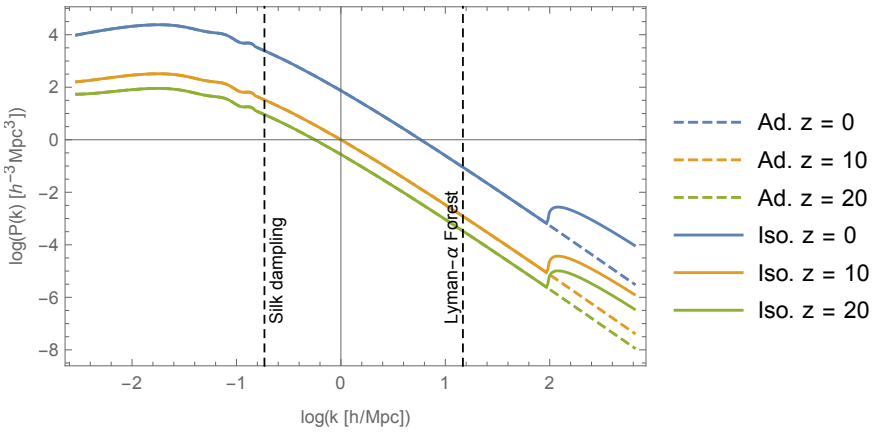

Figure 5.4: Total matter power spectra at $z = 0$, 10, and 20 for the cases that the primordial perturbations are produced by (1) only inflaton (dashed line), and (2) inflaton plus relaxation leptogenesis with $k_s = 65\,\mathrm{Mpc}^{-1}$ and $N_{\rm last} = 46.5$. Adiabatic perturbations to the right of the first dashed line are affected by Silk damping, although isocurvature contributions are not. The power spectrum to the left of the second dashed line are constrained by the Lyman-α constraints. The bump on the right edge of the plot describes the contribution on the isocurvature perturbations.

uncertainty associated with the removal of the foreground signal, galactic components, and zodiacal light. Therefore, recent measurements concern the anisotropies (spatial fluctuation) of the CIB [139]. From these measurements, one can infer the isotropic flux from the power in the fluctuations of the CIB.

In Sec. 5.1, we mentioned the currently unexplained excess in observations of anisotropies in the near-infrared cosmic radiation spectrum, $\delta F_{2-5\,\mu\mathrm{m}}\,(5') \simeq 0.09\,\mathrm{nW\,m^{-2}sr^{-1}}$ at 5 arcmin between 2 and 5 μm [140]. This relative fluctuation entails that the amplitude of the power in the fluctuations is $F_{\mathrm{CIB}} \approx \delta F_{\mathrm{CIB}}/\Delta_{5'} \sim 1\,\mathrm{nW\ m^{-2}sr^{-1}}$; one is then led to consider what sources could produce this radiation. One possibility is faint galaxies; such an explanation is consistent with AKARI observations but not the Spitzer observations, due to the fact that Spitzer is able to resolve fainter point sources [141]. As discussed in Refs. [139, 140], one possible source is early (population III) stars, at $z \approx 10$. Such stars, if they exist, will contribute significantly to the CIB and live only for a short cosmological time. In this case, the power in the fluctuations is equivalent to the isotropic flux due to the early stars [141].

However, Refs. [140, 150, 151] show that in the typical model of structure formation, with only adiabatic perturbations, one requires either an abnormally large stellar formation efficiency and/or an abnormally large radiation efficiency to produce the requisite amount of CIB radiation. We now demonstrate that the presence of isocurvature perturbations alters this conclusion. In our model, the isocurvature perturbations produced by Higgs relaxation leptogenesis cause a larger percentage of the mass in the early universe to be in collapsed halos which evolve nonlinearly and can support early star formation. Therefore, the comparably large isotropic CIB flux (that is, the power in the fluctuations) can be produced with a reasonable values for the stellar formation efficiency and radiation efficiency.

As the above discussion outlines, we are interested in the isotropic CIB flux due to early stars. The contribution from the first stars forming inside collapsed halos can be estimated

by [140]

$$F_{FS} \simeq \frac{c}{4\pi}\epsilon\rho_B c^2 f_{\rm Halo} f_* z_{\rm eff}^{-1}$$
$$= 9.1\times 10^5 \epsilon f_{\rm Halo} f_* \left(\frac{\Omega_B h^2}{0.0227}\right)\left(\frac{10}{z_{\rm eff}}\right)\,{\rm nW\,m^{-2}sr^{-1}}, \tag{5.32}$$

where $f_{\rm Halo}$ is the mass-fraction of the universe inside halos, f_* is the star formation efficiency, ϵ is the radiation efficiency, and $z_{\rm eff}$ is the effective redshift. One then finds that the halo fraction at $z = 10$ is given by

$$f_{\rm Halo} = 0.16\left(\frac{0.007}{\epsilon}\right)\left(\frac{10^{-3}}{f_*}\right)\left(\frac{F_{FS}}{F_{\rm CIB}}\right). \tag{5.33}$$

In order to have $F_{FS} = F_{\rm CIB} = 1\,{\rm nW\ m^{-2}\ sr^{-1}}$ (the value implied by the assumption that early stars explain the observed CIB anisotropy) for reasonable values of the parameters are $\epsilon \approx 0.007$ and $f_* \lesssim 10^{-3}$, one must have $f_{\rm Halo} \gtrsim 0.16$. [The value of ϵ comes from the hydrogen burning phase of early stars, which are fully convective and radiate close to the Eddington limit (see Ref. [144]); our preferred value of f_* comes from the same reference.] We fix ϵ and f_* at their upper bounds and show that with isocurvature perturbations one can have $f_{\rm Halo} \approx 0.16$, which one cannot accomplish with only adiabatic perturbations.

To compute the fraction of matter in collapsed halos, we adopt the Press-Schechter formalism [152]. An overdense region which in the linear theory would have present size R has in fact collapsed and formed structure by the time when the average density contrast $\delta_R(\boldsymbol{x}, t)$ exceeds $\delta_c \cong 1.686$, as calculated in the linearized theory defined by Eqs. (5.25) above. The average matter density contrast is computed by smoothing the spectrum

$$\delta_R(\boldsymbol{x}, t) = \int d^3y\, \delta_m(\boldsymbol{x}+\boldsymbol{y}, t)\, W_R(\boldsymbol{y}), \tag{5.34}$$

where a window function $W_R(\boldsymbol{y})$ is used to smooth the matter density so that one attains an average; we use the top-hat function

$$W_R(\boldsymbol{y}) = \frac{3}{4\pi R^3}\theta(R - |\boldsymbol{y}|). \tag{5.35}$$

which has the Fourier transform $W_R(k) = 3j_1(kR)/kR$. Using this window function, the mass contained in a sphere of radius R is approximately

$$M(R) = \frac{4}{3}\pi R^3 \rho_{m,0}, \tag{5.36}$$

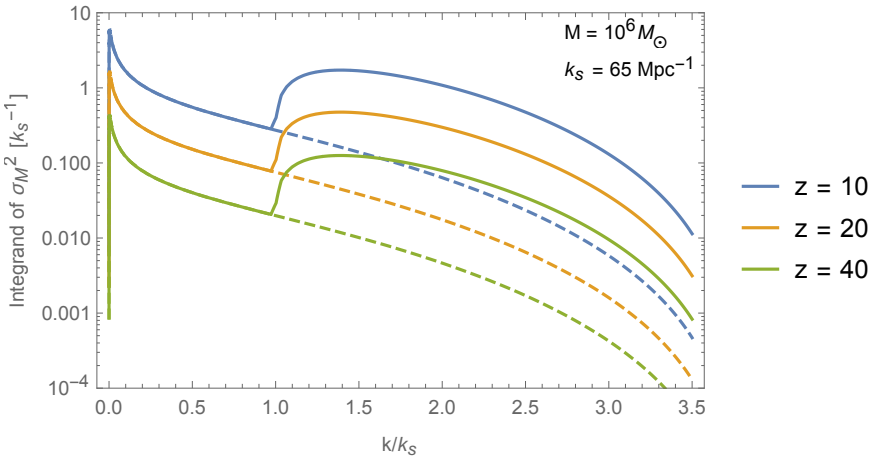

Figure 5.5: The integrand for σ_M^2 as a function of k/k_s for various redshifts z. The dashed lines are for the power spectrum with only adiabatic modes. The solid lines are for the power spectrum with isocurvature perturbation turned on at $k_s = 65\,\mathrm{Mpc}^{-1}$. We see that the integrand is dominated by $k/k_s \cong 1.4$ for the isocurvature case, neglecting the peak near zero which is present near for both the scenario with and without the isocurvature contribution.

where $\rho_{m,0}$ is the present average matter density of the universe. The smoothed matter density contrast $\delta_R(\boldsymbol{x}, t)$ computed in this way is itself a Gaussian random field, whose variance $\sigma_R(t)$ is given by

$$\sigma_R^2(t) \equiv \left\langle \delta_R^2(\boldsymbol{x}, t) \right\rangle = \int_0^\infty \frac{dk}{k} \mathcal{P}_m(k, t) \left| W_R(k) \right|^2, \tag{5.37}$$

Using Eq. (5.36), one can solve for radius R in terms of M, the total mass contained inside. Substituting this into $\sigma_R(t)$ gives the variance $\sigma_M(t) = \sigma_{M(R)}(t)$ as a function of enclosed mass M.

The integrand of Eq. (5.37) is shown in Fig. 5.5, where we have fixed the radius to correspond to a mass of $10^6 M_\odot$. This figure shows that for multiple redshifts, the integrand is peaked at $k \cong 1.4 k_s$. This justifies the claim that our signal is dominated by the contribution in this region, which was mentioned above and which motivated our choice of $k/k_s = 1.4$ as a reference point for characterizing δ_B.

Figure 5.6 shows this $\sigma_{M(R)}$ at various mass scales and redshifts. On both plots, the

dashed lines show $\sigma_{M(R)}$ including only adiabatic perturbations, while the solid and dotted lines includes the isocurvature perturbations generated by the Higgs relaxation mechanism, which we emphasize only exist for $k \geq k_s$. The plot of the left shows the results for $k_s = 65\,\mathrm{Mpc}^{-1}$ (solid) and $k_s = 100\,\mathrm{Mpc}^{-1}$ (dotted); on the right, we show the results for $k_s = 30\,\mathrm{Mpc}^{-1}$. As expected, we see that $k_s = 65\,\mathrm{Mpc}^{-1}$ leads to a larger deviation from the adiabatic-only model than $k_s = 100\,\mathrm{Mpc}^{-1}$. (We have used the initial value of $\delta_{B,0}$ and $\mathcal{R}$ given in the sections above.) On both plots, the black dash-dotted horizontal line corresponds to the critical variance; above this, a significant portion of the halos of a particular mass evolve nonlinearly.

Focusing on the $k_s = 65\,\mathrm{Mpc}^{-1}$ solid lines (left), we see that halos of mass $10^5 M_\odot$ would collapse around $z = 20$ while those of mass $10^6 M_\odot$ would collapse around $z = 10$ in the Higgs relaxation model; this contrasts to the standard picture, in which such halos would form later. At any given z, there are more halos with mass $M \lesssim 10^7 M_\odot$ in the Higgs relaxation scenario than in the typical scenario which has only adiabatic perturbations. Because the density contrast at mass scales $M \gtrsim 10^7 M_\odot$ is unaffected, the observed large scale structure is unchanged.

For the $k_s = 100\,\mathrm{Mpc}^{-1}$ (dotted) lines, the formation of small halos is still enhanced with respect to the adiabatic-perturbations only scenario; however, these halos form later. We focus on $10^6 M_\odot$ because such halos are near the lower bound of halos that can efficiently support star formation through molecular hydrogen cooling [153–157]. Production of these $10^6 M_\odot$ halos is not significantly enhanced for $k_s = 100\,\mathrm{Mpc}^{-1}$, which means that we require $k_s \lesssim 100\,\mathrm{Mpc}^{-1}$ to explain the CIB. The plot on the right shows the situation with $k_s = 30\,\mathrm{Mpc}^{-1}$; we see that halos of mass $10^6 M_\odot$ form earlier, around $z = 20$. We see that increasing k_s would bring us into conflict with optical depth measurements. Therefore, to explain the CIB excess, we require $k_s \approx 65\,\mathrm{Mpc}^{-1}$.

We now show that we make sufficiently many collapsed halos. Using the variance σ_M in the matter density contrast, we calculate the probability that a region with mass $M\,(R)$ has

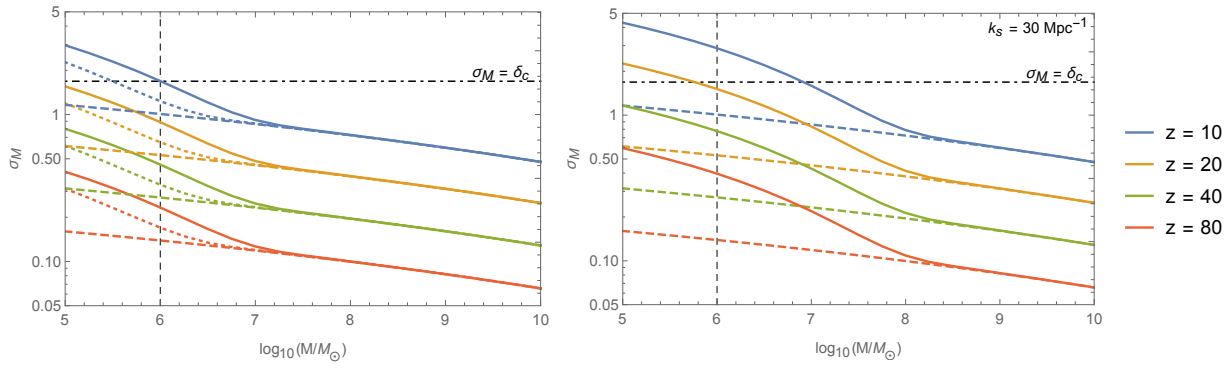

Figure 5.6: The variance σ_M of the smoothed density contrast at various redshifts and mass scales. Left: the dashed lines show the results with only adiabatic modes ($\mathcal{R} = \sqrt{A_S} \cong 4.7 \times 10^{-5}$), while the solid (dotted) lines also includes isocurvature perturbations for $k \geq 65\,\mathrm{Mpc}^{-1}$ ($100\,\mathrm{Mpc}^{-1}$), with $\delta_{B,0} = 0.025$ at $k = 1.4k_s$. Right: The solid lines correspond to $k_s = 30\,\mathrm{Mpc}^{-1}$. The black dash-dotted horizontal lines denotes the value $\sigma_M = \delta_c$; structure formation occurs above this line.

an average density contrast δ_R exceeding δ_c at redshift z [152], which is

$$f_{\mathrm{Halo}}(M,\, z) = P\left(\delta_{R(M)} > \delta_c\right) = \frac{1}{2}\left[1 - \mathrm{erf}\left(\frac{\delta_c}{\sqrt{2}\sigma_M(z)}\right)\right]. \tag{5.38}$$

This is equivalent to the fraction of mass which is collapsed halos of mass M, as smaller structures form earlier.

The results of this calculation are presented in Fig. 5.7 for $M = 10^6 M_\odot$ (solid lines) and $M = 10^8 M_\odot$ (dashed lines), first with only adiabatic modes (red lines) and then including the isocurvature modes (blue, yellow, and green lines). The Higgs relaxation scenario, with the isocurvature modes, is more efficient in halo formation; however, as expected from Fig. 5.6, the gain in efficiency is more pronounced for smaller halos. The vertical dashed line denotes $z = 10$; early stars at this time contribute significantly to the CIB. Therefore, we desire that halos large enough to support star formation ($\gtrsim 10^6 M_\odot$) have formed by this redshift.

As explained above, we will have sufficient stars to produce the inferred CIB excess for reasonable values of the radiation efficiency ϵ and star formation efficiency f_* if $f_{\mathrm{halo}} \approx 0.16$ for halos large enough to support star formation. Therefore, we have included a horizontal

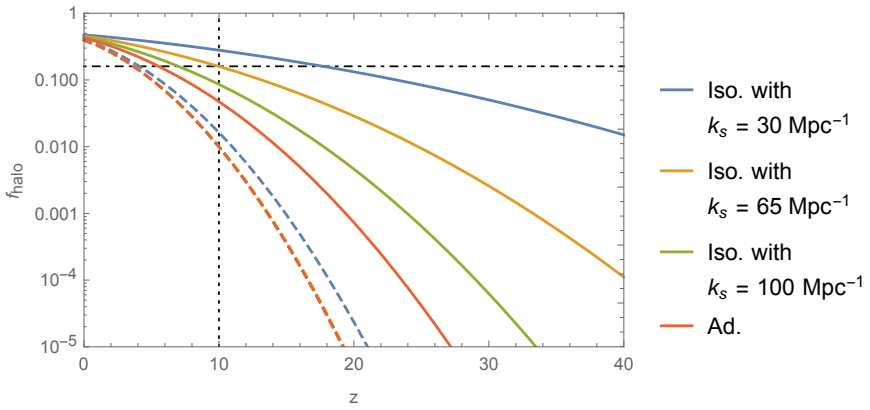

Figure 5.7: $f_{\rm Halo}\,(M,\,z)$, the mass fraction of the universe inside the collapsed halos of mass M, evaluated for $M = 10^6 M_\odot$ (solid lines) and $10^8 M_\odot$ (dashed lines), as a function of redshift z. Red lines represent the scenario with only adiabatic perturbations, while blue, yellow, and green lines represent the scenario which includes isocurvature perturbations for $k \geq k_s = 30$, 65, and $100\,{\rm Mpc}^{-1}$, respectively. The vertical dotted black line emphasizes $z = 10$; early stars at this redshift can potential explain the CIB excess. The horizontal dot-dashed black line indicated $f_{\rm Halo} = 0.16$; as discussed in the text, a model explains the CIB observations for reasonable ϵ and f_* values only if $f_{\rm Halo}$ takes this value for star-forming halos. ($\mathcal{R}$ and $\delta_{B,0}$ take the same values as in Fig. 5.6.)

black dot-dashed line at $f_{\rm halo} = 0.16$. In the scenario calculated with the Higgs relaxation isocurvature perturbations, the $10^6 M_\odot$ line indeed passes near $f_{\rm halo} = 0.16$ at $z = 10$ if we take $k_s = 65\,{\rm Mpc}^{-1}$ (yellow). As expected from the above discussion, $k_s = 30\,{\rm Mpc}^{-1}$ (blue) results in a larger percentage of the mass in collapsed halos and $k_s = 100\,{\rm Mpc}^{-1}$ (green) a smaller percentage. In the scenario which includes only adiabatic perturbations, the $f_{\rm Halo}$ line for $10^6 M_\odot$ is significantly suppressed; this is the source of the claim that unreasonably large radiation efficiency or star formation efficiency is required in the standard picture. We see that for $k_s \approx 65\,{\rm Mpc}^{-1}$ a sufficiently large percentage of the mass is in halos $\sim 10^6 M_\odot$ to account for the inferred contribution from early stars to the isotropic CIB flux.

Finally, we note that the isotropic CIB flux from early stars is inferred from the anisotropic flux measured at scales of 5 arcminutes, corresponding to $k \sim 0.45$ Mpc^{-1}, which is much

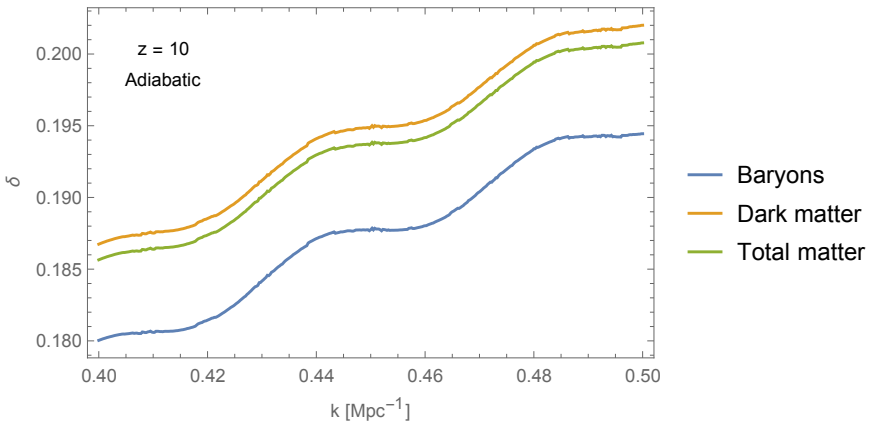

Figure 5.8: The density contrast at scales $k = 0.40$ Mpc^{-1} to $k = 0.50$ Mpc^{-1}, for which only the adiabatic perturbations contribute. The lines show the baryonic, dark matter, and total matter perturbations. $k \sim 0.45$ Mpc^{-1} corresponds to the 5 arcmin scale probed observationally.

smaller than $k_s = 65$ Mpc^{-1}. Therefore, only adiabatic modes contribute at this scale; the density contrast is shown in Fig. 5.8. We see that at $k \sim 0.45$ Mpc^{-1} the density contrast is $\sim 10\%$, consistent with the calculations in [140] and for similar reasons, consistent with the observational anisotropic data. (Note that although there is a difference between two-dimensional and three-dimensional power spectra, the difference should be order 1.) Therefore, the isocurvature perturbations considered here explain the inferred contribution of the early stars to the isotropic CIB excess without overproducing an anisotropic contribution.

To summarize, in our model, structure is generated by adiabatic perturbations at the large scale and the isocurvature perturbations at smaller scales. The isocurvature perturbations are responsible for causing more halos ($10^6 M_\odot$) to evolve nonlinearly, and hence, we make a sufficient number of stars to explain the isotropic CIB radiation inferred from the anisotropic measurements without a large stellar formation efficiency. However, these halos are distributed in accordance with the larger-scale adiabatic perturbations, and the scale of the CIB anisotropy is accounted for by this larger-scale structure. This provides an elegant solution as to the source of the observed CIB radiation fluctuations.

We also remark that in general, the early creation of population III stars is constrained

by the optical depth measurements of the CMB. We note that recent analyses of the Planck 2015 optical depth data in fact prefers early star formation, particularly if one includes self-regulated population III stars [158]. If star formation occurred much earlier than $z = 10$, as for $k_s \lesssim 30\,\mathrm{Mpc}^{-1}$, then this scenario would conflict with optical depth measurements. However, as noted, for $k_s = 65\,\mathrm{Mpc}^{-1}$ the star formation occurs around $z = 10$.

5.6 Available Parameter Space

In this section, we present plots of the parameter space in which Higgs relaxation leptogenesis can both explain the observed matter-antimatter asymmetry of the universe and the observations of the cosmic infrared background radiation. We note that Higgs relaxation leptogenesis is only one potential source of baryonic isocurvature perturbations; other sources include curvaton models (proposed in [159–161]; see also [162–165]) and warm inflation (e.g., [166, 167]). In general, any model which produces baryonic isocurvature perturbations similar to those discussed above can account for the observed CIB excess.

In these plots, we choose N_{last}, Λ_I, and Γ_I such that $k_s = 65\ \mathrm{Mpc}^{-1}$; then we determine the initial vacuum expectation value of the Higgs field using Eq. (5.6), which includes the curvature of the Higgs potential. As discussed in Sec. 5.3, and shown explicitly in Fig. 5.2, this leads to $\delta_B(k/k_s = 1.4) \approx 0.025$ throughout parameter space, sufficient to explain the CIB observations. (Regions where the requisite initial VEV probes the second vacuum in the Higgs potential are denoted on the plots.) We note that we include one-loop corrections to the Higgs potential and two-loop corrections to the running couplings; for details regarding the potential (including the specific values for the Higgs mass and top quark mass used), please see the Higgs relaxation leptogenesis analysis in [2].

As discussed in [1–3], there are several different mechanisms of generating the $\mathcal{O}_6$ operator; one can use thermal loops, leading the scale $\Lambda_n \sim T$, or one can introduce heavy fermions, leading to a scale $\Lambda_n \sim M_n$, a constant. The parameter space for these two options was explored extensively in Ref. [2], with the result that when the initial Higgs vacuum ex-

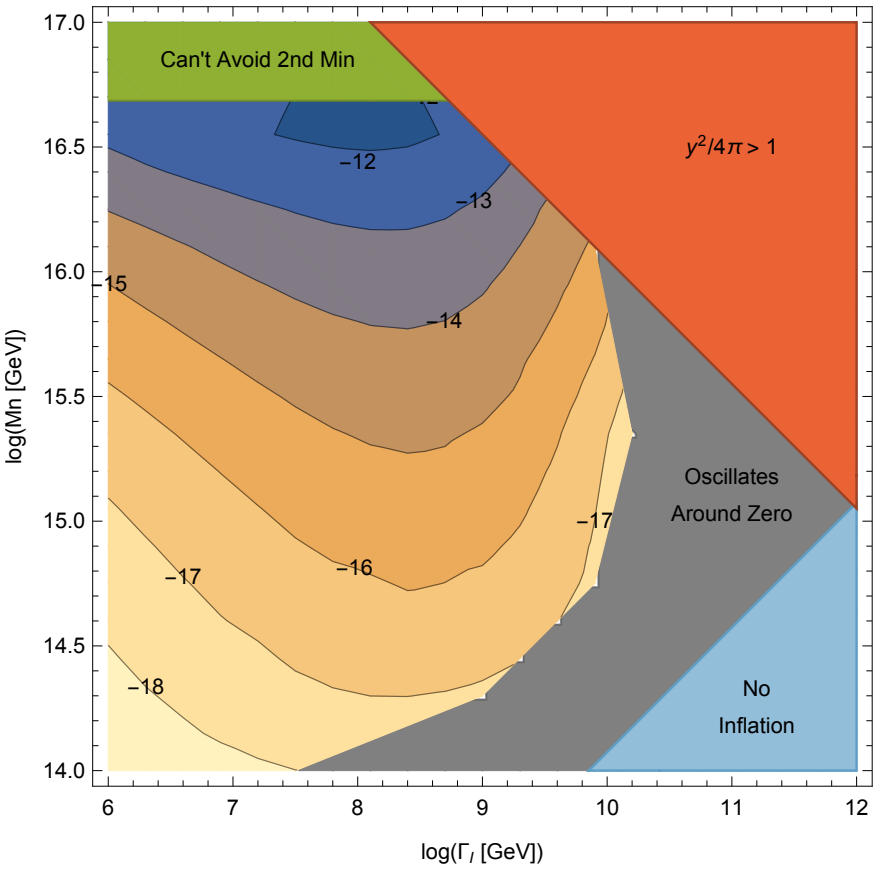

Figure 5.9: The lepton-number-to-entropy ratio, Y, from Higgs relaxation leptogenesis, with $N_{\rm last}$ set in order to explain the CIB excess and with the effective operator (5.1) generator by thermal loops, so that $\Lambda_n \sim T$. In the upper left corner, the $N_{\rm last}$ required to explain the CIB excess is such that the Higgs VEV probes the second minimum in the Higgs potential. In the lower right, $\Gamma_I > 3H_I$ and inflation is not successful. In the gray region, washout is sufficiently large to cause the lepton asymmetry to oscillate around zero at the end of our numerical analysis; the final value will be quite small. As in Refs. [2, 4], the neutrino Yukawa coupling is chosen to suppress thermal leptogenesis; in the upper right of the plot, this condition leads into the nonperturbative regime. We see the parameter space for generating sufficient lepton asymmetry is constrained in this case.

pectation value was set by quantum fluctuations, the largest lepton-asymmetry-to-entropy ratio that was possible with $\Lambda_n \sim T$ was $Y \sim 10^{-12}$ (Fig. 12 of Ref. [2]), while for $\Lambda_n \sim M_n$, parameter space was available, but in the regime in which the use of effective field theory to describe the $\mathcal{O}_6$ operator was questionable.

We mentioned above that in Refs. [1, 2, 4], we took $N_{\rm last} = 8$ out of an abundance of caution to avoid baryonic isocurvature constraints, but the actual limit is much weaker. Here, $N_{\rm last}$ is set by (5.18), which is generally larger ($N_{\rm last} \sim 40$ typically). As explained in Appendix D.1, the final asymmetry is proportional to ϕ_0^2, which grows as $N_{\rm last}$ in the limit of a flat potential. [However, in our numerical analysis, we use Eq. (5.6) which accounts for the curvature of the potential.] Therefore, we expect the asymmetry to be enhanced as compared to our previous analysis, although not significantly.

This is illustrated for the $\Lambda_n = T$ case in Fig. 5.9. This figure shows contours of the lepton asymmetry to entropy ratio Y; regions with $Y \gtrsim 10^{-9}$ can account for the observed baryonic matter-antimatter asymmetry of the universe. (We note that the original lepton asymmetry is redistributed between leptons and baryons by sphalerons.) As compared to Fig. 12 of Ref. [2], the asymmetry is enhanced by about a little less than an order of magnitude; however, this is not sufficient to ensure a region of parameter space in which both a sufficiently large asymmetry is generated and the CIB excess is explained.

Therefore, we turn our attention to Fig. 5.10, which instead has $\Lambda_n = M_n$, a constant. We see that a sufficiently large asymmetry is generated for a wide range of inflaton couplings Γ_I provided that the scale M_n is small enough; the upper bound on M_n becomes stronger as the inflation scale Λ_I decreases. Decreasing Λ_I decreases the asymmetry, if M_n and Γ_I are held constant.

The red and gray lines illustrate where M_n, the scale in the $\mathcal{O}_6$ effective operator, becomes less than ϕ_0 and $T_{\rm max}$ respectively. Below these lines, the use of effective field theory for $\mathcal{O}_6$ is somewhat questionable. This is not surprising as the same remark applied to the parameter space plots presented in [2, 4]. As discussed in [2], although the effective field theory description is questionable, we use it as an approximation as what would be found if

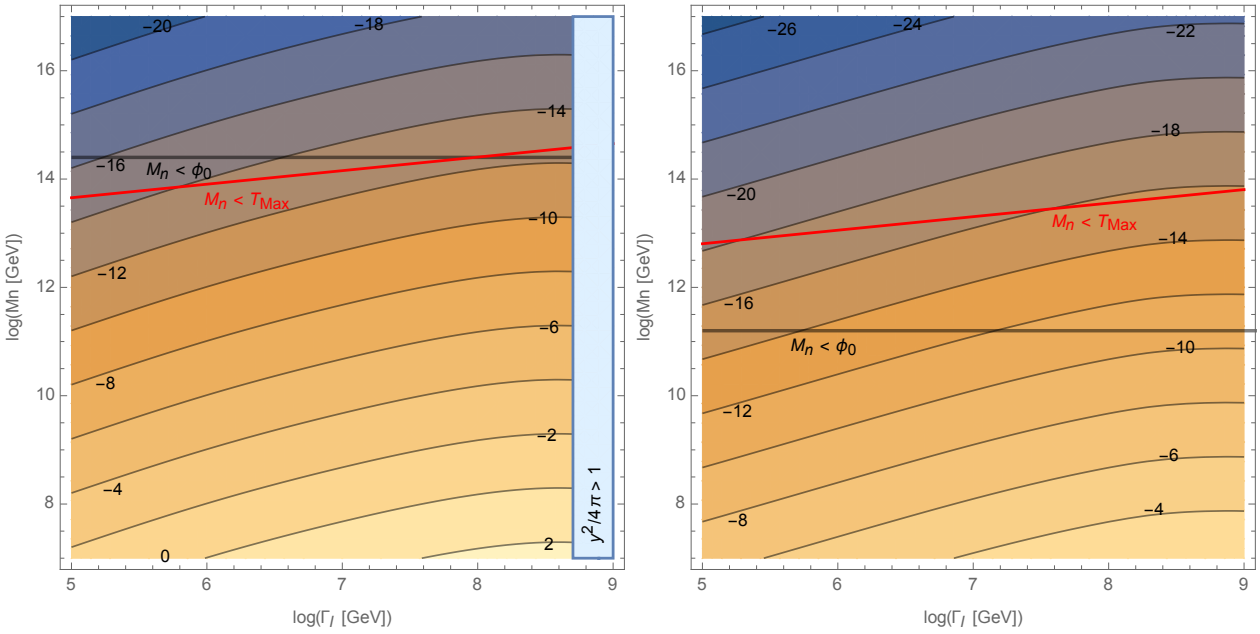

Figure 5.10: The lepton-number-to-entropy ratio, Y, from Higgs relaxation leptogenesis, with $N_{\rm last}$ set in order to explain the CIB observations and with the effective operator (5.1) generator by new massive particles, so that $\Lambda_n \sim M_n$. For these plots, $\Lambda_I = 5 \times 10^{16}\,\text{GeV}$ (left) and $\Lambda_I = 10^{15}\,\text{GeV}$ (right). As in Refs. [2, 4], the neutrino Yukawa coupling is chosen to suppress thermal leptogenesis; for sufficiently large Γ_I, this condition leads into the non-perturbative regime. We see that as sufficiently large asymmetry is generated, but in the regime in which the use of effective field theory with the operator (5.1) is questionable.

an exact calculation in some UV-complete theory were done. It was also shown in Ref. [4] that this can be avoided in models with an extended scalar sector.

Subject to this caveat regarding the effective theory, we conclude that Higgs relaxation leptogenesis can successfully generate the observed matter-antimatter asymmetry while also generating isocurvature perturbations which enhance early star formation, explaining the observed CIB excess. Thus, Higgs relaxation leptogenesis is a promising source for the desired baryonic isocurvature perturbations.

5.7 Conclusion for Chapter 5

In this chapter, we have demonstrated that baryonic isocurvature perturbations at very small scales can cause halos of mass $10^6 M_\odot$ to collapse earlier than they would in the typical model of structure formation, which includes only adiabatic perturbations from inflation. Since these halos can support the formation of population III stars, this leads to enhanced star formation in the early universe. Therefore, the power in the fluctuations of the cosmic infrared background radiation measured by the Spitzer and AKARI space telescopes can be explained without invoking unreasonably large stellar formation efficiency or radiation efficiency.

As a source for these perturbations, we have used the Higgs relaxation leptogenesis model, in which the matter-antimatter asymmetry is produced via lepton-number-violating interactions in a plasma influenced by a time-dependent chemical potential produced by the relaxing Higgs vacuum expectation value. If the initial vacuum expectation value of the Higgs field is set by quantum fluctuations, it will vary in different Hubble volumes, giving rise to slightly different baryon asymmetries. These are the desired isocurvature perturbations. The scale of these perturbations is set by number of e-folds the Higgs VEV grows through; we determined that we can explain the CIB observations if isocurvature perturbations exist for $k \gtrsim 65\ \mathrm{Mpc}^{-1}$. Finally, we illustrated the parameter space in which the Higgs relaxation model gives both successful leptogenesis and explains the CIB observations.

APPENDIX A

Vacuum Expectation Value for Scalar Fields with Polynomial Potential during Inflation

In Sec. 1.1.2, we have discussed that during inflation a scalar field can obtain a large VEV via quantum fluctuation. The VEV that a scalar field can obtain is such that $V\left(\sqrt{\langle\phi^2\rangle}\right) \sim H^4$. In this appendix, we strengthen this point by calculating the equilibrium VEV of ϕ with the potential of the general form

$$V(\phi) = \beta_n \phi^{2n} \quad , \quad n \in \mathbb{N}. \tag{A.1}$$

We consider only even function as $V(\phi)$ so that the potential is bounded from below. As we have explained in Sec. 1.1.2, the Fokker-Planck equation for a general potential in equilibrium can reduce to

$$\frac{\partial P(\phi)}{\partial \phi} = -\frac{8\pi^2}{3H^4} P(\phi) \frac{dV(\phi)}{d\phi}, \tag{A.2}$$

which give the equilibrium probability distribution as

$$P(\phi) = N \exp\left[-\frac{8\pi^2}{3H^4} V(\phi)\right] = N \exp\left(-\frac{8\pi^2}{3H^4}\beta_n \phi^{2n}\right). \tag{A.3}$$

Since the $V(\phi)$ is even under $\phi \to -\phi$, the expectation value $\langle\phi\rangle$ vanishes. Thus, we are interested in the expectation value of ϕ^2

$$\left\langle \phi^2 \right\rangle = \frac{\int \phi^2 P(\phi)\, d\phi}{\int P(\phi)\, d\phi}, \tag{A.4}$$

which can be computed by evaluating the integral of the form

$$W_m \equiv \int_{-\infty}^{\infty} P(\phi)\, \phi^m d\phi. \tag{A.5}$$

Defining $\alpha \equiv 8\pi^2/3H^4$, we have

$$W_m = N\int_{-\infty}^{\infty} \exp\left(-\alpha\beta_n\phi^{2n}\right)\phi^m d\phi = 2N\int_0^{\infty} \exp\left(-\alpha\beta_n\phi^{2n}\right)\phi^m d\phi. \tag{A.6}$$

Rescale $x \equiv \alpha\beta_n\phi^{2n}$, which gives $\phi = (x/\alpha\beta_n)^{1/2n}$, and

$$d\phi = \frac{1}{2n}\left(\frac{1}{\alpha\beta_n}\right)^{\frac{1}{2n}} x^{\frac{1}{2n}-1}dx. \tag{A.7}$$

Then one can find the close form for the integral W_m

$$W_m = \frac{N}{n}\left(\frac{1}{\alpha\beta_n}\right)^{\frac{m+1}{2n}}\int_0^{\infty} e^{-x}x^{\frac{m+1}{2n}-1}dx = \frac{N}{n}\left(\frac{1}{\alpha\beta_n}\right)^{\frac{m+1}{2n}}\Gamma\left(\frac{m+1}{2n}\right), \tag{A.8}$$

where $\Gamma(z)$ is the gamma function. The expectation value of ϕ^2 is then given by

$$\left\langle\phi^2\right\rangle = \frac{W_2}{W_0} = \left(\frac{3H^4}{8\pi^2\beta_n}\right)^{1/n}\frac{\Gamma\left(\frac{3}{2n}\right)}{\Gamma\left(\frac{1}{2n}\right)}, \tag{A.9}$$

as presented in Eq. (1.30). We then refer to the VEV of ϕ as $\phi_0 = \sqrt{\langle\phi^2\rangle}$ since $\langle\phi\rangle$ vanishes.

For a massive non-interacting scalar field with $V(\phi) = \frac{1}{2}m^2\phi^2$ potential, we have $n = 1$ and $\beta_n = \frac{1}{2}m^2$. Since $\Gamma\left(\frac{3}{2}\right)/\Gamma\left(\frac{1}{2}\right) = \frac{1}{2}$, the expectation value of ϕ^2 is

$$\left\langle\phi^2\right\rangle = \frac{3H^4}{8\pi^2m^2}, \tag{A.10}$$

as used in Eq. (1.27). The VEV of ϕ is

$$\sqrt{\langle\phi^2\rangle} = \sqrt{\frac{3}{8\pi^2}}\frac{H^2}{m} \approx 0.19\frac{H^2}{m}, \tag{A.11}$$

which accords with the claim that $V(\phi_0) \sim H^4$. For a massless interacting scalar field with $V(\phi) = \frac{1}{4}\lambda\phi^4$ potential, we have $n = 2$ and $\beta_n = \lambda/4$. The expectation value ϕ^2 is [12]

$$\left\langle\phi^2\right\rangle = \sqrt{\frac{3}{2\pi^2\lambda}}H^2\frac{\Gamma(3/4)}{\Gamma(1/4)}. \tag{A.12}$$

The corresponding equilibrium VEV of ϕ is

$$\sqrt{\langle\phi^2\rangle} = \sqrt{\frac{\Gamma(3/4)}{\Gamma(1/4)}}\left(\frac{3}{2\pi^2\lambda}\right)^{1/4}H \approx 0.36\frac{H}{\lambda^{1/4}}, \tag{A.13}$$

which also agrees with $V(\phi_0) \sim H^4$.

APPENDIX B

Appendices for Relaxation Leptogenesis

B.1 Interpretting the $\mathcal{O}_6$ Operator as an External Chemical Potential

In section 2.2, we remarked that the $\mathcal{O}_6$ operator in equation (2.12) acts like an external chemical potential. In this appendix, we explain why this is so and how this leads to a number density asymmetry in chemical equilibrium.

This $\mathcal{O}_6$ operator induces a term proportional to $(\partial_0\phi^2)/\Lambda_n^2 j^0_{B+L}$ in the Lagrangian. If ϕ is treated as an external field (which we discuss further below), then this produces a term of the form $-(\partial_0\phi^2)/\Lambda_n^2 j^0_{B+L}$ in the Hamiltonian, which has the appropriate form $-\mu_{\text{eff}} j^0_{B+L}$.

A term similar to this, using the phase of the Higgs VEV is frequently used in spontaneous baryogenesis scenarios, in which the phase of the Higgs VEV is used instead of its magnitude (e.g., [168]),

$$\mathcal{O}_6' = (\partial_t\theta) j^0_{B+L}. \tag{B.1}$$

However, in such scenarios, the asymmetry is produced via the decay of the Higgs condensate, and therefore, it is not appropriate to treat θ as an external degree of freedom. When the Hamiltonian is determined using

$$\mathcal{H} = \sum_i \frac{\partial \mathcal{L}}{\partial \dot{\phi}_i}\dot{\phi}_i - \mathcal{L}, \tag{B.2}$$

there is no contribution from $\mathcal{O}_6'$. Although an asymmetry may be produced in such cases [123, 124, 169], it is not appropriate to interpret $\dot{\theta}$ as a chemical potential.

In the scenario we consider in this work, the time scale for the reactions which maintain

the thermal distribution of the plasma is smaller than that of the evolution of the Higgs VEV. Therefore, for purposes of asymmetry generation, it is reasonable to consider the Higgs VEV as a background field, in which case it is appropriate to consider this as a chemical-potential-like term [169], as we explain below.

The $\mathcal{O}_6$ operator shifts $i\partial_0 \to i\partial_0 - (\partial_0\phi^2)/\Lambda_n^2$ in the Lagrangian. Consequently, the asymptotically free eigenfunctions are $\sim \exp(\mp i(E \mp (\partial_0\phi^2)/\Lambda_n^2)t)$, which justifies our comment that this is equivalent to decreasing the energy of particles by $E_0 = (\partial_0\phi^2)/\Lambda_n^2$ and increasing the energy of antiparticles by the same amount.

If we use the ideal gas approximation, then the phase space densities are

$$\begin{aligned} f_p &= \exp(-(E - E_0 - \mu_p)/T) \\ f_{\bar{p}} &= \exp(-(E + E_0 - \mu_{\bar{p}})/T) \end{aligned} \tag{B.3}$$

The number densities of particles and antiparticles can be found in the normal manner, using

$$\begin{aligned} n_p &= \int \frac{d^3p}{(2\pi)^3} \exp(-(E - E_0 - \mu_p)/T) \\ n_{\bar{p}} &= \int \frac{d^3p}{(2\pi)^3} \exp(-(E + E_0 - \mu_{\bar{p}})/T) \end{aligned} \tag{B.4}$$

If we use the non-relativistic relation $E = p^2/2m$, then we find

$$\begin{aligned} \mu_p &= -E_0 + T\ln(\lambda^3 n_p) \\ \mu_{\bar{p}} &= E_0 + T\ln(\lambda^3 n_{\bar{p}}), \end{aligned} \tag{B.5}$$

where $\lambda = \sqrt{2\pi mT}$. In the above relation, the first term can be interpretted as an external chemical potential (due to the "driving" effect of the $\mathcal{O}_6$ operator), while the $T\ln(\lambda^3 n_p)$ is the usual chemical potential of an ideal gas.

If a lepton-number-violating process or baryon-number-violating establishes chemical equilibrium between the species, then the chemical potentials will be equal, $\mu_p = \mu_{\bar{p}}$. This gives the expected result

$$\frac{n_p}{n_{\bar{p}}} = e^{2E_0/T}. \tag{B.6}$$

A similar result can be derived using the relativistic relation $E = p$ instead.

B.2 Calculation of Lepton-Number-Violating Cross Section and Reaction Rate

In this section, we calculate the cross section and reaction rate for the processes shown in Fig. 2.1, assuming a thermal number density for Higgs bosons and neutrinos, as discussed in Section 2.3. This improves the order of magnitude estimates used in [1]. As explained in the text, we can use the approximate cross section with the energy shift due to the $\mathcal{O}_6$ operator set equal to zero. In this approximation, the reaction rates for processes with neutrinos and antineutrinos are equal.

The top two diagrams of Fig. 2.1 are the s- and t-channel diagrams of the process $h^0\nu \to h^0\bar{\nu}$, whereas the bottom diagram describes the process $\nu\nu \to h^0h^0$. The s-channel has a resonance at $E \sim M_R$; however, the typical energy scale T is far beneath this. For completeness, we include the resonance, although it will have negligible effect. In calculating these cross sections, we follow the conventions of [170] for the Feynman rules of Majorana fermions.

The matrix element for the $\nu_\ell h^0 \to \bar{\nu}_L h^0$ process is

$$-i\mathcal{M} = i\sum_i \frac{Y_{Li}Y_{i\ell}^*}{2}\left[\frac{M_{Ri} - i\Gamma_i/2}{s - M_{Ri}^2 + i\Gamma_i M_{Ri} + \Gamma_i^2/4} + \frac{M_{Ri} - i\Gamma_i/2}{t - M_{Ri}^2 + i\Gamma_i M_{Ri} + \Gamma_i^2/4}\right] \times x_{L\alpha}(p_1, s_1)y_\ell^\beta(p_4, s_4)\delta_\beta^\alpha, \tag{B.7}$$

where s and t are the Mandelstam variables, and Γ_i is the width of the right-handed Majorana neutrino. (For a discussion of Breit-Wignar propagators, see [171]). The indices 1, 2, 3, and 4 refer to the incoming neutrino, incoming Higgs boson, outgoing Higgs boson, and outgoing antineutrino, in that order. The index i indicates a sum over the heavy right-handed Majorana neutrinos. Let us define

$$\begin{aligned} A_i &= s - M_{Ri}^2 + \Gamma_i^2/4, \\ B_i &= t - M_{Ri}^2 + \Gamma_i^2/4, \\ C_i &= \Gamma_i M_{Ri}. \end{aligned} \tag{B.8}$$

Then the matrix element squared, summed over both the initial and final spin states (as discussed in [75]), is

$$\sum_{s_1,s_2}|\mathcal{M}|^2=\sum_i 2p_1\times p_4\frac{|Y_{Li}|^2|Y_{i\ell}|^2}{4}\left(M_{Ri}^2+\frac{\Gamma_i^2}{4}\right)\times \left[\frac{1}{A_i^2+C_i^2}+\frac{1}{B_i^2+C_i^2}+\frac{2(A_iB_i+C_i^2)}{(A_iB_i+C_i^2)^2+C_i^2(A_i-B_i)^2}\right]. \tag{B.9}$$

In the center of mass reference frame, the cross section is

$$\sigma_{CM}(s)=\frac{1}{16\pi}\sum_i\frac{|Y_{Li}|^2|Y_{i\ell}|^2}{4}\left(M_{Ri}^2+\frac{\Gamma_i}{4}\right) \times\int_{-s}^0 dt\,(s+t)\left[\frac{1}{A_i^2+C_i^2}+\frac{1}{B_i^2+C_i^2}+\frac{2(A_iB_i+C_i^2)}{(A_iB_i+C_i^2)^2+C_i^2(A_i-B_i)^2}\right]. \tag{B.10}$$

Generically, the thermally averaged cross section is related to the CM cross section by [172]

$$\langle\sigma v\rangle_0=\frac{1}{8T\times m_1^2K_2(m_1/T)\times m_2^2K_2(m_2/T)} \times\int_{(m_1+m_2)^2}^\infty\frac{[s-(m_1-m_2)^2][s-(m_1+m_2)^2]}{\sqrt{s}}K_1(\sqrt{s}/T)\sigma_{CM}(s), \tag{B.11}$$

and so the thermally averaged cross section for $h^0\nu\to h^0\bar{\nu}$ is

$$\left\langle\sigma(h^0\nu\to h^0\bar{\nu})v\right\rangle_0=\sum_i\frac{|Y_{Li}|^2|Y_{i\ell}|^2}{512\pi}\left(M_{Ri}^2+\frac{\Gamma_i}{4}\right)\int_0^x dx\int_0^x dy(x^2-y^2)K_1(x) \left[\frac{1}{(x^2T^2-M_{Ri}^2+\Gamma_i^2/4)^2+\Gamma_i^2M_{Ri}^2}+\frac{1}{(y^2T^2+M_{Ri}^2-\Gamma_i^2/4)^2+\Gamma_i^2M_{Ri}^2} -\frac{2((x^2T^2-M_{Ri}^2+\Gamma_i^2/4)(y^2T^2+M_{Ri}^2-\Gamma_i^2/4)-\Gamma_i^2M_{Ri}^2)}{((x^2T^2-M_{Ri}^2+\Gamma_i^2/4)(y^2T^2+M_{Ri}^2-\Gamma_i^2/4)-\Gamma_i^2M_{Ri}^2)^2+\Gamma_i^2M_{Ri}^2(x^2+y^2)^2T^4}\right] \tag{B.12}$$

where we have introduced the dimensionless variables $x\equiv\sqrt{s}/T$ and $y\equiv\sqrt{-t}/T$. Since the temperature evolves in time, the cross section also does; however, when expanded in powers of T/M_{Ri}, the lowest order contribution is $\sim 1/M_{Ri}^2$, as expected. Repeating the same steps with the $\nu_\ell\nu_L\to h^0h^0$ cross section, which does not have a resonance, gives

$$\left\langle\sigma(\nu_\ell\nu_L\to h^0h^0)v\right\rangle_0=\sum_i\frac{|Y_{Li}|^2|Y_{i\ell}|^2}{64\pi M_{Ri}^2}. \tag{B.13}$$

The reaction rates are related to these cross sections by

$$\gamma_0^{eq}\left(\alpha\beta \to \gamma\delta\right) = n_{\alpha,0}^{eq} n_{\beta,0}^{eq} \left\langle \sigma\left(\alpha\beta \to \gamma\delta\right) v \right\rangle_0 , \tag{B.14}$$

which holds for any $2 \to 2$ process. Since we take $E_0 = 0$ in this section, the number densities for Higgs bosons, neutrinos, and antineutrinos are all equal to $n_0^{eq} \approx T^3/\pi^2$, and so for both processes,

$$\gamma_0^{eq} = \frac{T^6}{\pi^4} \left\langle \sigma v \right\rangle_0 . \tag{B.15}$$

As noted in the text, in order to simplify the calculation, we will consider only the case in which the flavor indices ℓ and L are equal, and the contribution of a single right-handed neutrino dominates. Its decay rate is $\Gamma \simeq y^2 M_R/16\pi$, from the only decay $N_R \to h^0 \nu_L$.

APPENDIX C

Lepton-Number-Violating Cross Section in the EGH Model

In Sec. 3.3.4, we remarked that the thermally averaged cross section of the lepton-number-violating processes in the EGH model is enhanced by a factor of 16 in comparison to the SM Higgs case. In this appendix, we discuss the calculation of the cross section, including this prefactor. The lepton-number-violating processes that we consider are (i) $\nu_L\phi_i \leftrightarrow \bar{\nu}_L\phi_j$ and (ii) $\nu_L\nu_L \leftrightarrow \phi_i\phi_j$ as shown in Fig. 3.1. The scalar fields that are involved in these processes are $\phi_i = \left\{\sigma,\, \Pi_4,\, \Theta,\, \tilde{\Pi}_4,\, \Pi_3,\, \tilde{\Pi}_3\right\}$. Their cross sections depend on the Yukawa couplings to LH and RH neutrinos, which can be read from Eq. (3.10) as

$$Y_i^\nu = \left\{Y^\nu \sin\theta,\, Y^\nu \cos\theta,\, iY^\nu \sin\theta,\, iY^\nu \cos\theta,\, iY^\nu,\, Y^\nu\right\}, \tag{C.1}$$

respectively.

For the (i) $\nu_L\phi_i \leftrightarrow \bar{\nu}_L\phi_j$ channel, the cross section depends on Y_i^ν as $\sigma\left(\nu_L\phi_i \to \bar{\nu}_L\phi_j\right) \propto \left|Y_i^\nu\right|^2 \left|Y_j^\nu\right|^2$. Summing the contribution from each i and j, the thermally averaged cross section from the channel (i) is

$$\left\langle\sigma v\right\rangle_{\text{(i)}} = \sum_{i,j} \left\langle\sigma\left(\nu_L\phi_i \leftrightarrow \bar{\nu}_L\phi_j\right) v\right\rangle = \frac{\left\langle\sigma\left(\nu_L\phi \leftrightarrow \bar{\nu}_L\phi\right) v\right\rangle}{\left|Y^\nu\right|^4} \sum_{i,j} \left|Y_i^\nu\right|^2 \left|Y_j^\nu\right|^2 \tag{C.2}$$

$$= 16 \left\langle\sigma\left(\nu_L\phi \leftrightarrow \bar{\nu}_L\phi\right) v\right\rangle, \tag{C.3}$$

where ϕ is a Standard Model-like scalar with the Yukawa coupling $|Y^\nu|$ to LH and RH neutrinos, and $\left\langle\sigma\left(\nu_L\phi \leftrightarrow \bar{\nu}_L\phi\right) v\right\rangle$ can be obtained from Eq. (3.35).

For the (ii) $\nu_L\nu_L \leftrightarrow \phi_i\phi_j$ channel, one has to consider the symmetry factor due to the

identical outgoing particles. The CM cross section in the limit $T \ll M_R$ is approximated as

$$\sigma\left(\nu_L\nu_L \to \phi_i\phi_j\right) \approx \frac{1}{4\pi S}\frac{\left|Y_i^\nu\right|^2\left|Y_j^\nu\right|^2}{M_R^2}, \tag{C.4}$$

where the symmetry factor $S = 2$ if $i = j$, and $S = 1$ if $i \neq j$. Summing different outgoing particles, the net CM cross section is

$$\sum_i\sum_{j\geq i}\sigma\left(\nu_L\nu_L \to \phi_i\phi_j\right) = \sum_i\left[\sigma\left(\nu_L\nu_L \to \phi_i\phi_i\right) + \sum_{j>i}\sigma\left(\nu_L\nu_L \to \phi_i\phi_j\right)\right] \tag{C.5}$$

$$= \frac{\sigma\left(\nu_L\nu_L \to \phi\phi\right)}{\left|Y^\nu\right|^4}\sum_i\left(\left|Y_i^\nu\right|^4 + 2\sum_{j>i}\left|Y_i^\nu\right|^2\left|Y_j^\nu\right|^2\right) \tag{C.6}$$

$$= \frac{\sigma\left(\nu_L\nu_L \to \phi\phi\right)}{\left|Y^\nu\right|^4}\sum_{i,j}\left|Y_i^\nu\right|^2\left|Y_j^\nu\right|^2 \tag{C.7}$$

$$= 16\,\sigma\left(\nu_L\nu_L \to \phi\phi\right), \tag{C.8}$$

where again ϕ denotes a Standard-Model like scalar which has a coupling constant Y^ν [which is related to the couplings of the EGH scalars via equation (C.1)]. Again, we see the enhancement by the factor of 16,

$$\left\langle\sigma v\right\rangle_{\text{(ii)}} = \sum_i\sum_{j\geq i}\left\langle\sigma\left(\nu_L\nu_L \leftrightarrow \phi_i\phi_j\right)v\right\rangle = 16\left\langle\sigma\left(\nu_L\nu_L \leftrightarrow \phi\phi\right)v\right\rangle. \tag{C.9}$$

APPENDIX D

Appendices for the Relaxation Leptogenesis, Isocurvature Perturbations, and the Cosmic Infrared Background

D.1 Relationship between Lepton Number Density and Initial Higgs VEV

Within the Higgs relaxation leptogenesis paradigm, the generation of the asymmetry can occur through several mechanisms, even when the lepton-number-violating operator appears in the neutrino sector due to heavy right-handed Majorana states. The asymmetry can be generated through particle production from the condensate as described by the Bogoliubov transformations [3], or via lepton-number-violating scatterings occurring in the plasma, e.g., [1, 2]. In this work, we are interested in the latter scenario, which requires a rapid production of plasma, perhaps even via some preheating mechanism. This in turn entails that the thermal corrections to the Higgs potential, $\sim T^2\phi^2$, tend to be large.

In this case, the Higgs VEV relaxes rather rapidly, and throughout all of the parameter space shown in Figs. 5.9 and 5.10, the relaxation time scale is faster than the reheat time scale, determined by the decay rate of the inflaton. This raises the concern that relaxation may proceed faster than the thermalization of the plasma, and therefore, that the finite temperature corrections to the Higgs potential are unreliable during relaxation.

According to Ref. [173], the thermalization time scale is

$$t_{\rm th} \approx \alpha^{-16/5} \frac{m_I^{4/5}}{M_{Pl}^{3/5} \Gamma_I^{6/5}}, \tag{D.1}$$

where m_I is the mass of the inflaton field, which is thus far undetermined in the Higgs relaxation scenario. We note that for successful reheating, the inflaton must have available decay channels, despite the relatively large Higgs VEV ϕ_0. However, even at values $m_I \sim 10^{-5}\phi_0$ the inflaton is able to efficiently decay into electrons. We have verified that in this limit, the thermalization time scale is faster than the relaxation time scale (using $\alpha \approx 1/40$ for the coupling, which accounts for its running at high scales). Thus, it is consistent to consider the regime in which the relaxation time scale is less than the reheat time scale, $t_{\rm rlx} < t_{RH}$, and also that the Higgs potential during relaxation is dominated by the $T^2\phi^2$ thermal correction.[1]

Therefore, we here consider only the case that the effective potential of the scalar field is dominated by the thermal mass term

$$V(\phi, T) = \frac{1}{2}\alpha_T^2 T^2 \phi^2. \tag{D.2}$$

For the standard model Higgs field, the coefficient is $\alpha_T \approx \sqrt{\left(\lambda + \frac{9}{4}g^2 + \frac{3}{4}g'^2 + 3h^2\right)/12} \approx 0.33$ at the energy scale $\mu \approx 10^{13}\,\text{GeV}$. During the epoch of coherent oscillations of the inflaton, the energy density of the radiation as a function of time can be described by

$$\rho_r(t) = \frac{m_{pl}^2 \Gamma_I}{10\pi\,(t + t_{\rm osc})} \left[1 - \left(\frac{t_{\rm osc}}{t + t_{\rm osc}}\right)^{5/3}\right], \tag{D.3}$$

where $t_{\rm osc} = \frac{2}{3}\sqrt{\frac{3}{8\pi}} m_{pl}/\Lambda_I^2$ and Γ_I is the decay rate of the inflaton. At all times we use an effective temperature for the plasma given by $\rho_r = \pi^2 g_* T^4/30$; as discussed, this is valid for $t > t_{th}$.

For $t_{\rm osc} < t < t_{RH}$, we approximate the temperature of the plasma by

$$T(t) \simeq T_{RH} \left(\frac{t_{RH}}{t}\right)^{1/4}, \tag{D.4}$$

[1] We note that for $\phi_0 \gg m_I$, the Higgs bosons that participate in the scattering $h^0\nu \leftrightarrow h^0\bar{\nu}$ are produced via the thermalization of the plasma. We also emphasize that we ensure that throughout the relaxation period, the energy density in the inflaton and produced radiation is greater than the energy density in the Higgs condensate.

where the reheat temperature is $T_{RH} \approx (3/\pi^3)^{1/4} g_{*S}^{-1/4}(T_{RH}) \sqrt{m_{pl}\Gamma_I}$ and $t_{RH} = 1/\Gamma_I$ is the time when reheating is complete. For times between $t_{\rm osc}$ and t_{RH}, the equation of motion for the scalar field is then

$$\ddot{\phi}(t) + \frac{2}{t}\dot{\phi}(t) + \alpha_T^2 \frac{T_{RH}^2 \sqrt{t_{RH}}}{\sqrt{t}} \phi(t) = 0 \tag{D.5}$$

if the thermal corrections dominate the effective potential, and we have taken $H(t) \approx 2/3t$ since during the epoch in which the inflaton undergoes coherent oscillation the universe evolves as if it were matter dominated. We can rescale $\phi(t = x t_{RH}) = \phi_0 y(x)$ and $t = x t_{RH}$ to rewrite Eq. (D.5) as

$$y''(x) + \frac{2}{x} y'(x) + \frac{\alpha_T^2 \beta^2}{\sqrt{x}} y(x) = 0, \tag{D.6}$$

where $\beta = T_{RH} t_{RH} = 6.06 \times 10^4 \left(\frac{10^8 \text{GeV}}{\Gamma_I}\right)^{1/2}$. The independent solutions for Eq. (D.6) are

$$y_1(x) = \left(\frac{3}{2}\right)^{2/3} \Gamma\left(\frac{5}{3}\right) J_{2/3}\left(\frac{4\alpha_T \beta}{3} x^{3/4}\right) \frac{1}{(\alpha_T \beta)^{2/3} \sqrt{x}}, \tag{D.7}$$

$$y_2(x) = \left(\frac{3}{2}\right)^{2/3} \Gamma\left(\frac{1}{3}\right) J_{-2/3}\left(\frac{4\alpha_T \beta}{3} x^{3/4}\right) \frac{1}{(\alpha_T \beta)^{2/3} \sqrt{x}}, \tag{D.8}$$

where $J_n(z)$ is the Bessel function of the first kind. Since $y_2(0)$ diverges, and $y_1(0) = 1$ and $y_1'(0) = 0$, we should take only y_1 as the physical solution, subject to the boundary condition that $\phi(t = 0) = \phi_0$ (where we shift our zero of time by $t_{\rm osc}$). Both the analytical solution given by Eq. (D.7) with this boundary condition and the actual numerical solution are shown in Fig. D.1.

As discussed in Sec. 2.4, one must be concerned with washout due to the subsequent oscillations of the Higgs VEV. This is avoided when the scattering processes are not too efficient in the early universe (which gives the result that a large chemical potential is needed to generate the asymmetry). Washout can be avoided either by having these interactions turn off rapidly, or by considering parameters such that there is significant damping of the Higgs oscillations, such as those in Fig. D.1. Regardless of the balance of factors, the end of the asymmetry production, $t_{\rm rlx}$, occurs around the time when the Higgs VEV passes zero. This can be approximated analytically by noting that the Bessel function with $n = 2/3$ has

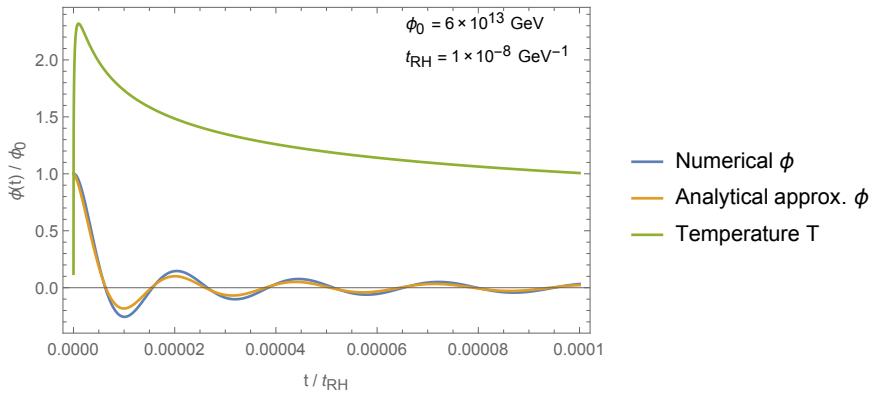

Figure D.1: Higgs evolution with $\Lambda_I = 1.5\times10^{16}\,\text{GeV}$, $\Gamma_I = 10^8\,\text{GeV}$, and $\phi_0 = 6\times10^{13}\,\text{GeV}$. First crossing times are $6.28\times10^{-14}\,\text{GeV}^{-1}$ (numerical) and $6.39\times10^{-14}\,\text{GeV}^{-1}$ (analytical approximation).

a first zero at $z_0 = 3.376$. The relaxation time of the scalar field can then be approximated using the first crossing at

$$z_0 = \frac{4\alpha_T\beta}{3}\, x_{\text{rlx}}^{3/4}, \tag{D.9}$$

which gives

$$t_{\text{rlx}} = t_{RH} x_{\text{rlx}} \approx t_{RH}\left(\frac{3z_0}{4\alpha_T T_{RH} t_{RH}}\right)^{4/3}. \tag{D.10}$$

Note that since Eq. (D.5) is linear in ϕ, the relaxation time is independent of the initial ϕ_0. Hence fluctuations in ϕ_0 does not affect the relaxation time, in the regime considered here: where the potential of the scalar field is dominated by the thermal mass and $t_{\text{rlx}} < t_{RH}$. In fact, as long as the potential is dominated by the thermal mass term (quadratic in ϕ), the relaxation time is always independent of ϕ_0.

The final lepton-to-entropy ratio can be estimated by

$$Y \approx \frac{45}{2\pi^2 g_{*S}}\frac{2\phi_0^2}{\pi^2\Lambda_n^2}\frac{T_{\text{rlx}}^2 t_{\text{rlx}}\Gamma_I^2}{T_{RH}^3}\min\left[1, \frac{2}{\pi^2}\sigma_R T_{\text{rlx}}^3 t_{\text{rlx}}\right]\exp\left(-\frac{8+\sqrt{15}}{\pi^2}\frac{\sigma_R T_{RH}^3}{\Gamma_I}\right), \tag{D.11}$$

which can be found in [4] and improves on the estimates in [1, 2] by $\mathcal{O}(1)$ factors. In this expression, σ_R is the thermally averaged cross section for the lepton-number-violating interaction, $h^0\bar{\nu} \leftrightarrow h^0\nu$, and a thermal distribution has been assumed for participating

particles. Using the above expressions, we have

$$Y \approx \frac{90\sigma_R}{\pi^6 g_{*S}} \left(\frac{\phi_0}{\Lambda_n}\right)^2 \frac{3 z_0 T_{RH}}{4\alpha_T t_{RH}} \exp\left(-\frac{8+\sqrt{15}}{\pi^2}\sigma_R T_{RH}^3 t_{RH}\right). \tag{D.12}$$

Since T_{RH} and t_{RH} are independent of ϕ_0, Eq. (D.12) entails that $Y \propto \phi_0^2$. Note that since $t_{\rm rlx}$ and therefore $T_{\rm rlx}$ are independent of ϕ_0, this is true whether the scale Λ_n in the $\mathcal{O}(6)$ operator (5.1) is a constant or whether it is the temperature of the plasma.

D.2 Power Spectrum of the Lepton Asymmetry

In the case that a scalar field $\phi(x)$ has a nonzero homogeneous part, $\langle\phi(x)\rangle \neq 0$, the fluctuation in any quantity that scales as $X \propto \phi^2$ is simply $\delta X \propto 2\,|\langle\phi(x)\rangle|\,\delta\phi$ for small $\delta\phi$, which gives

$$\frac{\delta X}{\langle X\rangle} \approx 2\frac{\delta\phi}{|\langle\phi(x)\rangle|}. \tag{D.13}$$

However, this is not applicable to the baryonic asymmetry in the relaxation leptogenesis model because the homogeneous part of ϕ is zero, $\langle\phi(x)\rangle = 0$, due to the symmetry of the potential. We note that it is $\phi_0 \equiv \sqrt{\langle\phi^2(x)\rangle}$ which is nonzero, and as we have explained in the Appendix D.1, the lepton asymmetry depends on the initial value of ϕ via $Y \propto \phi_0^2$. In this appendix, we now proceed to calculate the primordial power spectrum of the lepton asymmetry taking into account the fact that it is $\sqrt{\langle\phi^2(x)\rangle}$, not $\langle\phi(x)\rangle$, which is nonzero.

In the following analysis, we adopt the following conventions for the Fourier transform:

$$\phi(x) = \int \frac{d^3k}{(2\pi)^3} e^{i\vec{k}\cdot\vec{x}}\phi_{\vec{k}}, \tag{D.14}$$

$$\phi_{\vec{k}} = \int d^3x e^{-i\vec{k}\cdot\vec{x}}\phi(x). \tag{D.15}$$

The power spectrum of ϕ, $\mathcal{P}_\phi(k)$, is defined through the two-point correlation function of $\phi_{\vec{k}}$

$$\left\langle\phi_{\vec{k}}\phi_{\vec{k}'}\right\rangle = (2\pi)^3\delta^3\left(\vec{k}+\vec{k}'\right)\frac{2\pi^2}{k^3}\mathcal{P}_\phi(k). \tag{D.16}$$

As we mentioned in Eq. (5.8), we approximate the power spectrum of ϕ by

$$\mathcal{P}_\phi(k) = \left(\frac{H_I}{2\pi}\right)^2 \theta(k-k_s)\,\theta\left(k_s e^{N_{\rm last}} - k\right). \tag{D.17}$$

We remind the reader that k_s is the comoving scale which leaves the horizon when the Higgs VEV begins growing, $N_{\rm last}$ e-folds before the end of inflation. Our results are insensitive to very large values of k; however, for completeness, we have included a high-scale cutoff imposed by the fact that ϕ grows until the end of inflation. The comoving scale k that leaves the scale at the end of inflation is the highest scale on which isocurvature modes are produced; this scale is $k_s e^{N_{\rm last}}$. Again, though, such high k values are not relevant to our results, which means that we are insensitive to the end of inflation.

We now look at the fluctuation of $f(x) \equiv \phi^2(x)$ with respect to its expectation value,

$$\delta f(x) = \phi^2(x) - \left\langle \phi^2(x) \right\rangle = \int \frac{d^3k}{(2\pi)^3} e^{i\vec{k}\cdot\vec{x}} f_{\vec{k}}. \tag{D.18}$$

The power spectrum of $\delta f(x)$ can be computed from the two-point function of the Fourier transform of δf

$$\left\langle f_{\vec{k}} f_{\vec{k}'} \right\rangle = (2\pi)^3 \delta^3\left(\vec{k} + \vec{k}'\right) \frac{2\pi^2}{k^3} \mathcal{P}_{\delta f}(k), \tag{D.19}$$

which is

$$\left\langle f_{\vec{k}} f_{\vec{k}'} \right\rangle = \int d^3x d^3y e^{-i\vec{k}\cdot\vec{x} - i\vec{k}'\cdot\vec{y}} \left\langle \delta f(x)\, \delta f(y) \right\rangle \tag{D.20}$$

$$= \int d^3x d^3y e^{-i\vec{k}\cdot\vec{x} - i\vec{k}'\cdot\vec{y}} \left[\left\langle \phi^2(x)\, \phi^2(y) \right\rangle - \left\langle \phi^2(x) \right\rangle \left\langle \phi^2(y) \right\rangle \right] \tag{D.21}$$

$$= \int d^3x d^3y e^{-i\vec{k}\cdot\vec{x} - i\vec{k}'\cdot\vec{y}} \int \frac{d^3k_1 d^3k_2 d^3k_3 d^3k_4}{(2\pi)^{12}} e^{i\left(\vec{k}_1 + \vec{k}_2\right)\cdot\vec{x}} e^{i\left(\vec{k}_3 + \vec{k}_4\right)\cdot\vec{y}}$$
$$\times \left(\left\langle \phi_{\vec{k}_1} \phi_{\vec{k}_2} \phi_{\vec{k}_3} \phi_{\vec{k}_4} \right\rangle - \left\langle \phi_{\vec{k}_1} \phi_{\vec{k}_2} \right\rangle \left\langle \phi_{\vec{k}_3} \phi_{\vec{k}_4} \right\rangle \right). \tag{D.22}$$

Using Wick's theorem, one can express the 4-point function in terms of 2-point functions as

$$\left\langle \phi_{\vec{k}_1} \phi_{\vec{k}_2} \phi_{\vec{k}_3} \phi_{\vec{k}_4} \right\rangle = \left\langle \phi_{\vec{k}_1} \phi_{\vec{k}_2} \right\rangle \left\langle \phi_{\vec{k}_3} \phi_{\vec{k}_4} \right\rangle + \left\langle \phi_{\vec{k}_1} \phi_{\vec{k}_3} \right\rangle \left\langle \phi_{\vec{k}_2} \phi_{\vec{k}_4} \right\rangle + \left\langle \phi_{\vec{k}_1} \phi_{\vec{k}_4} \right\rangle \left\langle \phi_{\vec{k}_2} \phi_{\vec{k}_3} \right\rangle. \tag{D.23}$$

Integrating over $\vec{x}$ and $\vec{y}$, and making use of Eq. (D.16), we have

$$\begin{aligned}\left\langle f_{\vec{k}} f_{\vec{k}'}\right\rangle &= 2\int d^3k_1 d^3k_2 d^3k_3 d^3k_4 \delta^3\left(\vec{k}-\vec{k}_1-\vec{k}_2\right)\delta^3\left(\vec{k}'-\vec{k}_3-\vec{k}_4\right) \\ &\quad\times \delta^3\left(\vec{k}_1+\vec{k}_3\right)\delta^3\left(\vec{k}_2+\vec{k}_4\right)\frac{2\pi^2}{k_1^3}\frac{2\pi^2}{k_2^3}\mathcal{P}_\phi\left(k_1\right)\mathcal{P}_\phi\left(k_2\right) \qquad \text{(D.24)} \\ &= 2\int d^3k_1 d^3k_2 \delta^3\left(\vec{k}-\vec{k}_1-\vec{k}_2\right)\delta^3\left(\vec{k}'+\vec{k}_1+\vec{k}_2\right)\frac{4\pi^4}{k_1^3 k_2^3}\mathcal{P}_\phi\left(k_1\right)\mathcal{P}_\phi\left(k_2\right). \qquad \text{(D.25)} \\ &= 2\delta^3\left(\vec{k}+\vec{k}'\right)\int d^3k_1 \frac{4\pi^4}{k_1^3\left|\vec{k}_1-\vec{k}\right|^3}\mathcal{P}_\phi\left(k_1\right)\mathcal{P}_\phi\left(\left|\vec{k}_1-\vec{k}\right|\right). \qquad \text{(D.26)}\end{aligned}$$

Thus, the power spectrum of δf is

$$\mathcal{P}_{\delta f}\left(k\right) = \frac{k^3}{2\pi}\int d^3k_1 \frac{1}{k_1^3\left|\vec{k}_1-\vec{k}\right|^3}\mathcal{P}_\phi\left(k_1\right)\mathcal{P}_\phi\left(\left|\vec{k}_1-\vec{k}\right|\right). \qquad \text{(D.27)}$$

For the power spectrum of ϕ given by Eq. (D.17), this gives

$$\begin{aligned}\mathcal{P}_{\delta f}\left(k\right) &= \frac{k^3}{2\pi}\left(\frac{H_I}{2\pi}\right)^4\int d^3k_1 \frac{1}{k_1^3\left|\vec{k}_1-\vec{k}\right|^3}\theta\left(k_1-k_s\right)\theta\left(k_s e^{N_{\rm last}}-k_1\right) \\ &\quad\times\theta\left(\left|\vec{k}_1-\vec{k}\right|-k_s\right)\theta\left(k_s e^{N_{\rm last}}-\left|\vec{k}_1-\vec{k}\right|\right). \qquad \text{(D.28)}\end{aligned}$$

For $k \ll k_s$, the power spectrum is suppressed as

$$\mathcal{P}_{\delta f}\left(k\right) \approx \frac{k^3}{2\pi}\left(\frac{H_I}{2\pi}\right)^4\int_{k_s}^{\infty}\frac{4\pi dk_1}{k_1^4} = \frac{2}{3}\left(\frac{H_I}{2\pi}\right)^4\left(\frac{k}{k_s}\right)^3. \qquad \text{(D.29)}$$

For $k_s < k < k_s e^{N_{\rm last}}$, integral is dominated by $\vec{k}_1 \sim \vec{k}_s$ and $\vec{k}_1 \sim \vec{k}-\vec{k}_s$, so one can approximate (see also Appendix A of [174])

$$\begin{aligned}\mathcal{P}_{\delta f}\left(k\right) &\approx \frac{k^3}{2\pi}\left(\frac{H_I}{2\pi}\right)^4 2\int_{k_s}^{k}\frac{4\pi k_1^2 dk_1}{k_1^3 k^3} \qquad \text{(D.30)} \\ &= 4\left(\frac{H_I}{2\pi}\right)^4\ln\left(\frac{k}{k_s}\right). \qquad \text{(D.31)}\end{aligned}$$

The power spectrum reaches a maximum $\sim 4N_{\rm last}\left(H_I/2\pi\right)^4$ before being suppressed severely beyond $k = k_s e^{N_{\rm last}}$. However, as mentioned, this large scale cutoff does not affect our CIB signal, which is dominated by $k \approx 1.4k_s$. The behavior of Eqs. (D.28), (D.29), and (D.31) are shown in Figs. D.2 and D.3.

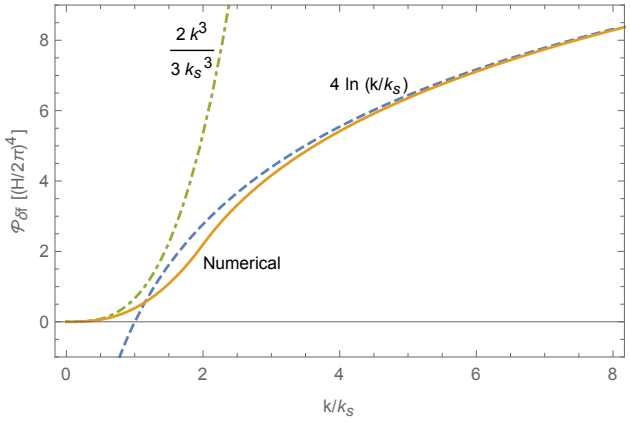

Figure D.2: Power spectrum of the fluctuation of $f = \phi^2$ with respect to its expectation value, $\langle\phi^2\rangle$. The yellow solid line denotes the numerical integration result of Eq. (D.28). The blue dashed curve shows the approximation (D.31) for $k > k_s$. The green dash-dotted line shows the $(k/k_s)^3$ suppression as described by Eq. (D.29), for $k < k_s$.

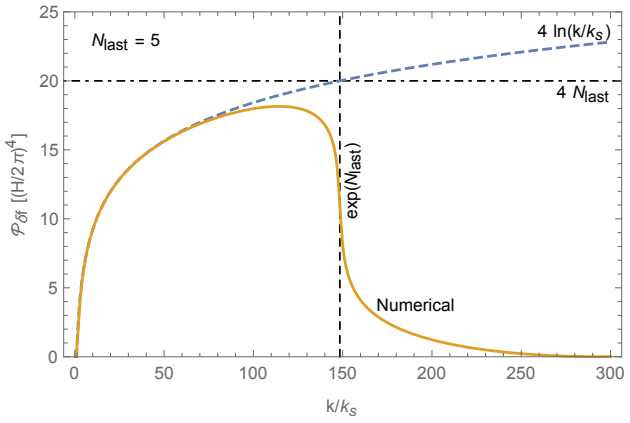

Figure D.3: Same plot as Fig. D.2 with $N_{\rm last} = 5$ as an example; this enables us to see the large scale cutoff. The yellow solid line denotes the numerical result. The blue dashed curve shows the approximation (D.31). The deviation between them appears at the scale $k \sim k_s e^{N_{\rm last}}$. The power spectrum reaches an upper limit around $4N_{\rm last}\,(H_I/2\pi)^4$. Since our calculation of the CIB is dominated by $k \approx 1.4k_s$, the large scale cutoff is irrelevant to our signal.

Since the fluctuation of δf is suppressed for $k < k_s$, we take

$$\mathcal{P}_{\delta f}(k) \approx 4 \left(\frac{H_I}{2\pi}\right)^4 \ln\left(\frac{k}{k_s}\right) \theta(k - k_s) \tag{D.32}$$

for $k \ll k_s e^{N_{\rm last}}$. The average fluctuation of f per $\ln k$ interval is then given by $\delta f_k = \sqrt{\mathcal{P}_{\delta f}(k)}$. Therefore, the spectrum of the fluctuation of Y_B is

$$\left.\frac{\delta Y_B}{Y_B}\right|_k = \frac{\delta f_k}{\langle f \rangle} \approx \frac{2 \ln^{1/2}(k/k_s)}{N_{\rm last}} \theta(k - k_s), \tag{D.33}$$

as used in Eq. (5.9).

References

[1] A. Kusenko, L. Pearce, and L. Yang, "Postinflationary Higgs relaxation and the origin of matter-antimatter asymmetry," Phys. Rev. Lett. **114**, 061302 (2015), arXiv:1410.0722 [hep-ph].

[2] L. Yang, L. Pearce, and A. Kusenko, "Leptogenesis via Higgs Condensate Relaxation," Phys. Rev. **D92**, 043506 (2015), arXiv:1505.07912 [hep-ph].

[3] L. Pearce, L. Yang, A. Kusenko, and M. Peloso, "Leptogenesis via neutrino production during Higgs condensate relaxation," Phys. Rev. **D92**, 023509 (2015), arXiv:1505.02461 [hep-ph].

[4] H. Gertov, L. Pearce, F. Sannino, and L. Yang, "Baryogenesis via Elementary Goldstone Higgs Relaxation," Phys. Rev. **D93**, 115042 (2016), arXiv:1601.07753 [hep-ph].

[5] A. Kusenko, L. Pearce, and L. Yang, "Leptogenesis via the 750 GeV pseudoscalar," Phys. Rev. **D93**, 115005 (2016), arXiv:1604.02382 [hep-ph].

[6] M. Kawasaki, A. Kusenko, L. Pearce, and L. Yang, "Relaxation leptogenesis, isocurvature perturbations, and the cosmic infrared background," Phys. Rev. **D95**, 103006 (2017), arXiv:1701.02175 [hep-ph].

[7] S. Chatrchyan *et al.* (CMS Collaboration), "Observation of a new boson at a mass of 125 GeV with the CMS experiment at the LHC," Phys. Lett. **B716**, 30–61 (2012), arXiv:1207.7235 [hep-ex].

[8] G. Aad *et al.* (ATLAS Collaboration), "Observation of a new particle in the search for the Standard Model Higgs boson with the ATLAS detector at the LHC," Phys. Lett. **B716**, 1–29 (2012), arXiv:1207.7214 [hep-ex].

[9] G. Degrassi, S. Di Vita, J. Elias-Miro, J. R. Espinosa, G. F. Giudice, G. Isidori, and A. Strumia, "Higgs mass and vacuum stability in the Standard Model at NNLO," JHEP **08**, 098 (2012), arXiv:1205.6497 [hep-ph].

[10] T. S. Bunch and P. C. W. Davies, "Quantum Field Theory in de Sitter Space: Renormalization by Point Splitting," Proc. Roy. Soc. Lond. **A360**, 117–134 (1978).

[11] A. D. Linde, "Scalar Field Fluctuations in Expanding Universe and the New Inflationary Universe Scenario," Phys. Lett. **B116**, 335–339 (1982).

[12] A. A. Starobinsky and J. Yokoyama, "Equilibrium state of a selfinteracting scalar field in the De Sitter background," Phys. Rev. **D50**, 6357–6368 (1994), arXiv:astro-ph/9407016 [astro-ph].

[13] A. D. Linde, *Particle Physics and Inflationary Cosmology*, Contemporary Concepts in Physics, Vol. 5 (Taylor and Francis, London, 1990) p. 362, arXiv:hep-th/0503203 [hep-th].

[14] A. Vilenkin and L. H. Ford, "Gravitational Effects upon Cosmological Phase Transitions," Phys. Rev. **D26**, 1231 (1982).

[15] A. A. Starobinsky, "Dynamics of Phase Transition in the New Inflationary Universe Scenario and Generation of Perturbations," Phys. Lett. **B117**, 175–178 (1982).

[16] A. Vilenkin, "Quantum Fluctuations in the New Inflationary Universe," Nucl. Phys. **B226**, 527–546 (1983).

[17] A. A. Starobinsky, "Cosmological models with the intermediate de sitter stage: Theory and observational consequences," in *Fundamental Interactions*, edited by V. N. Ponomarev (MGPI Press, Moscow, 1984) p. 55.

[18] A. A. Starobinsky, "Stochastic de sitter (inflationary) stage in the early universe," in *Field Theory, Quantum Gravity and Strings*, Lecture Notes in Physics, Vol. 246, edited by H. J. de Vega and N. Sánchez (Springer-Verlag, Berlin, 1986) p. 107.

[19] A. Vilenkin, "The Birth of Inflationary Universes," Phys. Rev. **D27**, 2848 (1983).

[20] S.-J. Rey, "Dynamics of Inflationary Phase Transition," Nucl. Phys. **B284**, 706–728 (1987).

[21] S. W. Hawking and I. G. Moss, "Supercooled Phase Transitions in the Very Early Universe," Phys. Lett. **B110**, 35–38 (1982).

[22] S. W. Hawking and I. G. Moss, "Fluctuations in the Inflationary Universe," Nucl. Phys. **B224**, 180 (1983).

[23] K. Enqvist, T. Meriniemi, and S. Nurmi, "Generation of the Higgs Condensate and Its Decay after Inflation," JCAP **1310**, 057 (2013), arXiv:1306.4511 [hep-ph].

[24] P. A. R. Ade *et al.* (Planck Collaboration), "Planck 2013 results. XXII. Constraints on inflation," Astron. Astrophys. **571**, A22 (2014), arXiv:1303.5082 [astro-ph.CO].

[25] P. A. R. Ade *et al.* (Planck Collaboration), "Planck 2015 results. XX. Constraints on inflation," Astron. Astrophys. **594**, A20 (2016), arXiv:1502.02114 [astro-ph.CO].

[26] L. Dai, M. Kamionkowski, and J. Wang, "Reheating constraints to inflationary models," Phys. Rev. Lett. **113**, 041302 (2014), arXiv:1404.6704 [astro-ph.CO].

[27] E. W. Kolb and M. S. Turner, *The Early Universe*, Frontiers in Physics, Vol. 69 (Addison-Wesley, Reading, MA, 1990) pp. 1–547.

[28] A. Andreassen, W. Frost, and M. D. Schwartz, "Consistent Use of the Standard Model Effective Potential," Phys.Rev.Lett. **113**, 241801 (2014), arXiv:1408.0292 [hep-ph].

[29] A. Andreassen, W. Frost, and M. D. Schwartz, "Consistent Use of Effective Potentials," Phys.Rev. **D91**, 016009 (2015), arXiv:1408.0287 [hep-ph].

[30] N. Nielsen, "On the Gauge Dependence of Spontaneous Symmetry Breaking in Gauge Theories," Nucl.Phys. **B101**, 173 (1975).

[31] R. Fukuda and T. Kugo, "Gauge Invariance in the Effective Action and Potential," Phys.Rev. **D13**, 3469 (1976).

[32] I. Aitchison and C. Fraser, "Gauge Invariance and the Effective Potential," Annals Phys. **156**, 1 (1984).

[33] L. Di Luzio and L. Mihaila, "On the gauge dependence of the Standard Model vacuum instability scale," JHEP **1406**, 079 (2014), arXiv:1404.7450 [hep-ph].

[34] J. A. Casas, J. R. Espinosa, and M. Quiros, "Improved Higgs mass stability bound in the standard model and implications for supersymmetry," Phys. Lett. **B342**, 171–179 (1995), arXiv:hep-ph/9409458 [hep-ph].

[35] M. Bando, T. Kugo, N. Maekawa, and H. Nakano, "Improving the effective potential: Multimass scale case," Prog. Theor. Phys. **90**, 405–418 (1993), arXiv:hep-ph/9210229 [hep-ph].

[36] C. Ford, "Multiscale renormalization group improvement of the effective potential," Phys. Rev. **D50**, 7531–7537 (1994), arXiv:hep-th/9404085 [hep-th].

[37] G. W. Anderson and L. J. Hall, "The Electroweak phase transition and baryogenesis," Phys. Rev. **D45**, 2685–2698 (1992).

[38] J. Kapusta and C. Gale, *Finite-temperature field theory: Principles and applications*, 2nd ed. (Cambridge University Press, Cambridge, England, 2006) p. 442.

[39] K. Enqvist, S. Nurmi, and S. Rusak, "Non-Abelian dynamics in the resonant decay of the Higgs after inflation," JCAP **1410**, 064 (2014), arXiv:1404.3631 [astro-ph.CO].

[40] P. Elmfors, K. Enqvist, and I. Vilja, "Thermalization of the Higgs field at the electroweak phase transition," Nucl.Phys. **B412**, 459–478 (1994), arXiv:hep-ph/9307210 [hep-ph].

[41] L. Kofman, A. D. Linde, and A. A. Starobinsky, "Towards the theory of reheating after inflation," Phys.Rev. **D56**, 3258–3295 (1997), arXiv:hep-ph/9704452 [hep-ph].

[42] J. Garcia-Bellido, D. G. Figueroa, and J. Rubio, "Preheating in the Standard Model with the Higgs-Inflaton coupled to gravity," Phys.Rev. **D79**, 063531 (2009), arXiv:0812.4624 [hep-ph].

[43] D. G. Figueroa, J. Garcia-Bellido, and F. Torrenti, "Decay of the standard model Higgs field after inflation," Phys. Rev. **D92**, 083511 (2015), arXiv:1504.04600 [astro-ph.CO].

[44] J. Garcia-Bellido, M. Garcia-Perez, and A. Gonzalez-Arroyo, "Chern-Simons production during preheating in hybrid inflation models," Phys.Rev. **D69**, 023504 (2004), arXiv:hep-ph/0304285 [hep-ph].

[45] H. A. Weldon, "Dynamical Holes in the Quark - Gluon Plasma," Phys.Rev. **D40**, 2410 (1989).

[46] K. Enqvist and J. Hogdahl, "Scalar condensate decay in a fermionic heat bath in the early universe," JCAP **0409**, 013 (2004), arXiv:hep-ph/0405299 [hep-ph].

[47] M. Drewes and J. U. Kang, "The Kinematics of Cosmic Reheating," Nucl.Phys. **B875**, 315–350 (2013), arXiv:1305.0267 [hep-ph].

[48] K. Enqvist, T. Meriniemi, and S. Nurmi, "Higgs Dynamics during Inflation," JCAP **1407**, 025 (2014), arXiv:1404.3699 [hep-ph].

[49] A. D. Sakharov, "Violation of CP Invariance, C Asymmetry, and Baryon Asymmetry of the Universe," Pis'ma Zh. Eksp. Teor. Fiz. **5**, 32–35 (1967), [JETP Lett. **5**, 24 (1967)]; "Violation of CP Invariance, C Asymmetry, and Baryon Asymmetry of the Universe," Usp. Fiz. Nauk **161**, 61 (1991), [Sov. Phys. Usp. **34**, 392 (1991)].

[50] P. Peebles, "Origin of the large-scale galaxy peculiar velocity field: a minimal isocurvature model," Nature **327**, 210–211 (1987).

[51] P. Peebles, "Cosmic background temperature anisotropy in a minimal isocurvature model for galaxy formation," Astrophys. J. Lett. **315**, L73–L76 (1987).

[52] K. Enqvist and J. McDonald, "Observable isocurvature fluctuations from the affleck-dine condensate," Phys. Rev. Lett. **83**, 2510–2513 (1999), arXiv:hep-ph/9811412 [hep-ph].

[53] K. Enqvist and J. McDonald, "Inflationary Affleck-Dine scalar dynamics and isocurvature perturbations," Phys. Rev. **D62**, 043502 (2000), arXiv:hep-ph/9912478 [hep-ph].

[54] K. Harigaya, A. Kamada, M. Kawasaki, K. Mukaida, and M. Yamada, "Affleck-dine baryogenesis and dark matter production after high-scale inflation," Phys. Rev. **D90**, 043510 (2014), arXiv:1404.3138 [hep-ph].

[55] A. Kusenko and P. Langacker, "Is the vacuum stable?" Phys. Lett. **B391**, 29–33 (1997), arXiv:hep-ph/9608340 [hep-ph].

[56] A. Kusenko, P. Langacker, and G. Segre, "Phase transitions and vacuum tunneling into charge and color breaking minima in the mssm," Phys. Rev. **D54**, 5824–5834 (1996), arXiv:hep-ph/9602414 [hep-ph].

[57] A. Kobakhidze and A. Spencer-Smith, "Electroweak vacuum (in)stability in an inflationary universe," Phys. Lett. **B722**, 130–134 (2013), arXiv:1301.2846 [hep-ph].

[58] M. E. Shaposhnikov, "Baryon Asymmetry of the Universe in Standard Electroweak Theory," Nucl. Phys. **B287**, 757–775 (1987).

[59] M. E. Shaposhnikov, "Structure of the High Temperature Gauge Ground State and Electroweak Production of the Baryon Asymmetry," Nucl. Phys. **B299**, 797–817 (1988).

[60] J. Smit, "Effective CP violation in the standard model," JHEP **0409**, 067 (2004), arXiv:hep-ph/0407161 [hep-ph].

[61] T. Brauner, O. Taanila, A. Tranberg, and A. Vuorinen, "Computing the temperature dependence of effective CP violation in the standard model," JHEP **1211**, 076 (2012), arXiv:1208.5609 [hep-ph].

[62] M. Dine, P. Huet, J. Singleton, Robert L., and L. Susskind, "Creating the baryon asymmetry at the electroweak phase transition," Phys. Lett. **B257**, 351–356 (1991).

[63] M. Ibe and K. Kaneta, "Spontaneous thermal Leptogenesis via Majoron oscillation," Phys. Rev. **D92**, 035019 (2015), arXiv:1504.04125 [hep-ph].

[64] R. Daido, N. Kitajima, and F. Takahashi, "Axion domain wall baryogenesis," JCAP **1507**, 046 (2015), arXiv:1504.07917 [hep-ph].

[65] A. G. Cohen and D. B. Kaplan, "Thermodynamic Generation of the Baryon Asymmetry," Phys. Lett. **B199**, 251 (1987).

[66] J. Garcia-Bellido, D. Yu. Grigoriev, A. Kusenko, and M. E. Shaposhnikov, "Nonequilibrium electroweak baryogenesis from preheating after inflation," Phys. Rev. **D60**, 123504 (1999), arXiv:hep-ph/9902449 [hep-ph].

[67] J. Garcia-Bellido and D. Y. Grigoriev, "Inflaton-induced sphaleron transitions," JHEP **0001**, 017 (2000), arXiv:hep-ph/9912515 [hep-ph].

[68] A. Tranberg and J. Smit, "Baryon asymmetry from electroweak tachyonic preheating," JHEP **0311**, 016 (2003), arXiv:hep-ph/0310342 [hep-ph].

[69] H. Davoudiasl, R. Kitano, G. D. Kribs, H. Murayama, and P. J. Steinhardt, "Gravitational baryogenesis," Phys.Rev.Lett. **93**, 201301 (2004), arXiv:hep-ph/0403019 [hep-ph].

[70] T. Yanagida, "HORIZONTAL SYMMETRY AND MASSES OF NEUTRINOS," in *Proceedings: Workshop on the Unified Theories and the Baryon Number in the Universe, Tsukuba, Japan, 1979*, edited by O. Sawada and A. Sugamoto (KEK, Tsukuba, 1979) pp. 95–99.

[71] T. Yanagida, "Horizontal Symmetry and Masses of Neutrinos," Prog. Theor. Phys. **64**, 1103 (1980).

[72] M. Gell-Mann, P. Ramond, and R. Slansky, "Complex Spinors and Unified Theories," in *Supergravity*, edited by D. Freedman and P. V. Nieuwenhuizen (North-Holland, Amsterdam, 1979) pp. 315–321, arXiv:1306.4669 [hep-th].

[73] P. Minkowski, "$\mu \to e\gamma$ at a Rate of One Out of 10^9 Muon Decays?" Phys. Lett. **B67**, 421–428 (1977).

[74] M. Fukugita and T. Yanagida, "Baryogenesis Without Grand Unification," Phys. Lett. **B174**, 45 (1986).

[75] G. F. Giudice, A. Notari, M. Raidal, A. Riotto, and A. Strumia, "Towards a complete theory of thermal leptogenesis in the SM and MSSM," Nucl. Phys. **B685**, 89–149 (2004), arXiv:hep-ph/0310123 [hep-ph].

[76] J. Kearney, H. Yoo, and K. M. Zurek, "Is a Higgs Vacuum Instability Fatal for High-Scale Inflation?" Phys. Rev. **D91**, 123537 (2015), arXiv:1503.05193 [hep-th].

[77] T. Chiba, F. Takahashi, and M. Yamaguchi, "Baryogenesis in a flat direction with neither baryon nor lepton charge," Phys. Rev. Lett. **92**, 011301 (2004), erratum: Phys. Rev. Lett. **114**, 209901 (2015), arXiv:hep-ph/0304102 [hep-ph].

[78] A. Kusenko, K. Schmitz, and T. T. Yanagida, "Leptogenesis via Axion Oscillations after Inflation," Phys. Rev. Lett. **115**, 011302 (2015), arXiv:1412.2043 [hep-ph].

[79] J. M. Cline, "Baryogenesis," in *Les Houches Summer School - Session 86: Particle Physics and Cosmology: The Fabric of Spacetime Les Houches, France, July 31-August 25, 2006* (2006) arXiv:hep-ph/0609145 [hep-ph].

[80] P. Adshead and E. I. Sfakianakis, "Leptogenesis from left-handed neutrino production during axion inflation," Phys. Rev. Lett. **116**, 091301 (2016), arXiv:1508.00881 [hep-ph].

[81] M.-z. Li, X.-l. Wang, B. Feng, and X.-m. Zhang, "Quintessence and spontaneous leptogenesis," Phys. Rev. **D65**, 103511 (2002), arXiv:hep-ph/0112069 [hep-ph].

[82] A. De Felice, S. Nasri, and M. Trodden, "Quintessential baryogenesis," Phys. Rev. **D67**, 043509 (2003), arXiv:hep-ph/0207211 [hep-ph].

[83] F. Takahashi and M. Yamaguchi, "Spontaneous baryogenesis in flat directions," Phys. Rev. **D69**, 083506 (2004), arXiv:hep-ph/0308173 [hep-ph].

[84] K. Kamada and M. Yamaguchi, "Asymmetric Dark Matter from Spontaneous Cogenesis in the Supersymmetric Standard Model," Phys. Rev. **D85**, 103530 (2012), arXiv:1201.2636 [hep-ph].

[85] T. Alanne, H. Gertov, F. Sannino, and K. Tuominen, "Elementary Goldstone Higgs boson and dark matter," Phys. Rev. **D91**, 095021 (2015), arXiv:1411.6132 [hep-ph].

[86] H. Gertov, A. Meroni, E. Molinaro, and F. Sannino, "Theory and phenomenology of the elementary Goldstone Higgs boson," Phys. Rev. **D92**, 095003 (2015), arXiv:1507.06666 [hep-ph].

[87] D. B. Kaplan and H. Georgi, "SU(2) x U(1) Breaking by Vacuum Misalignment," Phys. Lett. **B136**, 183 (1984).

[88] D. B. Kaplan, H. Georgi, and S. Dimopoulos, "Composite Higgs Scalars," Phys. Lett. **B136**, 187 (1984).

[89] G. Cacciapaglia and F. Sannino, "Fundamental Composite (Goldstone) Higgs Dynamics," JHEP **04**, 111 (2014), arXiv:1402.0233 [hep-ph].

[90] T. Alanne, A. Meroni, F. Sannino, and K. Tuominen, "Radiatively induced Fermi scale and unification," Phys. Rev. **D93**, 091701 (2016), arXiv:1511.01910 [hep-ph].

[91] T. Appelquist, P. S. Rodrigues da Silva, and F. Sannino, "Enhanced global symmetries and the chiral phase transition," Phys. Rev. **D60**, 116007 (1999), arXiv:hep-ph/9906555 [hep-ph].

[92] Z.-y. Duan, P. S. Rodrigues da Silva, and F. Sannino, "Enhanced global symmetry constraints on epsilon terms," Nucl. Phys. **B592**, 371–390 (2001), arXiv:hep-ph/0001303 [hep-ph].

[93] T. A. Ryttov and F. Sannino, "Ultra Minimal Technicolor and its Dark Matter TIMP," Phys. Rev. **D78**, 115010 (2008), arXiv:0809.0713 [hep-ph].

[94] J. Galloway, J. A. Evans, M. A. Luty, and R. A. Tacchi, "Minimal Conformal Technicolor and Precision Electroweak Tests," JHEP **10**, 086 (2010), arXiv:1001.1361 [hep-ph].

[95] R. N. Mohapatra and G. Senjanovic, "Neutrino Mass and Spontaneous Parity Violation," Phys. Rev. Lett. **44**, 912 (1980).

[96] S. Weinberg, *Cosmology* (Oxford Univ. Pr., Oxford, UK, 2008) pp. 1–593.

[97] A. Pilaftsis and T. E. J. Underwood, "Resonant leptogenesis," Nucl. Phys. **B692**, 303–345 (2004), arXiv:hep-ph/0309342 [hep-ph].

[98] A. Pilaftsis and T. E. J. Underwood, "Electroweak-scale resonant leptogenesis," Phys. Rev. **D72**, 113001 (2005), arXiv:hep-ph/0506107 [hep-ph].

[99] E. K. Akhmedov, V. A. Rubakov, and A. Yu. Smirnov, "Baryogenesis via neutrino oscillations," Phys. Rev. Lett. **81**, 1359–1362 (1998), arXiv:hep-ph/9803255 [hep-ph].

[100] M. Cannoni, "Relativistic &lt;$\sigma v_{\rm rel}$&gt; in the calculation of relics abundances: a closer look," Phys. Rev. **D89**, 103533 (2014), arXiv:1311.4494 [astro-ph.CO].

[101] ATLAS Collaboration, *Search for resonances decaying to photon pairs in 3.2 fb^{-1} of pp collisions at $\sqrt{s}$ = 13 TeV with the ATLAS detector*, Report No. ATLAS-CONF-2015-081 (CERN, Geneva, 2015).

[102] CMS Collaboration, *Search for new physics in high mass diphoton events in proton-proton collisions at $\sqrt{s} = 13$ TeV*, Report No. CMS-PAS-EXO-15-004 (CERN, Geneva, 2015).

[103] D. Buttazzo, A. Greljo, and D. Marzocca, "Knocking on new physics' door with a scalar resonance," Eur. Phys. J. **C76**, 116 (2016), arXiv:1512.04929 [hep-ph].

[104] R. Franceschini, G. F. Giudice, J. F. Kamenik, M. McCullough, A. Pomarol, R. Rattazzi, M. Redi, F. Riva, A. Strumia, and R. Torre, "What is the $\gamma\gamma$ resonance at 750 GeV?" JHEP **03**, 144 (2016), arXiv:1512.04933 [hep-ph].

[105] W. Altmannshofer, J. Galloway, S. Gori, A. L. Kagan, A. Martin, and J. Zupan, "750 GeV diphoton excess," Phys. Rev. **D93**, 095015 (2016), arXiv:1512.07616 [hep-ph].

[106] Y. Mambrini, G. Arcadi, and A. Djouadi, "The LHC diphoton resonance and dark matter," Phys. Lett. **B755**, 426–432 (2016), arXiv:1512.04913 [hep-ph].

[107] M. Backovic, A. Mariotti, and D. Redigolo, "Di-photon excess illuminates Dark Matter," JHEP **03**, 157 (2016), arXiv:1512.04917 [hep-ph].

[108] C. Han, H. M. Lee, M. Park, and V. Sanz, "The diphoton resonance as a gravity mediator of dark matter," Phys. Lett. **B755**, 371–379 (2016), arXiv:1512.06376 [hep-ph].

[109] P. S. B. Dev and D. Teresi, "Asymmetric dark matter in the Sun and diphoton excess at the LHC," Phys. Rev. **D94**, 025001 (2016), arXiv:1512.07243 [hep-ph].

[110] H. Han, S. Wang, and S. Zheng, "Dark Matter Theories in the Light of Diphoton Excess," (2015), arXiv:1512.07992 [hep-ph].

[111] J.-C. Park and S. C. Park, "Indirect signature of dark matter with the diphoton resonance at 750 GeV," Phys. Dark Univ. **14**, 4–10 (2016), arXiv:1512.08117 [hep-ph].

[112] F. D'Eramo, J. de Vries, and P. Panci, "A 750 GeV Portal: LHC Phenomenology and Dark Matter Candidates," JHEP **05**, 089 (2016), arXiv:1601.01571 [hep-ph].

[113] A. Berlin, "Diphoton and diboson excesses in a left-right symmetric theory of dark matter," Phys. Rev. **D93**, 055015 (2016), arXiv:1601.01381 [hep-ph].

[114] W. Chao, "The Diphoton Excess Inspired Electroweak Baryogenesis," (2016), arXiv:1601.04678 [hep-ph].

[115] M.-L. Xiao and J.-H. Yu, "Electroweak baryogenesis in a scalar-assisted vectorlike fermion model," Phys. Rev. **D94**, 015011 (2016), arXiv:1509.02931 [hep-ph].

[116] P. Adshead and E. I. Sfakianakis, "Fermion production during and after axion inflation," JCAP **1511**, 021 (2015), arXiv:1508.00891 [hep-ph].

[117] K. Schmitz, "Leptogenesis during Axion Relaxation after Inflation," in *2nd Toyama International Workshop on Higgs as a Probe of New Physics (HPNP2015) Toyama, Japan, February 11-15, 2015* (2015) arXiv:1503.08908 [hep-ph].

[118] F. Takahashi and M. Yamada, "Strongly broken Peccei-Quinn symmetry in the early Universe," JCAP **1510**, 010 (2015), arXiv:1507.06387 [hep-ph].

[119] F. Takahashi and M. Yamada, "Spontaneous Baryogenesis from Asymmetric Inflaton," Phys. Lett. **B756**, 216–220 (2016), arXiv:1510.07822 [hep-ph].

[120] K. Kainulainen, S. Nurmi, T. Tenkanen, K. Tuominen, and V. Vaskonen, "Isocurvature Constraints on Portal Couplings," JCAP **1606**, 022 (2016), arXiv:1601.07733 [astro-ph.CO].

[121] B. Shi and S. Raby, "Basis invariant description of chemical equilibrium with implications for a recent axionic leptogenesis model," Phys. Rev. **D92**, 085008 (2015), arXiv:1507.08392 [hep-ph].

[122] A. G. Cohen and D. B. Kaplan, "SPONTANEOUS BARYOGENESIS," Nucl. Phys. **B308**, 913 (1988).

[123] A. Dolgov and K. Freese, "Calculation of particle production by Nambu Goldstone bosons with application to inflation reheating and baryogenesis," Phys. Rev. **D51**, 2693–2702 (1995), arXiv:hep-ph/9410346 [hep-ph].

[124] A. Dolgov, K. Freese, R. Rangarajan, and M. Srednicki, "Baryogenesis during reheating in natural inflation and comments on spontaneous baryogenesis," Phys. Rev. **D56**, 6155–6165 (1997), arXiv:hep-ph/9610405 [hep-ph].

[125] K. Enqvist, S. Nurmi, S. Rusak, and D. Weir, "Lattice Calculation of the Decay of Primordial Higgs Condensate," JCAP **1602**, 057 (2016), arXiv:1506.06895 [astro-ph.CO].

[126] R. N. Mohapatra and G. Senjanovic, "Neutrino Masses and Mixings in Gauge Models with Spontaneous Parity Violation," Phys. Rev. **D23**, 165 (1981).

[127] L. Covi, E. Roulet, and F. Vissani, "CP violating decays in leptogenesis scenarios," Phys. Lett. **B384**, 169–174 (1996), arXiv:hep-ph/9605319 [hep-ph].

[128] P. A. R. Ade *et al.* (Planck Collaboration), "Planck 2013 results. XVI. Cosmological parameters," Astron. Astrophys. **571**, A16 (2014), arXiv:1303.5076 [astro-ph.CO].

[129] W. Buchmuller, R. D. Peccei, and T. Yanagida, "Leptogenesis as the origin of matter," Ann. Rev. Nucl. Part. Sci. **55**, 311–355 (2005), arXiv:hep-ph/0502169 [hep-ph].

[130] I. Affleck and M. Dine, "A New Mechanism for Baryogenesis," Nucl. Phys. **B249**, 361 (1985).

[131] M. Dine, L. Randall, and S. D. Thomas, "Baryogenesis from flat directions of the supersymmetric standard model," Nucl. Phys. **B458**, 291–326 (1996), arXiv:hep-ph/9507453 [hep-ph].

[132] ATLAS Collaboration, *Search for scalar diphoton resonances with 15.4 fb^{-1} of data collected at $\sqrt{s}$=13 TeV in 2015 and 2016 with the ATLAS detector*, Report No. ATLAS-CONF-2016-059 (CERN, Geneva, 2016).

[133] CMS Collaboration, *Search for resonant production of high mass photon pairs using 12.9 fb^{-1} of proton-proton collisions at $\sqrt{s}$ = 13 TeV and combined interpretation of searches at 8 and 13 TeV*, Report No. CMS-PAS-EXO-16-027 (CERN, Geneva, 2016).

[134] A. Kashlinsky, R. G. Arendt, J. C. Mather, and S. H. Moseley, "Tracing the first stars with fluctuations of the cosmic infrared background," Nature **438**, 45–50 (2005), arXiv:astro-ph/0511105 [astro-ph].

[135] A. Kashlinsky, R. G. Arendt, J. Mather, and S. H. Moseley, "New Measurements of Cosmic Infrared Background Fluctuations from Early Epochs," Astrophys. J. **654**, L5–L8 (2007).

[136] A. Kashlinsky, R. G. Arendt, M. L. N. Ashby, G. G. Fazio, J. Mather, and S. H. Moseley, "New Measurements of the Cosmic Infrared Background Fluctuations in Deep Spitzer/IRAC Survey Data and Their Cosmological Implications," Astrophys. J. **753**, 63 (2012), arXiv:1201.5617.

[137] A. Cooray *et al.*, "A measurement of the intrahalo light fraction with near-infrared background anisotropies," Nature **490**, 514–517 (2012), arXiv:1210.6031 [astro-ph.CO].

[138] H. J. Seo, H. M. Lee, T. Matsumoto, W. S. Jeong, M. G. Lee, and J. Pyo, "AKARI Observation of the Sub-degree Scale Fluctuation of the Near-infrared Background," Astrophys. J. **807**, 140 (2015), arXiv:1504.05681 [astro-ph.CO].

[139] K. Helgason, M. Ricotti, A. Kashlinsky, and V. Bromm, "On the Physical Requirements for a Pre-Reionization Origin of the Unresolved Near-Infrared Background," Mon. Not. Roy. Astron. Soc. **455**, 282–294 (2016), arXiv:1505.07226 [astro-ph.CO].

[140] A. Kashlinsky, J. C. Mather, K. Helgason, R. G. Arendt, V. Bromm, and S. H. Moseley, "Reconstructing emission from pre-reionization sources with cosmic infrared background fluctuation measurements by the jwst," Astrophys. J. **804**, 99 (2015), arXiv:1412.5566 [astro-ph.CO].

[141] K. Helgason and E. Komatsu, "AKARI near-infrared background fluctuations arise from normal galaxy populations," Mon. Not. Roy. Astron. Soc. **467**, L36 (2017), arXiv:1611.00042 [astro-ph.GA].

[142] R. G. Arendt, A. Kashlinsky, S. H. Moseley, and J. Mather, "Cosmic Infrared Background Fluctuations and Zodiacal Light," Astrophys. J. **824**, 26 (2016), arXiv:1604.07291 [astro-ph.CO].

[143] N. Cappelluti, A. Kashlinsky, R. G. Arendt, A. Comastri, G. G. Fazio, A. Finoguenov, G. Hasinger, J. C. Mather, T. Miyaji, and S. H. Moseley, "Cross-correlating Cosmic Infrared and X-Ray Background Fluctuations: Evidence of Significant Black Hole Populations among the CIB Sources," Astrophys. J. **769**, 68 (2013), arXiv:1210.5302 [astro-ph.CO].

[144] A. Kashlinsky, "LIGO gravitational wave detection, primordial black holes and the near-IR cosmic infrared background anisotropies," Astrophys. J. **823**, L25 (2016), arXiv:1605.04023 [astro-ph.CO].

[145] A. Dolgov and J. Silk, "Baryon isocurvature fluctuations at small scales and baryonic dark matter," Phys. Rev. **D47**, 4244–4255 (1993).

[146] A. D. Dolgov, M. Kawasaki, and N. Kevlishvili, "Inhomogeneous baryogenesis, cosmic antimatter, and dark matter," Nucl. Phys. **B807**, 229–250 (2009), arXiv:0806.2986 [hep-ph].

[147] W. Hu, E. F. Bunn, and N. Sugiyama, "COBE constraints on baryon isocurvature models," Astrophys. J. **447**, L59–L64 (1995), arXiv:astro-ph/9501034 [astro-ph].

[148] M. Beltran, J. Garcia-Bellido, J. Lesgourgues, and M. Viel, "Squeezing the window on isocurvature modes with the lyman-alpha forest," Phys. Rev. **D72**, 103515 (2005), arXiv:astro-ph/0509209 [astro-ph].

[149] D. S. Gorbunov and V. A. Rubakov, *Introduction to the Theory of the Early Universe: Cosmological Perturbations and Inflationary Theory* (World Scientific, Singapore, 2011) p. 489.

[150] A. Cooray, Y. Gong, J. Smidt, and M. G. Santos, "The Near-IR Background Intensity and Anisotropies During The Epoch of Reionization," Astrophys. J. **756**, 92 (2012), arXiv:1205.2316 [astro-ph.CO].

[151] B. Yue, A. Ferrara, R. Salvaterra, and X. Chen, "The Contribution of High Redshift Galaxies to the Near-Infrared Background," Mon. Not. Roy. Astron. Soc. **431**, 383 (2013), arXiv:1208.6234 [astro-ph.CO].

[152] W. H. Press and P. Schechter, "Formation of Galaxies and Clusters of Galaxies by Self-Similar Gravitational Condensation," Astrophys. J. **187**, 425–438 (1974).

[153] T. Abel, P. Anninos, Y. Zhang, and M. L. Norman, "Modeling primordial gas in numerical cosmology," New Astron. **2**, 181–207 (1997), arXiv:astro-ph/9608040 [astro-ph].

[154] M. Tegmark, J. Silk, M. J. Rees, A. Blanchard, T. Abel, and F. Palla, "How small were the first cosmological objects?" Astrophys. J. **474**, 1–12 (1997), arXiv:astro-ph/9603007 [astro-ph].

[155] T. Abel, G. L. Bryan, and M. L. Norman, "The formation of the first star in the Universe," Science **295**, 93 (2002), arXiv:astro-ph/0112088 [astro-ph].

[156] V. Bromm, P. S. Coppi, and R. B. Larson, "The formation of the first stars. I. The Primordial star forming cloud," Astrophys. J. **564**, 23–51 (2002), arXiv:astro-ph/0102503 [astro-ph].

[157] V. Bromm, N. Yoshida, L. Hernquist, and C. F. McKee, "The formation of the first stars and galaxies," Nature **459**, 49–54 (2009), arXiv:0905.0929 [astro-ph.CO].

[158] V. Miranda, A. Lidz, C. H. Heinrich, and W. Hu, "Signatures of metal-free star formation in Planck 2015 Polarization Data," Mon. Not. Roy. Astron. Soc. **467**, 4050 (2017), arXiv:1610.00691 [astro-ph.CO].

[159] K. Enqvist and M. S. Sloth, "Adiabatic CMB perturbations in pre - big bang string cosmology," Nucl. Phys. **B626**, 395–409 (2002), arXiv:hep-ph/0109214 [hep-ph].

[160] D. H. Lyth and D. Wands, "Generating the curvature perturbation without an inflaton," Phys. Lett. **B524**, 5–14 (2002), arXiv:hep-ph/0110002 [hep-ph].

[161] T. Moroi and T. Takahashi, "Effects of cosmological moduli fields on cosmic microwave background," Phys. Lett. **B522**, 215–221 (2001), Erratum: Phys. Lett. **B539**, 303 (2002), arXiv:hep-ph/0110096 [hep-ph].

[162] M. Postma, "The Curvaton scenario in supersymmetric theories," Phys. Rev. **D67**, 063518 (2003), arXiv:hep-ph/0212005 [hep-ph].

[163] M. Postma and A. Mazumdar, "Resonant decay of flat directions: Applications to curvaton scenarios, Affleck-Dine baryogenesis, and leptogenesis from a sneutrino condensate," JCAP **0401**, 005 (2004), arXiv:hep-ph/0304246 [hep-ph].

[164] M. Postma, "Curvaton scenario with low scale inflation revisited," JCAP **0405**, 002 (2004), arXiv:astro-ph/0403213 [astro-ph].

[165] K. Harigaya, T. Hayakawa, M. Kawasaki, and S. Yokoyama, "CDM/baryon isocurvature perturbations in a sneutrino curvaton model," JCAP **1410**, 068 (2014), arXiv:1409.1669 [hep-ph].

[166] M. Bastero-Gil, A. Berera, R. O. Ramos, and J. G. Rosa, "Warm baryogenesis," Phys. Lett. **B712**, 425–429 (2012), arXiv:1110.3971 [hep-ph].

[167] M. Bastero-Gil, A. Berera, R. O. Ramos, and J. G. Rosa, "Observational implications of mattergenesis during inflation," JCAP **1410**, 053 (2014), arXiv:1404.4976 [astro-ph.CO].

[168] A. G. Cohen, D. B. Kaplan, and A. E. Nelson, "Baryogenesis at the weak phase transition," Nucl. Phys. **B349**, 727–742 (1991).

[169] A. Dolgov, "Baryogenesis, 30 years after," (1997), arXiv:hep-ph/9707419 [hep-ph].

[170] H. K. Dreiner, H. E. Haber, and S. P. Martin, "Two-component spinor techniques and Feynman rules for quantum field theory and supersymmetry," Phys. Rept. **494**, 1–196 (2010), arXiv:0812.1594 [hep-ph].

[171] M. Nowakowski and A. Pilaftsis, "On gauge invariance of Breit-Wigner propagators," Z. Phys. **C60**, 121–126 (1993), arXiv:hep-ph/9305321 [hep-ph].

[172] M. Cannoni, "Probability distribution for the relative velocity of colliding particles in a relativistic classical gas," Phys. Rev. **D89**, 103533 (2014), arXiv:1311.4494 [astro-ph.CO].

[173] K. Harigaya and K. Mukaida, "Thermalization after/during Reheating," JHEP **05**, 006 (2014), arXiv:1312.3097 [hep-ph].

[174] D. H. Lyth, "Axions and inflation: Sitting in the vacuum," Phys. Rev. **D45**, 3394–3404 (1992).